

Dual-Band Multi-Channel Airborne Radar for Mapping the Internal and Basal Layers of Polar Ice Sheets

By

Kiran C. Marathe

B.E (With Distinction)., Electronics and Communication Engineering,
Bapuji Institute of Engineering and Technology,
Kuvempu University, India 2001

Submitted to the Department of Electrical Engineering and
Computer Science and the Faculty of the Graduate School
of the University of Kansas in partial fulfillment of
the requirements for the degree of Master's of Science

Thesis Committee:

Dr. Christopher Allen

Dr. Sivaprasad Gogineni

Dr. Fernando Rodriguez-Morales

Date Defended: 02/15/2008

The Thesis Committee for Kiran C. Marathe certifies
That this is the approved version of the following thesis:

**Dual-Band Multi-Channel Airborne Radar for Mapping the Internal and
Basal Layers of Polar Ice Sheets**

Committee:

Chairperson

Date Approved

Abstract

Rapid thinning of the Jakobshavn and a few other outlet glaciers in Greenland and the Antarctic has been observed in the past few years. The key to understanding these dramatic changes is basal conditions. None of the spaceborne radars, that have been providing a wealth of information about the ice surface, is capable of measuring ice thickness or mapping bed conditions. At the Center for Remote Sensing of Ice Sheets (CReSIS), we have developed an airborne radar system to map the internal and basal layers to obtain a 3-dimensional representation of the ice sheets in Polar Regions. We have also devised advanced signal processing techniques to overcome the effects of surface clutter.

We have developed a radar for measuring ice thickness up to a 5000 m depth from low-altitude (500 m) and high-altitude (7000 m) aircraft. This airborne radar system can operate at two bands: very high frequency band (VHF-band) (140 MHz to 160 MHz) with a peak power of 800 W and P-band (435 MHz to 465 MHz) with a peak power of 1.6 kW for collecting data to develop effective ice sheet models. The pulse signal has a duration of 3 μ s or 10 μ s. The radar has 1 transmitter and 6 receivers inside the aircraft and an 8 element dipole antenna array mounted beneath the wings of the aircraft. This system is designed to have 32 coherent integrations and pulse compression due to which a high loop sensitivity of at least 208 dB was obtained. This system was tested and data were collected in the recent September 2007 field experiment over various parts of Greenland. From the initial observations of the collected data it can be deduced that the signal losses at 450 MHz are more than predicted by existing models and clutter masked the weak bed echoes when the data were collected at higher altitudes both at 150 MHz and 450 MHz.

Acknowledgments

I would like to thank Dr. Gogineni for providing me a wonderful opportunity to know and explore the field of radars. His philosophy of giving importance to student learning is really worth mentioning. I remember of him helping me in the lab, in spite of his busy schedule and other commitments. Further, he has been an excellent support during those difficult times both in my personal and professional life.

I would like to thank Dr. Allen for serving on my committee as the Chairperson. He is always there to answer any questions related to course work or research.

Initially I was little concerned about meeting a new person with whom I would have to work for my thesis and the rest of my graduate research period. But I was surprised when I met Dr. Rodriguez-Morales since he made me feel comfortable instantly with his carefree and cheerful smile. Later during the course of our everyday interaction, I realized that I have found a wise mentor who would help me in growing to greater heights with all his vast knowledge. I am very lucky to discover a friend and a philosopher in him. Thank you Fernando!

I would like to acknowledge John Ledford for helping me during the initial stages of the project when I had hardware problems and I was clueless! I would like to express my gratitude to Anthony Hoch, Jilu Li and Chandini Veeramachaneni for sharing their knowledge in signal processing and data processing. My thanks to Torry Akins and John Paden for the initial radar design ideas and special thanks to Keron Hopkins and Dennis Sundermeyer for providing hassle-free administrative and machining lab support respectively. My special thanks to Uday Kiran who offered guidance with latex programming which helped in producing a professional thesis document.

Mrs. Suseela Gogineni is not directly related to my thesis work. Nevertheless, I would like to remember her for the excellent moral support and providing me the required encouragement during the hard days when my confidence was really low. It was important!

Sahana, Victor, Deepthi and Dileepa are four important people of my more than two years of life in USA. They have been with me and done everything possible and

have encouraged me in my work and personal life to the fullest.

Without Sahana it would have been impossible to complete this project meeting all the deadlines. She toiled selflessly for the project and helped me during times when I was technically ignorant or my mind went blank.

Victor is my first true non-Indian friend and he proved that people from opposite parts of the globe can indeed be best friends, understand, value and respect mutual cultures.

Deepthi has been invaluable support to my work and my well-being. She helped me relentlessly when I was working non-stop towards my career and thesis research.

My room mate Dileepa could sense whenever assistance was required and he was happy to keep aside his personal work to help me out when I had any problems.

Nazia, Kevin, Cameron, Logan, Aqsa, Dinesh to name a few are those wonderful friends whom I met at CReSIS and during my stay at Lawrence. I would cherish all those unforgettable moments which will remind me of the wonderful graduate school days!

It is impossible to acknowledge my parents who have given me all that I need to cultivate and imbibe in me the human values. The dedication of this thesis is the least that I can offer in gratitude to all the hardships that they have experienced in fulfilling my dreams of pursuing higher studies.

Contents

Acceptance Page	i
Abstract	ii
Acknowledgments	iii
1 Introduction	1
1.1 Previous work	4
1.2 Thesis goals and outline	5
2 System Design and Implementation	7
2.1 Science requirements	7
2.2 System description	8
2.2.1 Radar transmitter	10
2.2.2 Radar receiver	13
2.3 System specifications	15
2.4 RF system design	20
2.4.1 Low power transmitter design	21
2.4.2 Low power receiver design	24
2.5 Antenna sub-system	26
2.6 Digital system and radar software	28
2.7 Fabrication	30
3 Laboratory Testing and Results	34
3.1 Receiver testing	34
3.1.1 S-parameter measurement	35
3.1.2 Noise floor measurements	37
3.1.3 Receiver noise figure measurements	39
3.1.4 Compression point measurements	40

3.2	Arbitrary waveform generation spectra	41
3.3	Transmitter testing	44
3.3.1	tx_input testing	45
3.3.2	tx_output testing	45
3.3.3	Transmitter output spectrum	47
3.4	Thermal stress testing	49
3.5	System loopback and calibration testing	49
4	Field Experiment and Results	52
4.1	Field experiment description	52
4.2	Sample results and discussion	55
5	Future Improvements	59
5.1	EMI testing	59
5.2	High power amplifier characterization	61
5.2.1	150 MHz amplifier	62
5.2.2	450 MHz amplifier	67
5.3	Transmitter design	68
5.3.1	AWG improvements	68
5.3.2	IQ modulator	68
5.3.3	Lowpass and bandpass filters	70
5.4	Receiver modifications	71
5.4.1	Blanking switches	71
5.5	General improvements	73
6	Conclusion	75
	Appendices	76
A	Schematic and PCB Layout	76
B	Matlab Listing	81
B.1	Program listing 1	81
B.2	Program listing 2	85
B.3	Program listing 3	92
B.4	Program listing 4	93
B.5	Program listing 5	94
C	Bill of Materials	96

D Publications	102
References	104

List of Figures

1.1	World estimation map of inundation effect due to 1 m sea level rise . . .	2
1.2	World estimation map of inundation effect due to 6 m sea level rise . . .	2
2.1	Radar system diagram	9
2.2	Block diagram of dual-band multi-channel imaging and depth sounding radar	10
2.3	Block diagram of low power radar RF transmitter	11
2.4	Block diagram of low power radar RF receiver	13
2.5	(a) High power blanking switches box with the switching logic circuit (top left) and (b) High power filter box	14
2.6	Pictorial representation of radar echo times	19
2.7	ADS harmonic balance simulation of P-band IQ modulator	21
2.8	Simulated results of IQ modulator	22
2.9	(a) Antenna array at 450 MHz. 3-D antenna simulation results in high frequency structure simulator (HFSS) software for (b) 450 MHz system and (c) 150 MHz system.	27
2.10	Antenna feed network used in the depth sounder mode	28
2.11	Pictorial representation of under-sampling concept	29
2.12	Aluminum chassis with frequency synthesizer, input and output transmitter sections	31
2.13	Aluminum chassis with 2 receiver channels and data cable for programming the Xilinx CPLD	32
2.14	(a) Transmitter chassis ports (b) Receiver chassis ports	33
3.1	Preliminary receiver validation outside the chassis	36
3.2	Transmitter validation using a RF tested board	36
3.3	Measured s-parameters for receiver channel 0 for (a) 150 MHz system and (b) 450 MHz system	37

3.4	Measured effective noise power spectrum of (a) Spectrum analyzer (b) Receiver at 150 MHz and (c) Receiver at 450 MHz	38
3.5	Measured compression point values for receiver channel 0 at (a) 150 MHz and (b) 450 MHz	41
3.6	Measured AWG output spectrum with (a) 20 MHz bandwidth and (b) 30 MHz bandwidth	42
3.7	Simulated time domain 10 MHz to 30 MHz chirp signal: (a) Ideal rectangular chirp (b) Pre-distorted chirp (c) Amplitude tapered chirp (d) Pre-distorted and amplitude tapered chirp	43
3.8	Simulated frequency domain 10 MHz to 30 MHz chirp signal: (a) Ideal rectangular chirp (b) Pre-distorted chirp (c) Amplitude tapered chirp (d) Pre-distorted and amplitude tapered chirp	44
3.9	Measured output spectrum of transmitter input section for (a) 150 MHz system and (b) 450 MHz system	46
3.10	Measured s-parameters for tx_output for (a) 150 MHz system and (b) 450 MHz system	46
3.11	Measured output spectrum of integrated transmitter section for (a) 150 MHz system and (b) 450 MHz system	47
3.12	System loopback and calibration block diagram	50
3.13	System loopback set-up and the optical fiber spools (inset)	51
4.1	Flight lines for September 2007 Greenland field experiment	53
4.2	System installed on NASA P-3 aircraft	54
4.3	Dipole antenna array installed beneath the aircraft wings	54
4.4	Locations of the field experiment for the presented sample data results	56
4.5	(a) Echogram and (b) A-scope of data collected for 450 MHz system at high elevation in interferometric mode	56
4.6	(a) Echogram and (b) A-scope of data collected for 450 MHz system at low elevation in depth sounder mode	57
4.7	(a) Echogram and (b) A-scope of data collected for 150 MHz system at high elevation in interferometric mode	57
4.8	(a) Echogram and (b) A-scope of data collected for 150 MHz system at an elevation of 1700 m in depth sounder mode	57
5.1	Sprint anechoic chamber test set-up	61
5.2	Measured EMI test results	62
5.3	150 MHz power amplifier P1-dB characterization test set-up	62

5.4	Measured response of (a) PA 0 for 150 MHz tone as input and (b) PA 1 for 150 MHz tone as input	64
5.5	Measured response of PA 0 and PA1 for 150 MHz tone as input for comparison	64
5.6	Calibration test set-up for the (a) 3-dB power splitter and (b) high power amplifiers	65
5.7	Measured amplitude and phase difference response between 150 MHz PA 0 and PA 1 high power amplifier modules	66
5.8	Measured response for the 450 MHz high power amplifier	67
5.9	(a) Analog Devices IQ modulator circuit. (b) In-house designed bias circuit	70
5.10	(a) Lowpass filter designed at CReSIS. (b) Measured s-parameters of the filter	71
5.11	Skyworks switches (a) with bandpass filter and (b) without bandpass filter in the receiver path	73
A.1	Transmitter input schematic	76
A.2	Transmitter output schematic	77
A.3	Receiver output schematic	77
A.4	Transmitter and receiver PCBs	78
A.5	Receiver input with Skyworks AS216-339 switch introduced between Trilithic band-pass filter and Miteq LNA	79
A.6	In-house developed CReSIS-MiniCircuits IQ modulator	80
C.1	Receiver front-end board bill of materials	97
C.2	Frequency synthesizer bill of materials	98
C.3	Transmitter input board bill of materials	99
C.4	Transmitter output board bill of materials	100
C.5	Miscellaneous parts bill of materials	101

List of Tables

2.1	Specifications relating to radar system hardware	16
2.2	Theoretical transmitter input section link budget for 150 MHz and 450 MHz systems	23
2.3	Theoretical transmitter output section link budget for 150 MHz and 450 MHz systems	23
2.4	Theoretical transmitter system power budget for 150 MHz and 450 MHz systems	23
2.5	Theoretical receiver link budget for 150 MHz and 450 MHz systems	24
3.1	Receiver test parameters	34
3.2	Receiver settings for the s-parameter measurements of 150 MHz and 450 MHz systems	37
3.3	Measured noise floor values with noise power normalized to 1 Hz bandwidth	38
3.4	Measured and calculated noise figure values for 2 receiver channels both for 150 MHz and 450 MHz systems	40
3.5	Typical Lorch Microwave bandpass filter specifications used in the transmitter and receiver	48
4.1	Parameters for September 2007 field mission sample results	55
5.1	Sample test cases for the study of EMI effect on the system response	60
5.2	Measured output power for the 150 MHz power amplifier module PA 0	63
5.3	Measured output power for the 150 MHz power amplifier module PA 1	63
5.4	Measured amplitude and phase imbalance values for the two 150 MHz power amplifiers	66

Chapter 1

Introduction

The mass balance of Greenland and Antarctica ice sheets is varying rapidly due to the climate change on planet earth. These variations of the ice sheets caused by the global warming phenomenon is one of the major contributors to the sea-level rise. Glaciers and ice sheets modulate the sea level by storing water deposited as snow on the surface and discharging water back in to the ocean through melting and via icebergs. The sea level is rising at a rate of approximately 3.1 mm/year. The contribution from the polar ice caps is about 15% while a major portion (about 57%) is due to thermal expansion of water. Even though the sea level variations have been happening for many centuries, it is remarkable to note that the sea level rise has been enormously high from past few decades. Figures 1.1 and 1.2 illustrate the potential effects of drastic changes in the global sea level [1]. Global mean sea level rose at an average rate of 1.8 mm/year over 1961 to 2003. The rate was faster over 1993 to 2003, about 3.1 mm/year as per the latest Intergovernmental Panel on Climate Change (IPCC) report [2]. Undoubtedly it has become important to understand and predict the role of polar ice caps in the sea level change.

The various working groups of the IPCC have released their reports on climate change. In the past much of the debate was focused on whether climate change exists and if human beings are responsible. But currently with the latest IPCC 2007 reports,

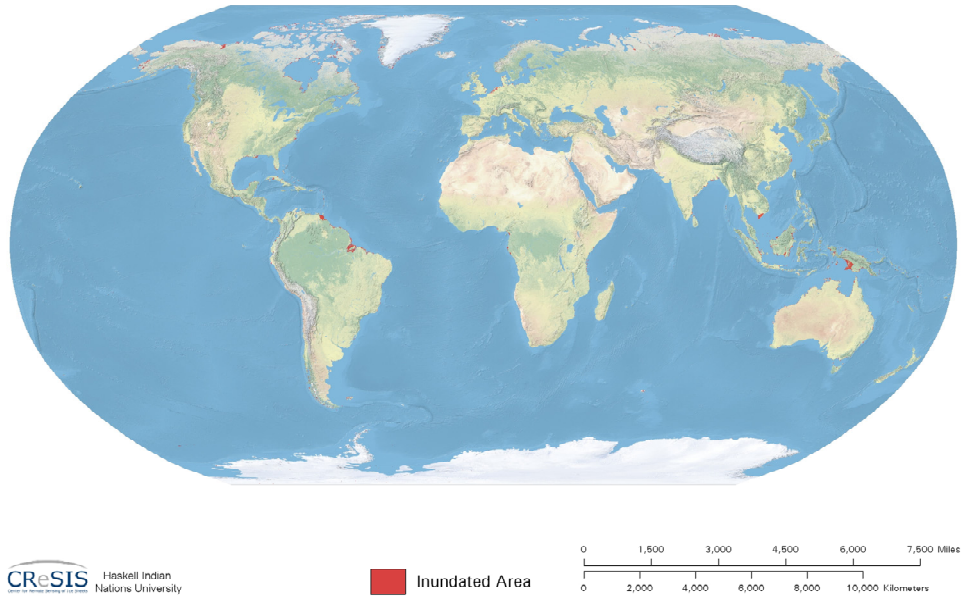


Figure 1.1. World estimation map of inundation effect due to 1 m sea level rise

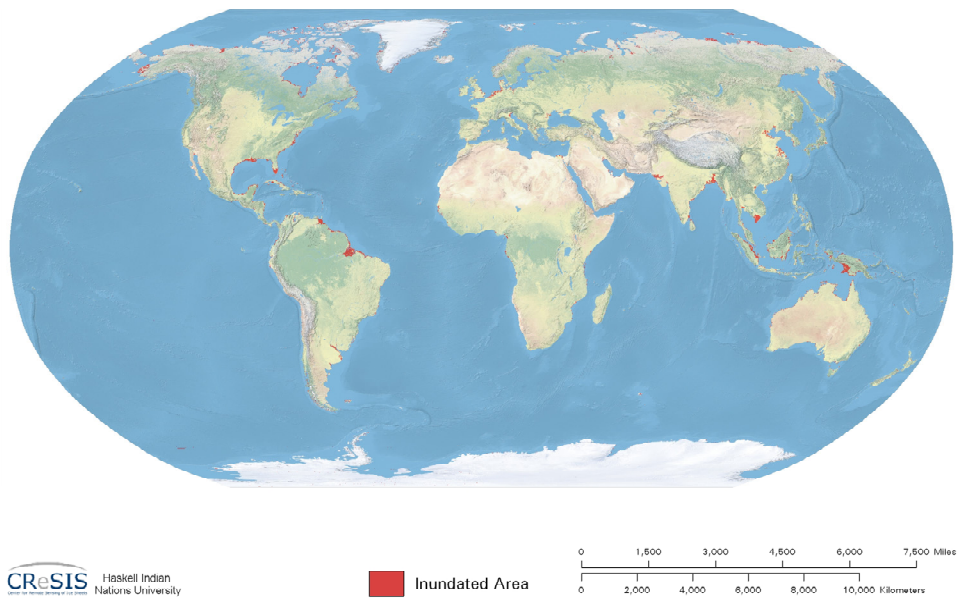


Figure 1.2. World estimation map of inundation effect due to 6 m sea level rise

it has been concluded that indeed climate change is happening and that human activity is a major contributor compared to the natural phenomenon. As summarized by the reports, one of the major challenges is to reduce the greenhouse emissions to mitigate the effects of climate variations [3].

Further, year 2007 set a new record of highest melting in Greenland. Areas higher than 2000 m in elevation melted up to 25 days to 30 days longer than the average number of days calculated for the previous 18 years. Since melting at higher elevations implies rising temperatures a check on the emissions is important [4]. Even the Antarctica has a lamentable story of its own. The potential for rapid deglaciation, or collapse of the 2-million-sq-kilometer West Antarctic Ice Sheet (WAIS) due to the change in climate, is a biggest threat to mankind. This would result in increasing sea-levels to an extent where several low-lying areas in many continents would lose the land mass. Even though this would not happen in next few centuries it is necessary to contain such likely events [5].

One of the key factors in understanding the variations in ice sheets is the basal conditions or the bed conditions of the ice sheets. The study of the ice-bed variations can provide a wealth of information to understand the mass balance change of the ice sheets. Nevertheless, there are quite few uncertainties in understanding how these greater polar ice sheets are receding and the current data is insufficient to model the rapidly changing behavior. We at CReSIS are constantly focusing our efforts to develop new technologies and systems to fill in these gaps and thus provide better inputs to modelers. The team at CReSIS, University of Kansas has been developing radar instrumentation for quite few years to image the ice-bed interface and map the ice sheets with very high resolution. Radar is one of the primary sensor techniques used in remote sensing of ice sheets.

The invention of radio frequency detection and ranging (radar) and the applications date back to the 'golden years' of microwave engineering during the 1930s and 1940s [6]. Even though it had the early usage only in military, today radar is used for many peaceful and scientific purposes including but not limited to air traffic control, weather studies and remote sensing. At CReSIS the goal is to 'To Understand and Predict the

Role of Polar Ice Sheets in Sea Level Change’ and the primary application of radar in this context is related to remote sensing of polar ice caps.

1.1 Previous work

Similar radar systems have been developed in the past at University of Kansas under different group names such as Remote Sensing Laboratory (RSL), Polar Radar for Ice Sheet Measurement (PRISM) and currently CRISIS.

During 2004 a multi-band multi-static synthetic aperture radar was developed for measuring the basal conditions of ice sheets. This system operated at 3 different frequencies: 80 MHz, 150 MHz and 350 MHz with 2 receivers and a single transmitter operating at a peak power of 100 W. This was a ground based system designed with connectorized components and which operated in both monostatic and bistatic modes. It used a log periodic antenna system mounted on a sled over the ice surface. This system used novel signal processing techniques (0/pi phase modulation) to reduce the coherent system noise [7].

During 2006 an airborne Multi-Channel Radar Depth Sounder (MCRDS) was developed operating at a frequency of 150 MHz and a peak power of 800 W. This system had 1 transmitter and 5 receivers for data collection. This was an airborne miniaturized system fabricated on printed circuit boards (PCBs) using surface mount components used in depth sounding of ice sheets. MCRDS operated at an altitude of 500 m from the ice surface with the system installed on a Twin Otter aircraft with a 5-element linear quarter-wave folded dipole antenna array mounted beneath the wings of the aircraft. MCRDS has successfully provided the first depth sounding results of the Jacobshavn glacier within 90 km of the calving front, to a depth of 800 m [8].

The current system was developed during 2006-2007 for measuring the ice thickness, mapping the ice-bed and to estimate the surface clutter. This system operates at 2 different frequencies: 150 MHz and 450 MHz with peak power of 800 W and 1600 W

respectively. The system has a single switched transmitter (VHF-band or P-band) and 6 receivers for data collection. The system was fabricated on PCBs using surface mount components as a process towards miniaturization. The system operated at an altitude ranging from 500 m up to 7000 m from the ice surface with the system installed on a NASA P-3 aircraft with a 8-element linear half-wave dipole antenna array mounted beneath the wings of the aircraft. The operating modes were termed as depth sounder and interferometric mode which provided the first ever high altitude (7000 m) data at 450 MHz of the Jacobshavn glacier. Finally, compared to the previously discussed radars this system has the $0/\pi$ feature for coherent noise suppression.

1.2 Thesis goals and outline

The goal of the project under which this thesis is developed was to optimize the previous MCRDS system for better performance at 150 MHz as well as introducing the capability of 450 MHz operation so has to have an integrated system without expanding the hardware board layout.

This work comprises the development of the radio frequency (RF) sub-system which was used as a 'proof-of-concept' for Global Ice Sheets Mapping Orbiter (GISMO) project. This thesis describes the design, implementation and testing of an airborne radar system operating at 150 MHz and 450 MHz for ice sheet mapping. The instrument is optimized for both depth sounding and interferometry applications. The sensor was successfully deployed and data were collected during the Fall 2007 Greenland field experiment.

The thesis is divided in to 6 chapters. Chapter 2 describes system design, implementation and the specifications. Chapter 3 focuses on the laboratory testing of the system both at module-level and complete system loop-back test. Chapter 4 has some sample results obtained during the Greenland field experiments along with a preliminary discussion of the results. Chapter 5 lists several enhancements for the transmitter, receiver and the integrated system which would aid in developing a robust, compact

and a well-defined radar system for future. Finally the thesis concludes with a brief summary of accomplishments in chapter 6.

Chapter 2

System Design and Implementation

The design constraints for the system are driven by the science requirements put forth by the scientists for the study of surface and basal topography of terrestrial ice sheets and to determine the physical properties of glacier bed. Further considerations from an engineering perspective previously gained experience was used to introduce modifications at the system level. These modifications to the hardware were intended to optimize the performance of the system at 150 MHz.

This chapter describes the requirements, design and implementation of the RF hardware system.

2.1 Science requirements

The science requirements are listed below. A thorough discussion on these requirements can be found in [9].

1. Measure ice thickness and basal topography to an accuracy of 20 m or better;
2. Measure ice thickness every 1000 m (in some cases 500 m);

3. Measure ice thickness ranging from 100 m to 5000 m;
4. Measure radar reflectivity from basal interfaces;
5. Pole-to-pole observations

The above requirements are intimately related to the radar hardware system design. The measurement accuracy depends on the system bandwidth and the required signal to noise ratio (SNR). The measurement resolution also depends on system bandwidth. The range of measurement is a factor deciding the loop sensitivity of the system where receiver parameters and transmit power are of primary consideration. Radar reflectivity is based on transmit and receive power and other parameters such as antenna gain and dielectric contrast of the target. The last requirement stems from the fact that the current airborne system is a potential proof-of-concept for an observation platform with the goal of sounding the greater ice sheets from space.

2.2 System description

The primary focus of this work are the design, construction and testing of the radar transmitter and receiver. Other sub-systems are also briefly discussed. Figure 2.1 shows overview of radar system. The radar transmitter obtains the baseband chirp signal generated digitally by arbitrary waveform generator (AWG) which is essentially a digital to analog converter (DAC) output. The AWG produces in-phase 'I' and quadrature 'Q' signals that are in turn mixed with the local oscillator (LO) frequency (120 MHz or 420 MHz) using a quadrature modulator. The up-converted chirp signal is then amplified by low power amplifier and a pre-amplifier before fed in to the high power amplifier which is then sent to the antenna array.

The received signal after suitable analog signal conditioning is sent through an analog to digital converter (ADC) with under-sampling to recover the signal and finally stored on the digital data hard drives.

The timing and control block provides critical timing, trigger and enable signals for the radar system. The radar controller is a miniature computer which runs the operating system and also hosts the custom designed graphical user interface (GUI). It has the overall control of the system and also allows the operator to set parameters on the GUI. The user can set parameters for example, number of coherent integrations, receiver gain, receiver blanking control, transmit chirp center frequency, bandwidth and pulse duration. The GUI is also used to observe the real-time signal returns during the experiment. The entire low power section is housed in a compact peripheral component interface (cPCI) chassis.

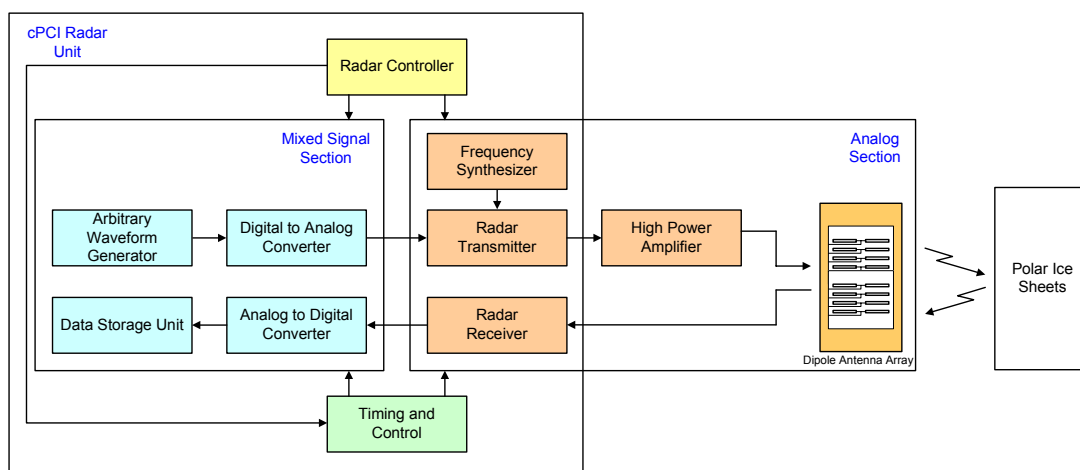


Figure 2.1. Radar system diagram

Figure 2.2 shows the radar system overall block diagram. The main blocks of the system are digital system and clock generation section, RF electronics section comprising of transmitter and receiver sections and a dipole antenna array system.

The radar RF system is broadly categorized in to 'low power' and 'high power' blocks. The low power block comprises of radar transmitter and receiver modules while the high power block comprises of the high power amplifiers, high power capacity cables, high power attenuators and antenna sub-system. The following subsections describe in detail the low power block since this is the primary focus of this thesis.

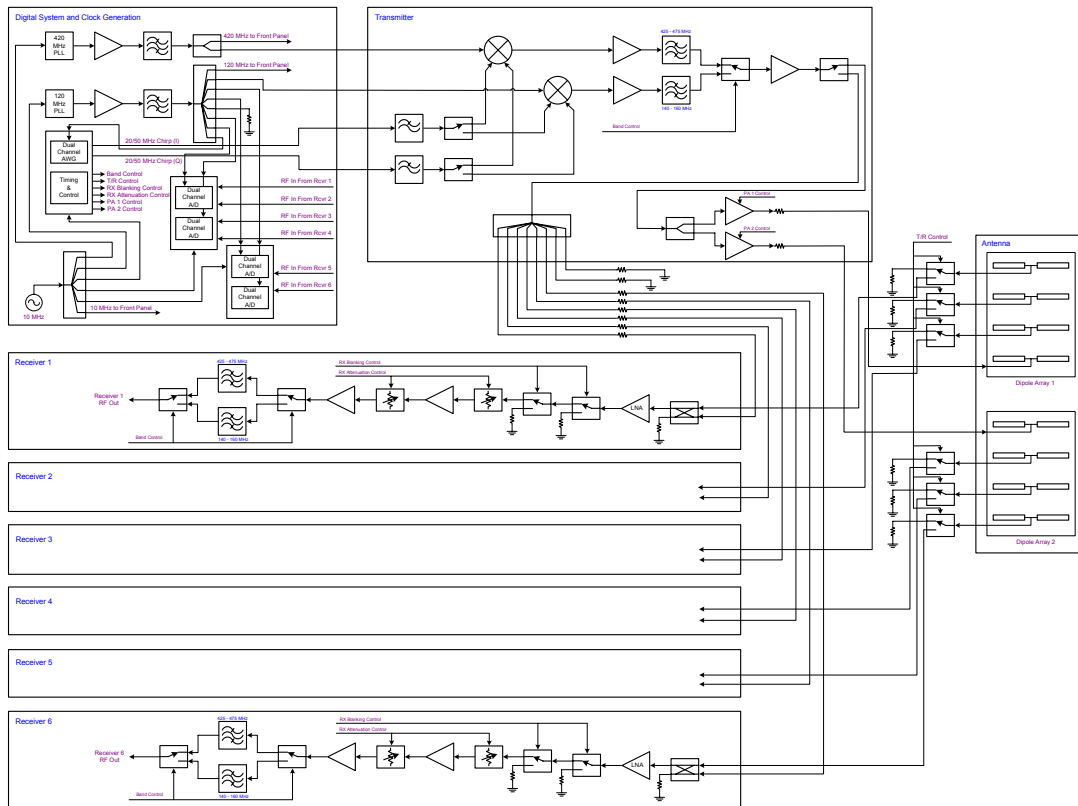


Figure 2.2. Block diagram of dual-band multi-channel imaging and depth sounding radar

2.2.1 Radar transmitter

Figure 2.3 shows the low power radar RF transmitter block diagram. The low power transmitter block is further sectioned in to 'transmitter input' and 'transmitter output' sections. This sectioning enables easy analysis and debugging of the transmitter. The diagram also depicts a typical configuration for 150 MHz and 450 MHz operation.

The input to the transmitter is a quadrature (I and Q) baseband signal with a bandwidth of 20 MHz to 40 MHz and a power level of 0 dBm for 150 MHz system and a chirp of 15 MHz to 45 MHz with power of 0 dBm for the 450 MHz system. A 120 MHz LO with 13 dBm for the 150 MHz system and 420 MHz LO at 10.8 dBm for the 450 MHz system is provided from the frequency synthesizer section to the IQ modulator [10]. The baseband signal is initially lowpass filtered to remove the harmonics originating from

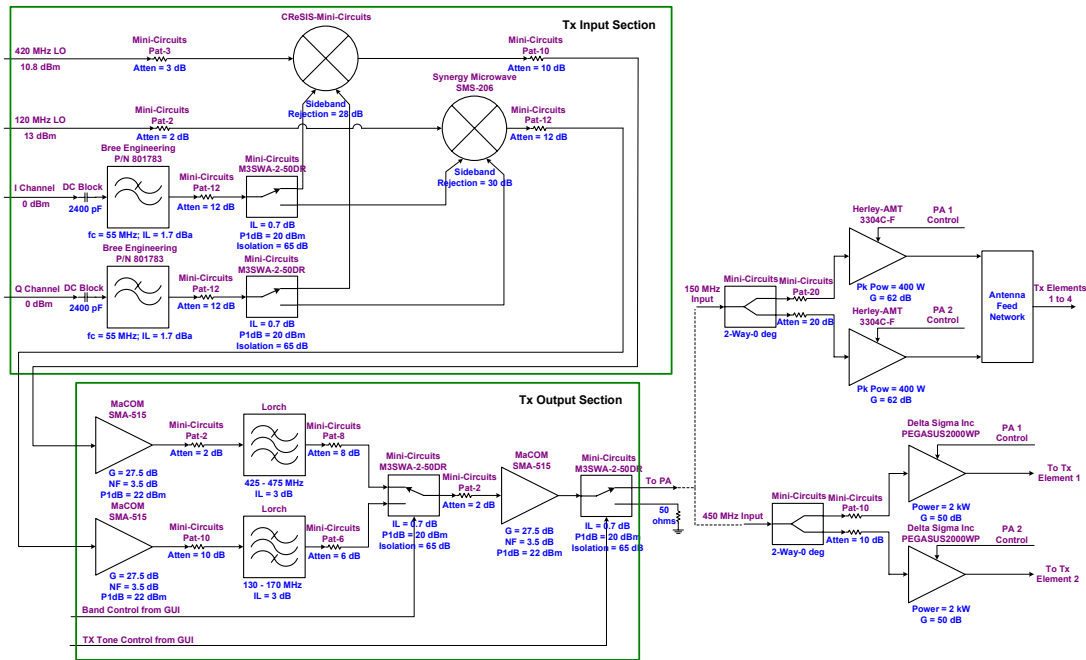


Figure 2.3. Block diagram of low power radar RF transmitter

the chirp signal and LO frequency and then fed in to the switches. Thus the custom-designed front end Bree Engineering lowpass filter acts as an anti-imaging filter. The lowpass filters have a 1.7 dB cut-off frequency at 55 MHz. Since the maximum usable baseband signal is only 48 MHz (due to sinc frequency roll-off effect, section 3.2) there is an alternate design using lowpass filter (KR2740) with 45 MHz as the 0.5 dB cut-off frequency from KR Electronics. Both designs have been developed and tested and their performance is comparable for the frequency band of operation. Since the system uses a single waveform generator to generate the chirp signals Mini-Circuits switches (M3SWA-2-50DR) with very low insertion loss of 0.7 dB are used to select the path for 150 MHz or 450 MHz system.

For the 150 MHz system SMS206 IQ modulator from Synergy Microwave is used for up-conversion. This mixer possesses a conversion loss of 8 dB and a minimum sideband rejection of 30 dB. Since off-the-shelf IQ modulator was not available for operation at 450 MHz, an IQ modulator was designed in-house using 2 double balanced mixers (Mini-

Circuits ADEX-10L), 2 Way-90° power splitter (Mini-Circuits HPQ-05) and 2 Way-0° power combiner (Mini-Circuits ADP-2-10). Section 2.4.1 details the simulation of the P-band IQ modulator.

The DC block capacitors are required at the front end of the transmitter section to protect the switches from potential damage due to the DC signal from the AWG-DAC combination.

The MaCOM SMA515 first amplifier stage in the 'transmitter output' section, provides sufficient gain (27.5 dB) to the up-converted signal followed by custom designed Lorch Microwave bandpass filter which removes out of band frequency components generated at the mixer output. The bandpass filter has a maximum of 3 dB insertion loss in the passband. A Mini-Circuits M3SWA-2-50DR band control switch is introduced to switch between the bands (150 MHz and 450 MHz) based on the experiment plan. The final MaCOM SMA515 amplifier provides the required boost (27.5 dB gain) to the signal before being fed to the power amplifier section. A Mini-Circuits M3SWA-2-50DR switch after the final amplifier stage in the transmitter output section is mainly legacy but can be used to switch the transmit signal to the receivers for calibration purposes. This calibration method was not used in the current system and hence the other port of the switch is terminated with a 50 ohm termination. A different approach is adopted for the system calibration and loopback testing which is outlined in section 3.5.

Finally, at least 2 dB pads are placed between most of the components throughout the transmitter chain to minimize signal reflection and saturation. Mixer, amplifiers and switches are the components which have saturation specifications and thus pads are required not to exceed their input power limits.

The signal output from the 'transmitter output' section is divided in to 2 paths using a 3-dB power splitter and provided to the power amplifiers. Figure 2.3 shows an example configuration for operation at 150 MHz and 450 MHz. A detailed discussion on configurations is provided in section 4.1.

2.2.2 Radar receiver

Figure 2.4 shows the radar RF receiver block diagram excluding the high power switches and high power filters.

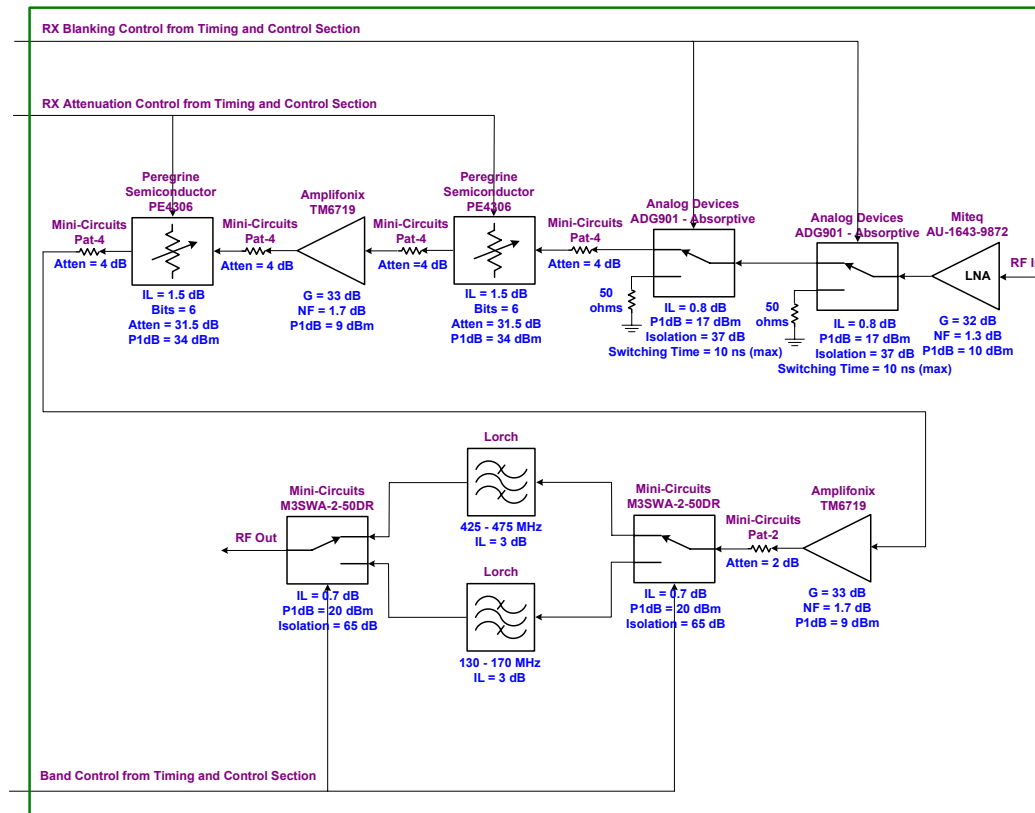


Figure 2.4. Block diagram of low power radar RF receiver

The back scattered energy from the target reaches the antenna which is then fed in to high power blanking switches and high power bandpass filters. The high power switches 50S-1532, from JFW Industries can operate over a frequency range of 140 MHz to 480 MHz and has a very low insertion loss of about 0.4 dB. It provides 50 dB isolation when maximum power of 2 kW is transmitted, thus safe-guarding the front-end of the receivers. Its switching time is approximately 10 μ s and can handle a peak power of 200 W for a 20 μ s pulse. The custom built Trilithic bandpass filters have a very low insertion loss of less than 0.5 dB with a peak power handling capacity of 2 kW.

There are 6 blanking switches and 12 Trilithic filters (6 each for 150 MHz and 450 MHz) housed in individual aluminum boxes as shown in figure 2.5. Each box measures about 17 inches by 24 inch in dimension. The blanking switch box uses an in-house designed switching logic circuit to provide suitable control voltages to the control lines of the switches such that at any time both the control lines are not TTL high, which may damage the switch.

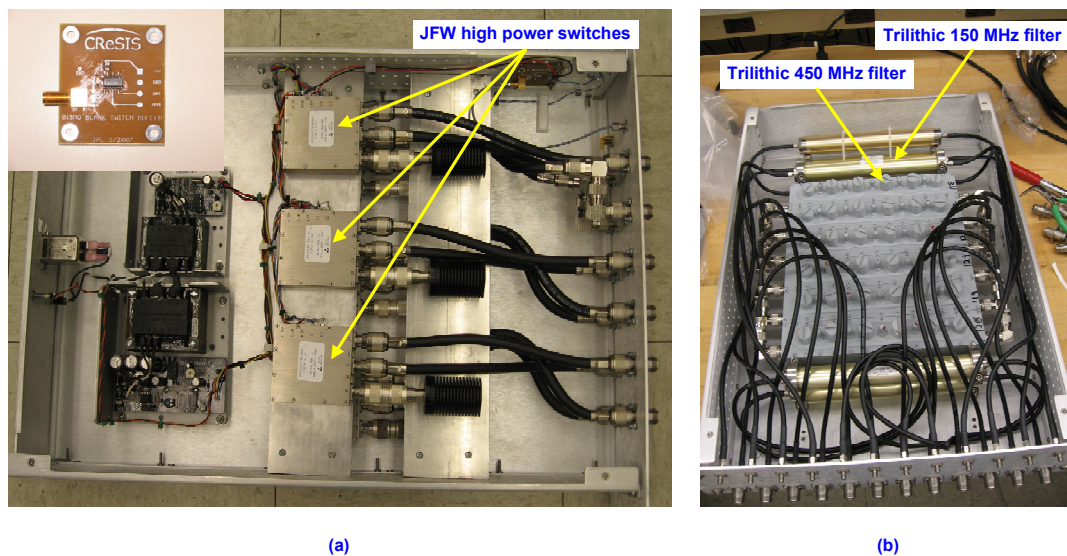


Figure 2.5. (a) High power blanking switches box with the switching logic circuit (top left) and (b) High power filter box

The output of the each high power filter goes in to each of the 6 receiver channels. The front-end project specific Miteq low noise amplifier (LNA) has a typical gain of 32 dB and a typical noise figure (NF) of 1.3 dB over the frequency range from 50 MHz to 500 MHz. It has a recovery time of approximately $0.5 \mu\text{s}$ if it enters in to saturation. Two low power ADG901 Analog Devices blanking switches provide an isolation of at least 74 dB in addition to the high power external blanking switch isolation. Thus the receiver output section is well protected from saturation and high power signals. The blanking switches receive the switching control and blanking duration information from the timing and control section. The values are set on the GUI by the user based on the pulse duration. There are two PE4308 Peregrine Semiconductor digital attenuators

each providing an attenuation ranging from 1.5 dB (insertion loss) up to 33 dB. The attenuators are used to set the 'low-gain' condition when the receiver receives strong surface returns and 'high-gain' setting for extremely weak ice-bed returns. The gain values are set on the GUI by the user based on the signal strength. The system has two amplifiers from Spectrum Microwave (TM6719) in the chain which are placed apart so that they do not saturate the next stages. The first amplifier after the LNA provides a gain of 33 dB and it is placed between digital attenuators to make sure that it is not saturated or that it does not saturate the next amplifier in the chain. The second amplifier provides an additional gain of 33 dB for the signal. It should be noted that a single amplifier with 66 dB gain is not used since the gain needs to be distributed along the receiver chain to have better NF and P1-dB values. Further, the P1-dB specification of amplifiers is not very high (+9 dBm) since the maximum non-saturating input to the data acquisition (DAQ) system following the receiver is +4 dBm. The last two Mini-Circuits M3SWA-2-50DR switches control the band by switching to the appropriate Lorch Microwave (similar parts as in transmitter) anti-aliasing bandpass filter based on the operating frequency. The switches receive the control from the timing and control section but they are initiated from the GUI by the user. As a matter of fact once the experiment has started the switches will be in a fixed position only, since there is no on-the-fly switching of bands during the experiment. Finally, at least 2 dB pads (higher value can be selected based on the system gain) are placed between most of the components throughout the receiver chain to minimize signal reflection and saturation. Amplifiers, switches and digital attenuators are the components which have saturation specifications and thus pads are required not to exceed their input power specifications.

2.3 System specifications

Table 2.1 lists the system specifications.

As discussed before, the radar operates at 2 frequency bands: 150 MHz and 450

Table 2.1. Specifications relating to radar system hardware

Radar Parameter	Parameter Value/Description
Radar type	Depth sounder/Interferometry
Number of transmitters	1 (VHF-band/P-Band)
Number of receiver channels	4 (depth sounder)/6 (interferometry)
RF carrier frequency	150 MHz (VHF-band)/450 MHz (P-band)
RF bandwidth	20 MHz (VHF-band)/30 MHz (P-band)
Transmit pulse duration	3 μ sec and 10 μ sec
Duty cycle	10%
Peak transmit power	800 W (VHF-band)/1600 W (P-band)
Pulse repetition frequency(PRF)	10 kHz
Receiver noise figure	2.14 dB
Loop sensitivity	208 dB
Range resolution in ice	2.8 m to 4.2 m
Sampling frequency	120 MHz
A/D dynamic range	12-bit, 72 dB
Antenna	8 half-wave dipoles

MHz. Systems designed and operating at 150 MHz are reported to be working and data were collected over various parts of Greenland during the field seasons between 2004 to 2006 [8] [11] [12]. Thus, 150 MHz frequency was selected to be used for the current experiment.

Selection of 450 MHz as the operating frequency was based on considerable research and analysis.

1. As reported in [12] the estimated basal power reflection coefficient (ratio of reflected to incident power) loss increases from 166.8 dB to 174.6 dB over the frequency range from 110 MHz to 500 MHz. This clearly shows that the loss variations are slightly dependent on the frequency but are small compared to the wideband of operation. Hence the natural choice was to be on the far end of this range which in the current design is 450 MHz (435 MHz to 465 MHz band), where the loss is about 172 dB compared to the loss at 150 MHz which is about 168 dB.
2. Another clear reason for choosing a higher frequency over lower frequencies is the antenna size reduction. This is an important factor considering that the system

will be transitioned to a spaceborne platform where antenna size is a major design constraint.

3. With reduced antenna size at high frequency (450 MHz), considering an example of using a phased dipole antenna array, the spacing between the elements is also reduced when compared to 150 MHz antenna array. Thus the baseline is reduced which results in using just 1 spacecraft for interferometry [13].
4. Finally, with higher center frequency the chirp bandwidth can be higher which improves range resolution, since range resolution is inversely proportional to signal bandwidth.

In spite of all these factors leading to selection of 450 MHz it is observed that at P-band frequencies the surface clutter is high [13] and hence a fall back system at 150 MHz which is a proven system is in place. To make the system clutter-free at 450 MHz novel clutter rejection algorithms can be developed and the discussion is beyond the scope of current thesis work.

The RF bandwidth for 150 MHz is selected to be 20 MHz (baseband 20 MHz to 40 MHz) and for 450 MHz as 30 MHz (baseband 15 MHz to 45 MHz). Selecting the system bandwidth is based on certain criteria.

1. The design uses narrow band chirp signals which implies narrow band filters and as a rule of thumb the 'fractional bandwidth' is selected to be $\leq 20\%$ [14]. The fractional bandwidth is defined as

$$\text{fractional bandwidth} = 100 \left(\frac{\text{chirp bandwidth}}{\text{carrier frequency}} \right) \quad (2.1)$$

For 150 MHz and 450 MHz the percentage bandwidth is approximately 13.34% and 6.67% respectively which is acceptable.

2. The chirp bandwidth is also based on the sampling rate of the DAC and the current system uses a DAC with a Nyquist frequency of 60 MHz. The usable

frequency not limited by the sinc roll-off effect is about 80% of the Nyquist rate implying that the far-end of the chirp can go up to 48 MHz [15].

3. The DAQ system used in the current radar operates with single sampling clock of 120 MHz. This removes the need for changing the clock rates (120 MHz or 420 MHz) when either of the 2 systems are operating (150 MHz or 450 MHz). But this requires that the chirp bandwidth be selected such that the received signal can be under-sampled with the same sampling clock at 120 MHz. Clearly 435 MHz to 465 MHz band falls in to the baseband spectrum of 15 MHz to 45 MHz due to aliasing when sampled at 120 MHz which is then detected.
4. The lower end of chirp bandwidth in the current system is limited by inherent spectral impurity of the AWG output which results in degraded signals below 5 MHz. This degradation has been observed during laboratory tests but no recorded results exist.

To image the ice surface and map the ice-bed with a dual-band radar system at varying altitudes (from 500 m up to 7000 m from the ice surface) requires certain amount of energy. Clearly at higher altitudes (7000 m) more energy is required to detect the weak ice-bed signals than at lower altitudes (500 m). A long duration pulse implies more energy impinged on the target which is required in the case of ice-bed detection where the signal losses are very high. Long pulse also implies degraded range resolution. A solution is to use a chirp signal with high bandwidth and pulse compress the received signal and thus achieve better resolution and additional pulse compression gain. Further, the pulse duration also specifies the duty cycle (ON time) for a selected PRF. The basis for selecting the pulse duration and the duty cycle is listed below.

1. The specifications for both Herley 3304C and Delta Sigma PEGASUS2000WP power amplifier suggest a maximum duty cycle of 10% and 20% respectively which implies that the maximum transmit pulse duration is restricted to less than 20 μ s

for a 100 μs pulse repetition time (PRT).

2. With PRT set to 100 μs for the current radar system, the transmitter is ON for certain period of the time (termed as 'duty cycle') and then it is OFF (receiver is ON) for the rest of the PRT. Figure 2.6 shows that the received pulse from the farthest target (basal echo at 20°) arrives at 87.6 μs [16]. To fully process the

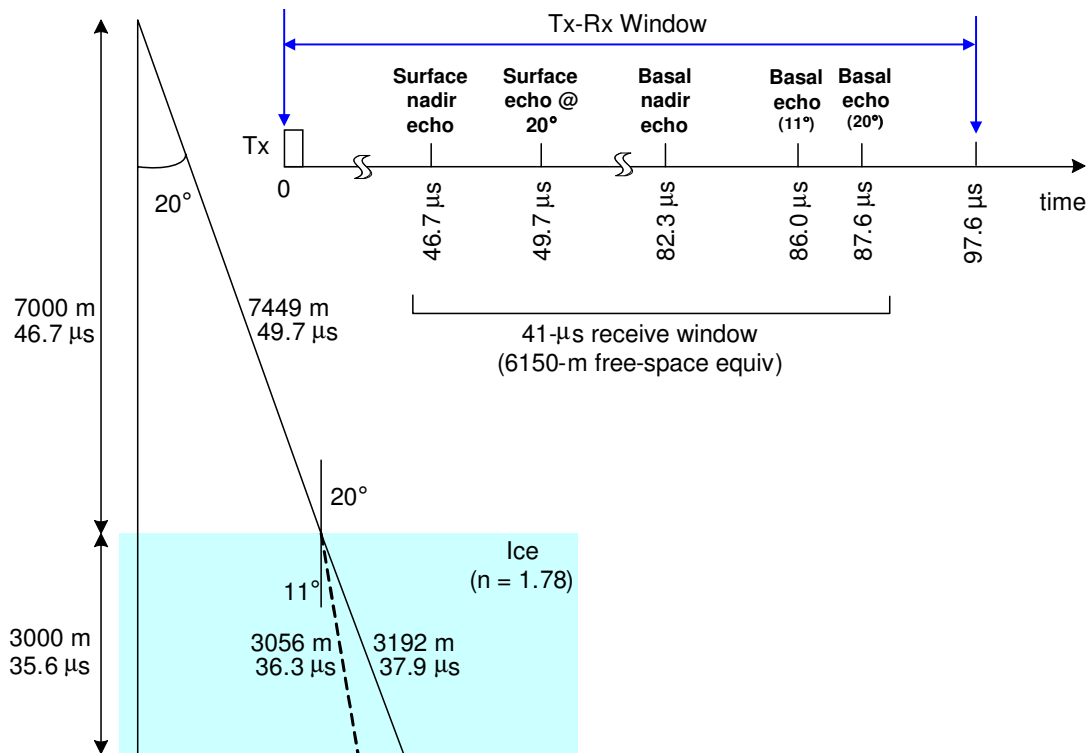


Figure 2.6. Pictorial representation of radar echo times

pulse, the pulse duration (if assumed to be 10 μs) needs to be added which results in a signal return time of 97.6 μs . It can be concluded that the pulse duration in fact cannot be beyond 12.4 μs theoretically so as to avoid running in to next transmit pulse. To be on the safer side the upper limit on pulse duration is set at

10 μs for the designed PRT. The equation for the calculation is given below.

$$\text{Tx-Rx Window} = 2 \left(\frac{\text{range in air}}{c} \right) + (2 * 1.78) \left(\frac{\text{range in ice}}{c} \right) + (\text{pulse duration}) \quad (2.2)$$

'c' is the velocity of an electromagnetic wave in air and pulse duration is the time for the pulse to fully engage with the target. The factor 1.78 is the refractive index for ice.

The explanation can be continued to calculate the minimum pulse duration which is based on the distance to the nearest target from minimum altitude. At 500 m above the ice surface the required pulse duration is 3.33 μs . Thus to account for the finite switching time of the blanking switches in the receiver section the pulse duration is set to 3 μs [8].

3. The switching time of the high power blanking switches is 10 μs [17]. With a longer pulse clearly there is a risk of damaging the receivers if the switches are turned ON (indicates receive mode) while the switches are still taking time to switch OFF (implies transmit mode). Hence a buffer time is required for the switches to completely reach the steady state condition.

The transmit power selection is based on the attenuation that the signal encounters as it passes through air and various layers of ice sheets. The transmit power should be sufficient to overcome these losses and the parameter which quantifies the fact is 'loop sensitivity'. As mentioned before, from the *insitu* measurements the loss at the ice-bed is determined to be 168 dB for a 3000 m thick ice at 150 MHz which the radar should be able to overcome and detect the signal.

2.4 RF system design

This section primarily describes the low power transmitter and low power receiver design with link budget calculations.

2.4.1 Low power transmitter design

The transmitter system parameters are mainly system gain, system saturation limits, sideband and carrier frequency suppression. The design of the transmitter system hence focuses on achieving the best values for these parameters.

As discussed in section 2.2.1 the P-band IQ modulator was developed in-house. The simulation of the IQ modulator on Agilent Advanced Design System (ADS) is depicted in figure 2.7 and a detailed schematic is shown in appendix A. The component parameter values used in the simulation are directly read off from the data sheet typical values. Modulator simulation is performed before proceeding towards schematic and PCB layout to validate the concept. Figure 2.8 shows the results for simulation. A single tone at 15

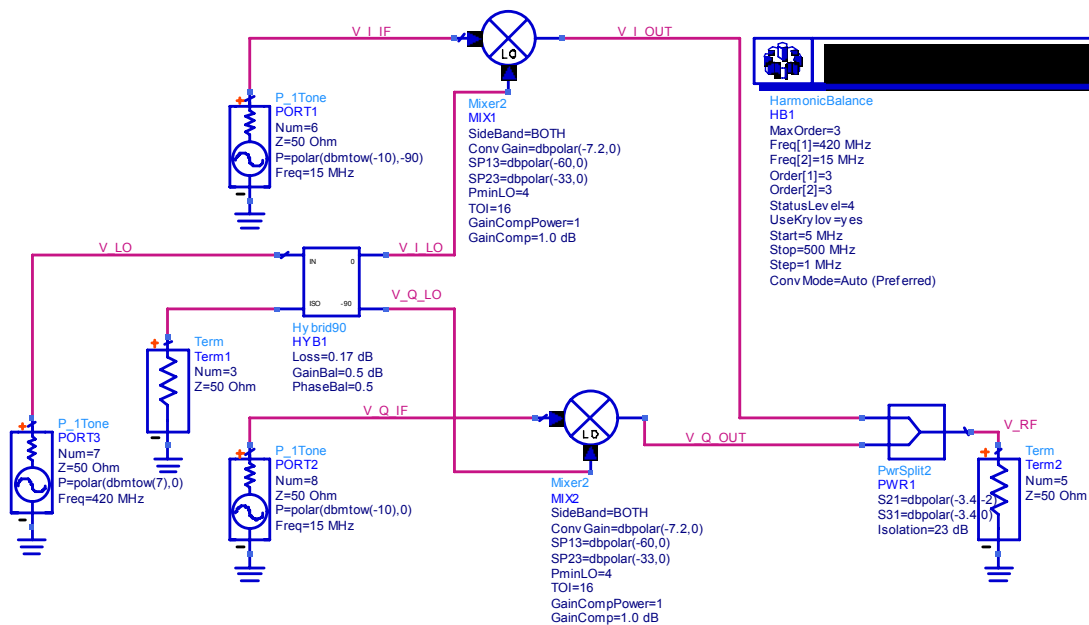


Figure 2.7. ADS harmonic balance simulation of P-band IQ modulator

MHz which is the lower edge of the baseband chirp for the 450 MHz system is selected since this lies very close to the LO (420 MHz) after up-conversion. The simulation gives a fair idea of the LO and sideband suppression which can be used as a reference for hardware implementation.

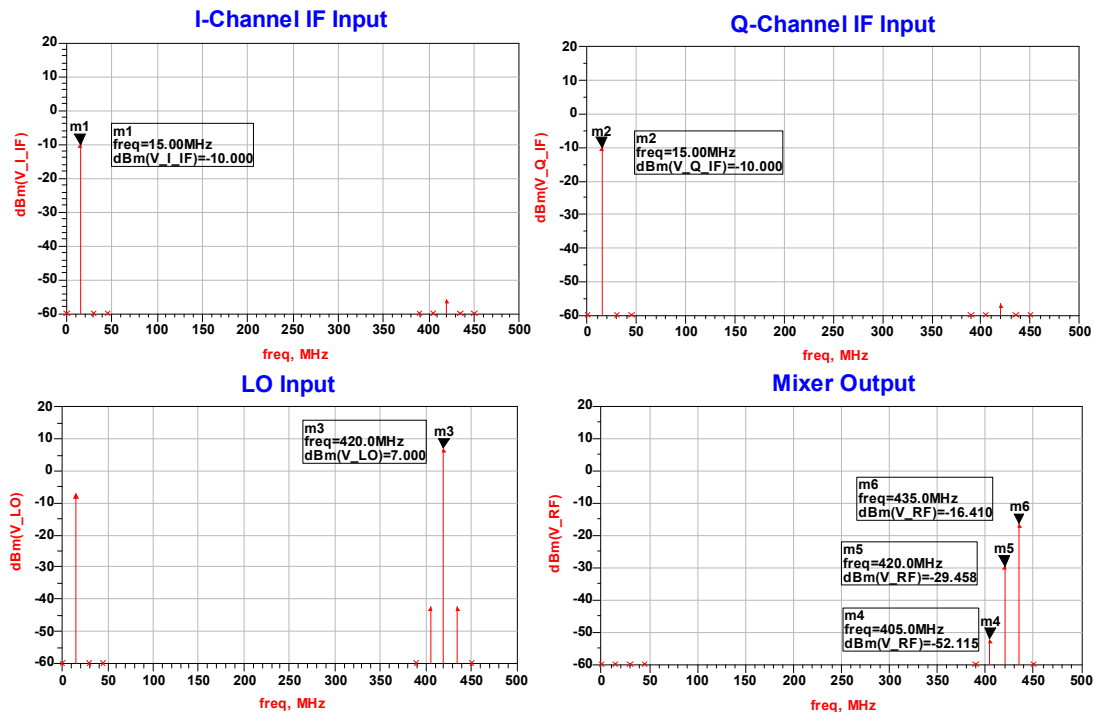


Figure 2.8. Simulated results of IQ modulator

It can be observed that the mixer has at least 13 dB LO suppression and 30 dB of sideband suppression with respect to the required upper sideband frequency (435 MHz).

The aim of transmitter link budget analysis is to verify that the input power to the transmitter is not high enough to saturate the system. Further, it provides an estimation of output power obtained from the low power transmitter before feeding in to the high power amplifier.

Tables 2.2, 2.3 and 2.4 are with reference to the block diagram 2.3.

From table 2.4 the maximum input power for high power amplifiers can be calculated to be -6 dBm (150 MHz) and 13 dBm (450 MHz). To operate the amplifiers in the linear region the input power is backed-off by at least 10 dB. Thus external attenuators are provided after the 3-dB power splitter just before the power amplifiers as shown in figure 2.3. The attenuators also serve as a way to reduce signal reflections in the transmitter path. The power values mentioned in the above tables are based on the

Table 2.2. Theoretical transmitter input section link budget for 150 MHz and 450 MHz systems

Device	Gain (dB) (150 MHz)	Gain (dB) (450 MHz)	P1-dB (dBm) (150 MHz)	P1-dB (dBm) (450 MHz)	Pin-sat (dBm) (150 MHz)	Pin-sat (dBm) (450 MHz)
LPF	-1.7	-1.7	–	–	–	–
Pad	-12	-12	–	–	–	–
Switch	-0.7	-0.7	20	20	33.7	33.7
Mixer	-8	-7.2	0	1	14.4	15.4
Hyb-90	–	-3.9	–	–	–	–
Pad	-12	-10	–	–	–	–

Table 2.3. Theoretical transmitter output section link budget for 150 MHz and 450 MHz systems

Device	Gain (dB) (150 MHz)	Gain (dB) (450 MHz)	P1-dB (dBm) (150 MHz)	P1-dB (dBm) (450 MHz)	Pin-sat (dBm) (150 MHz)	Pin-sat (dBm) (450 MHz)
Amplifier	27.5	27.5	22	22	-5.5	-5.5
Pad	-10	-2	–	–	–	–
BPF	-3	-3	–	–	–	–
Pad	-6	-8	–	–	–	–
Switch	-0.7	-0.7	20	20	11.5	5.5
Pad	-2	-2	–	–	–	–
Amplifier	27.5	27.5	22	22	-11.3	-11.3
Switch	-0.7	-0.7	20	20	-13.3	-19.3

Table 2.4. Theoretical transmitter system power budget for 150 MHz and 450 MHz systems

fc (MHz)	Baseband power (dBm)	Tx-in gain (dB)	Tx-out gain (dB)	PA gain (dB)	PA P1-dB (dBm)
150	0	-34.4	32.6	62	56
450	0	-35.5	38.6	50	63

data sheet specifications and the values obtained via actual s-parameter measurement are discussed in section 3.3.2. A close observation of table 2.3 reveals that the input power to the transmitter should be less than -13.3 dBm and -19.3 dBm for 150 MHz and 450 MHz systems respectively such that the final switch in the transmitter is not saturated.

2.4.2 Low power receiver design

The receiver section is designed to have a very low noise figure, high dynamic range and the ability to receive and detect the weak bed signals. Initially the link budget is discussed and the various receiver parameters are calculated.

The receiver link budget is detailed in table 2.5. This is with reference to block diagram 2.4.

Table 2.5. Theoretical receiver link budget for 150 MHz and 450 MHz systems

Device	Gain (dB)	P1-dB (dBm)	Pin-sat (dBm)	NF (dB)
External blank switch	-0.4	63	–	0.4
External BPF	-1	–	–	1
LNA	32	10	-20.6	1.4
Blank switch	-0.8	17	-13.6	0.8
Blank switch	-0.8	17	-12.8	0.8
Pad	-4	–	–	4
Digital attenuator	-1.5	24	-1	1.5
Pad	-4	–	–	4
Amplifier	33	9	-43.5	1.7
Pad	-4	–	–	4
Digital attenuator	-1.5	24	-24.5	1.5
Pad	-4	–	–	4
Amplifier	33	9	-67	1.7
Pad	-2	–	–	2
Switch	-0.7	20	-54	0.7
BPF	-3	–	–	3
Switch	-0.7	20	-50.3	0.7

The approximate noise factor (F) in linear units of cascaded 2 port devices can be

calculated by the standard Friss formula. Only the first 4 components (high power blanking switches, high power bandpass filters, LNA and the first low power blanking switch) are considered for the calculation and the approximate noise figure (NF) is 2.14 dB with standard temperature at 290 K.

The receiver minimum detectable signal (MDS) is determined to be

$$MDS(dBm) = 10\log_{10}(kT) + 10\log_{10}(BW) + NF - G_{PC} - G_{CI} + SNR_{min} \quad (2.3)$$

The pulse compression gain is calculated as $G_{PC} = BW * \text{pulse duration}$. For the 150 MHz system ($BW = 20$ MHz), with a $3 \mu\text{s}$ pulse, the pulse compression gain (G_{PC}) is 17.78 dB and with 32 coherent integrations of the received signal the coherent integration gain (G_{CI}) is 15 dB. 'k' is the standard Boltzmann's constant and $T = 290$ K is the reference temperature. If SNR_{min} is 0 dB, then it is termed as MDS and the value is -131.6 dBm. If SNR_{min} is considered to be 13 dB for interferometric synthetic aperture radar (SAR) [18], then it is termed as sensitivity ($SNR_{min} \neq 0$) and the resulting value is -118.6 dBm. Similar calculations for the 450 MHz case with 30 MHz bandwidth results in same MDS and sensitivity values indicating the importance of pulse compression, which accounts for extra gain which is lost due to more noise entering the system when the bandwidth is increased.

From table 2.5, the receiver theoretical input saturation power is noted to be -67 dBm and to ensure that the system is operating in the linear region the power is backed-off to -75 dBm. The theoretical dynamic range of the receiver is 64.6 dB (Pin-sat - MDS).

The output of the RF receiver section is fed in to the DAQ system. The DAQ system has an input damage power rated at +15 dBm, clips any input power above +4 dBm and the noise floor noted to be approximately -58 dBm [8]. To avoid DAQ system saturation, the expected input power to the DAQ system is restricted between 0 dBm and -50 dBm by suitable setting of the digital attenuators on the receiver.

Radar loop sensitivity can be defined as the total loss that the signal can incur

after it has been transmitted and yet be detected and demodulated successfully by the receiver [8]. The total radar loop sensitivity is calculated to be:

$$LS(dB) = 10\log_{10}(P_T) - 10\log_{10}(kT) - 30 - 10\log_{10}(BW * F) + G_{PC} + G_{CI} + G_{TX} + G_{RX} \quad (2.4)$$

For 150 MHz system ($BW = 20$ MHz) with a peak transmit power (P_T) of 800 W and with antenna gains (G_{TX} and G_{RX}) of ~ 8.6 dB the loop sensitivity is 208 dB. For the 450 MHz system ($BW = 30$ MHz) with a peak transmit power (P_T) of 1600 W and with antenna gains (G_{TX} and G_{RX}) of ~ 8.6 dB the loop sensitivity is similar to 150 MHz case.

2.5 Antenna sub-system

Two 4-element half-wave length dipole antenna arrays are used for both transmission and reception. Initially, a feasibility study of using the existing antenna array developed for the 150 MHz system for operation at 450 MHz was investigated and issues were reported due to non consistent antenna dimensions [19]. Clearly a 3 times increase in frequency from 150 MHz to 450 MHz corresponds to wavelength reduction of 3. The antenna array spacing is approximately 1 m, which is half-wavelength at 150 MHz but it is 1.5 times the half wavelength at 450 MHz as shown in figure 2.9. Even though suitable length dipole elements can be designed for the 450 MHz system, the spacing between the elements and the spacing between the wing (ground plane) and the dipole array is still suitable for the 150 MHz operation, which was a design constraint. This is due to the fact that the antenna array mounted underneath the wings of the NASA P-3 aircraft has holes drilled at spacing suited for the 150 MHz frequency. Further, the spacing between the wing of the aircraft and the dipole antenna array are also fixed mechanical structures suited for the 150 MHz operation. Figure 2.9.(a) depicts the antenna structure at 450 MHz where the distance between dipoles is expected to be ~ 0.3 m but in reality it is ~ 1 m which is half-wave length at 150 MHz.

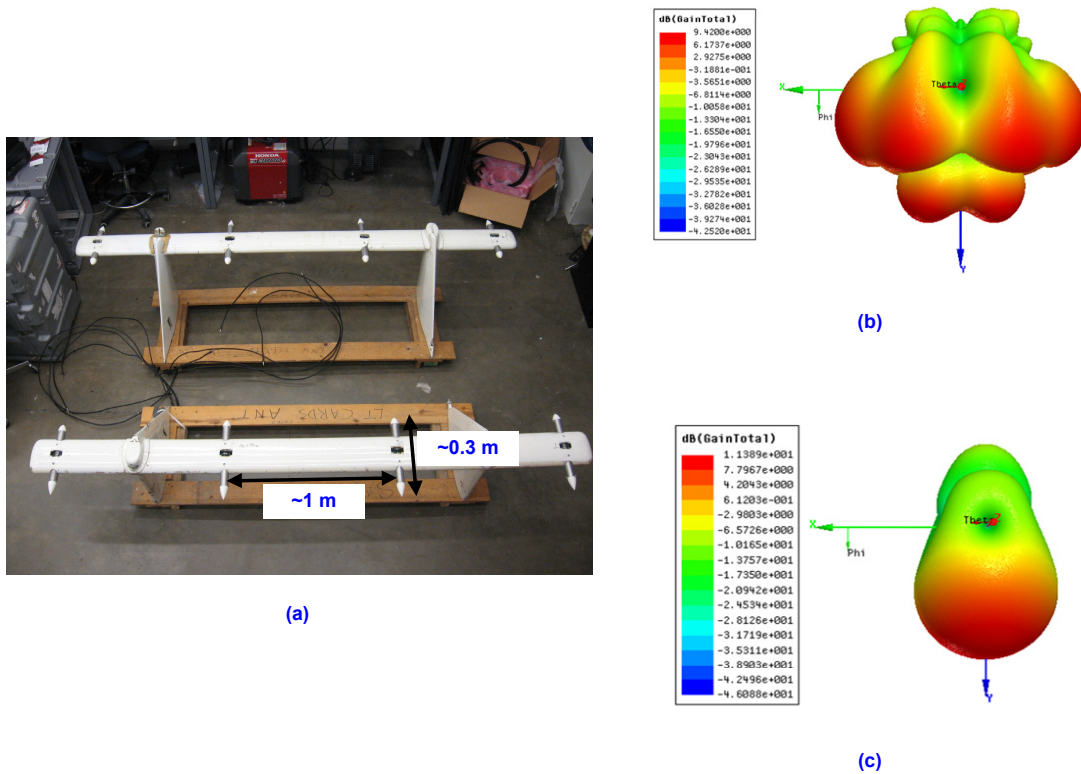


Figure 2.9. (a) Antenna array at 450 MHz. 3-D antenna simulation results in high frequency structure simulator (HFSS) software for (b) 450 MHz system and (c) 150 MHz system.

Since the spacing between the elements is greater than half-wavelength at the center frequency of 450 MHz, multiple lobes of the same magnitude as the main lobe called 'grating lobes' are formed. Figure 2.9.(b) illustrates the grating lobes at 450 MHz and 2.9.(c) the antenna pattern with pronounced main lobe which is the desired condition in the case of 150 MHz [19].

Clearly with grating lobes the radiation pattern is worse at 450 MHz compared to 150 MHz. In the final design, modified dipoles of half-wave length at 450 MHz were constructed. Further, careful antenna balun tuning was performed to achieve better performance in terms of antenna gain pattern. With all these modifications, the s-parameter measurements of the antenna array at both 150 MHz and 450 MHz yielded a return loss of at least 10 dB which is an acceptable value [20].

Finally, from figure 2.3 it can be observed that for the 150 MHz, depth sounder configuration, an antenna feed network is used to distribute the transmit signal from the power amplifiers into 4 dipole elements for transmission. The power into each antenna element is based on the Dolph-Chebyshev weighting to obtain low (< 30 dB) side-lobes at 60° to 80° incidence angle [21] of the transmit signal on the target. Figure 2.10 shows the antenna feed network used in this case.

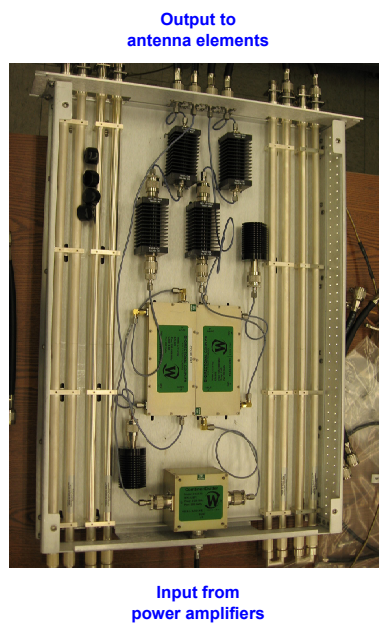


Figure 2.10. Antenna feed network used in the depth sounder mode

2.6 Digital system and radar software

The digital system has numerous modules and explanation of every module is beyond the scope of current work and only a brief account is given here. The digital system has a waveform generator card to generate the chirp signals and a data acquisition card to record the received signal. The waveform creation is done by a dual channel 16-bit 160 mega samples per second (MSPS) AWG Card and a single channel 10-bit 1 giga sample per second (GSPS) direct digital synthesizer (DDS) Card. The data acquisition is done by a dual channel 12-bit 160 MSPS DAQ card. All the cards are of same form

factors. These cards are plugged onto carrier cards which are then plugged into a cPCI slot. Each carrier card can hold two plug-on cards. Different combinations of plug-on cards can be placed on multiple carrier cards to make up the desired data system [22].

The current system has a sampling rate of 120 MHz for both 150 MHz and 450 MHz systems. The under-sampling concept as depicted in figure 2.11, is employed to recover the baseband chirp signal of 20 MHz to 40 MHz (150 MHz system) and 15 MHz to 45 MHz (450 MHz system).

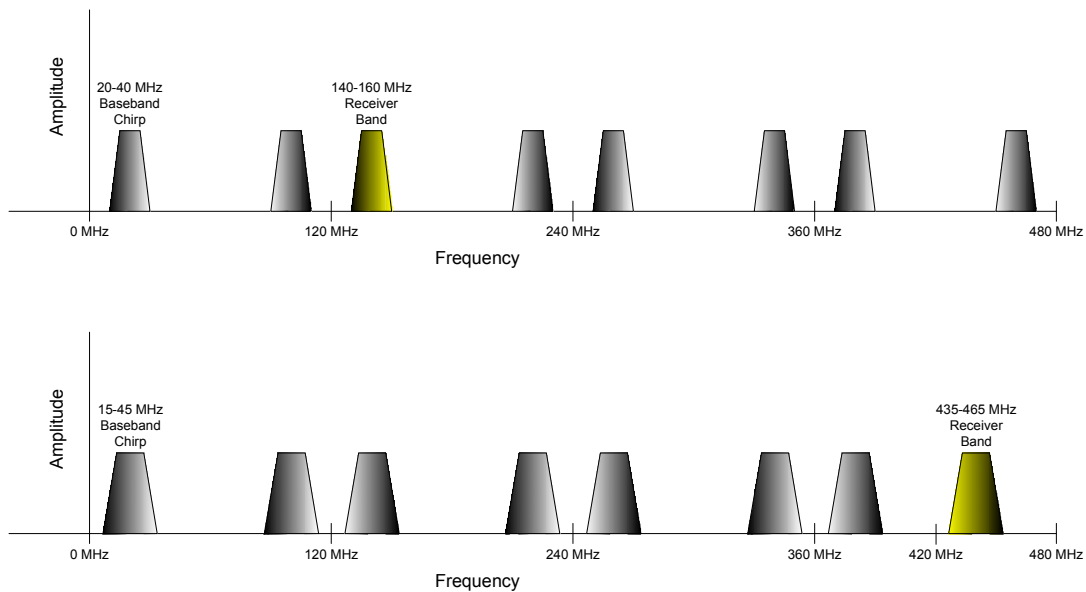


Figure 2.11. Pictorial representation of under-sampling concept

The system has an on-board computer, which hosts the CentOS operating system and loaded programs for GUI, waveform generation and signal processing. An X-server based custom-designed GUI is used for setting the various radar and global positioning system (GPS) parameters and viewing the real-time results during the field experiments. A detailed user manual for the system is created briefing the GUI usage [23].

2.7 Fabrication

The theoretical RF system design as outlined in previous sections is later realized in hardware via PCB manufacturing and assembly. Suitable components are selected to implement the hardware which result in achieving the parameters calculated theoretically. Figures 2.12 and 2.13 show the fabricated and assembled RF transmitter and receiver circuits respectively. The circuit schematic, PCB design and layout is done on Altium Designer 6 with SP3 (also formerly called Protel) and then outsourced for PCB manufacturing. The manufactured PCBs are thoroughly inspected and then followed by component assembly and testing at the CReSIS state-of-art facility. The assembled transmitter and receiver PCBs are installed in the aluminum chassis as shown. Further, power supply and control signals are provided from the backplane of the system. Note the data cable in figure 2.13 for programming the Xilinx complex programmable logic device (CPLD). This device is used to control the blanking switches, band control and the digital attenuators and thus the values are programmable by the user.

Figure 2.14 depicts the ports of the transmitter and receiver chassis. The frequency synthesizer section requires a 10 MHz clock signal from the common system clock. The transmitter chassis has external ports to tap the 120 MHz and 420 MHz LO frequencies for other applications. The 150 MHz and 450 MHz mixers receive their LO inputs internal to the chassis as shown in figure 2.12. The 120 MHz LO to the AWG requires a 5 dB external pad inserted at the port before being connected to the LO port of the AWG chassis (not shown). Further, the 2 frequency synthesizer LEDs indicate the proper operation by signalling that the phase locked loop (PLL) is locked on to the required LO frequency. On the receiver, two columns of LEDs indicate the 5-bit digital attenuator value which is set through the GUI. The rotary switch is used to set a unique identifiable value between 0 to 9 manually for the receivers. As an example receiver 6 and receiver 7 are shown with the values set through the switch.

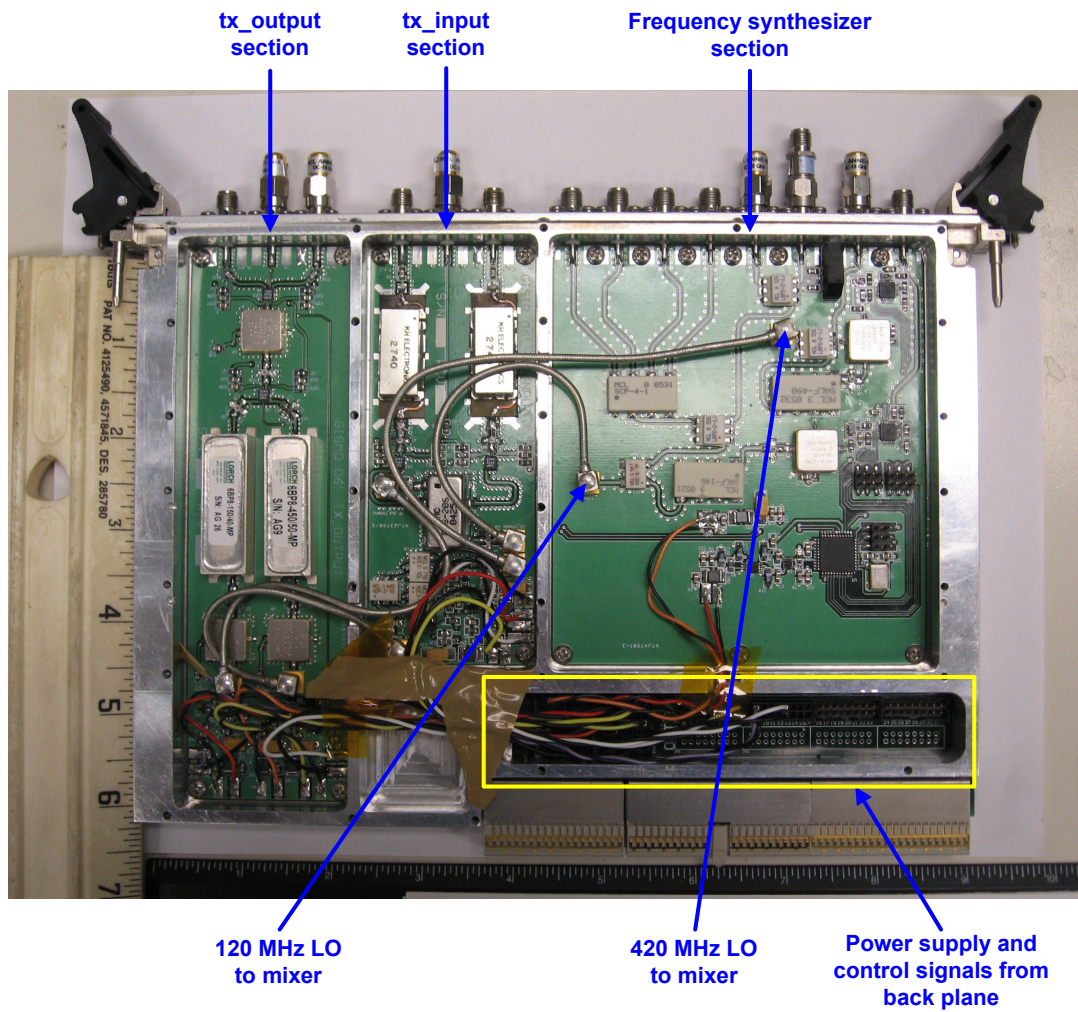


Figure 2.12. Aluminum chassis with frequency synthesizer, input and output transmitter sections

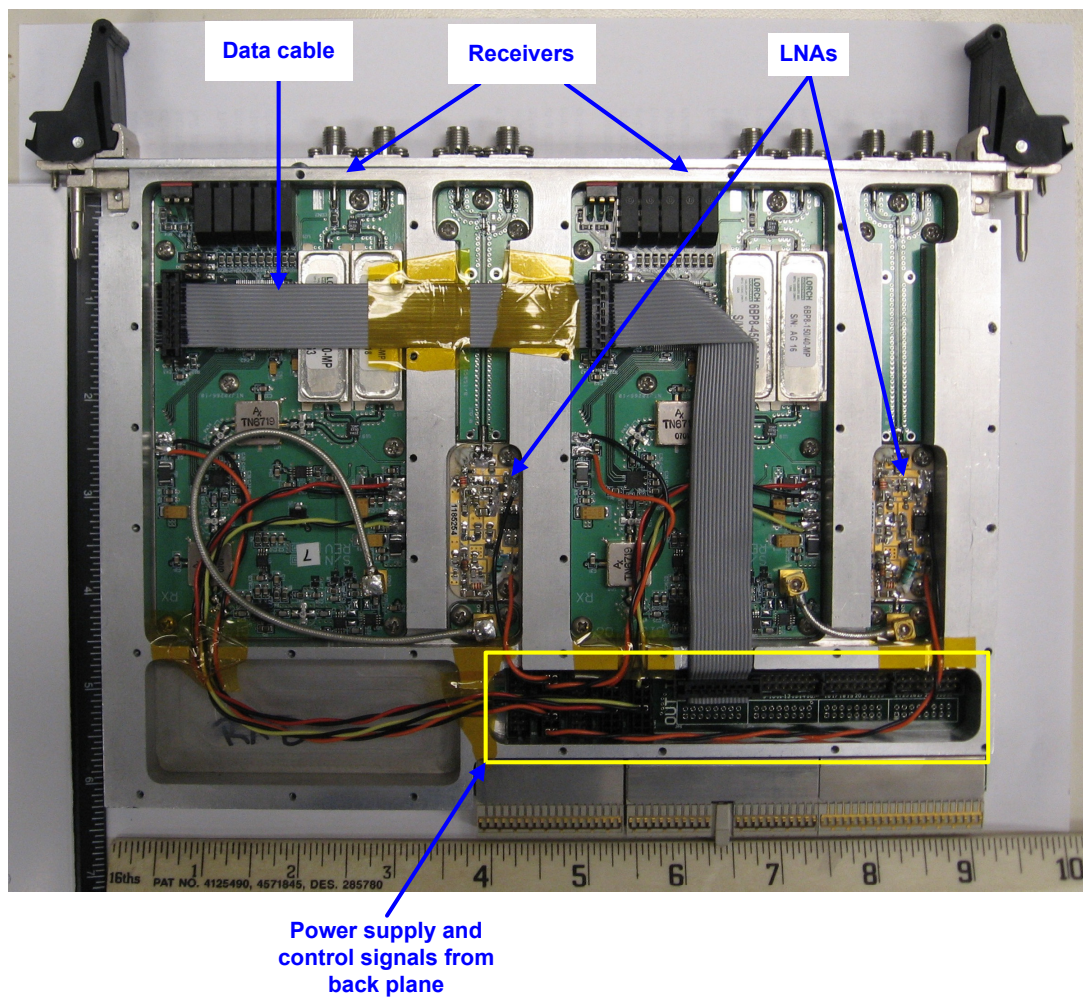


Figure 2.13. Aluminum chassis with 2 receiver channels and data cable for programming the Xilinx CPLD

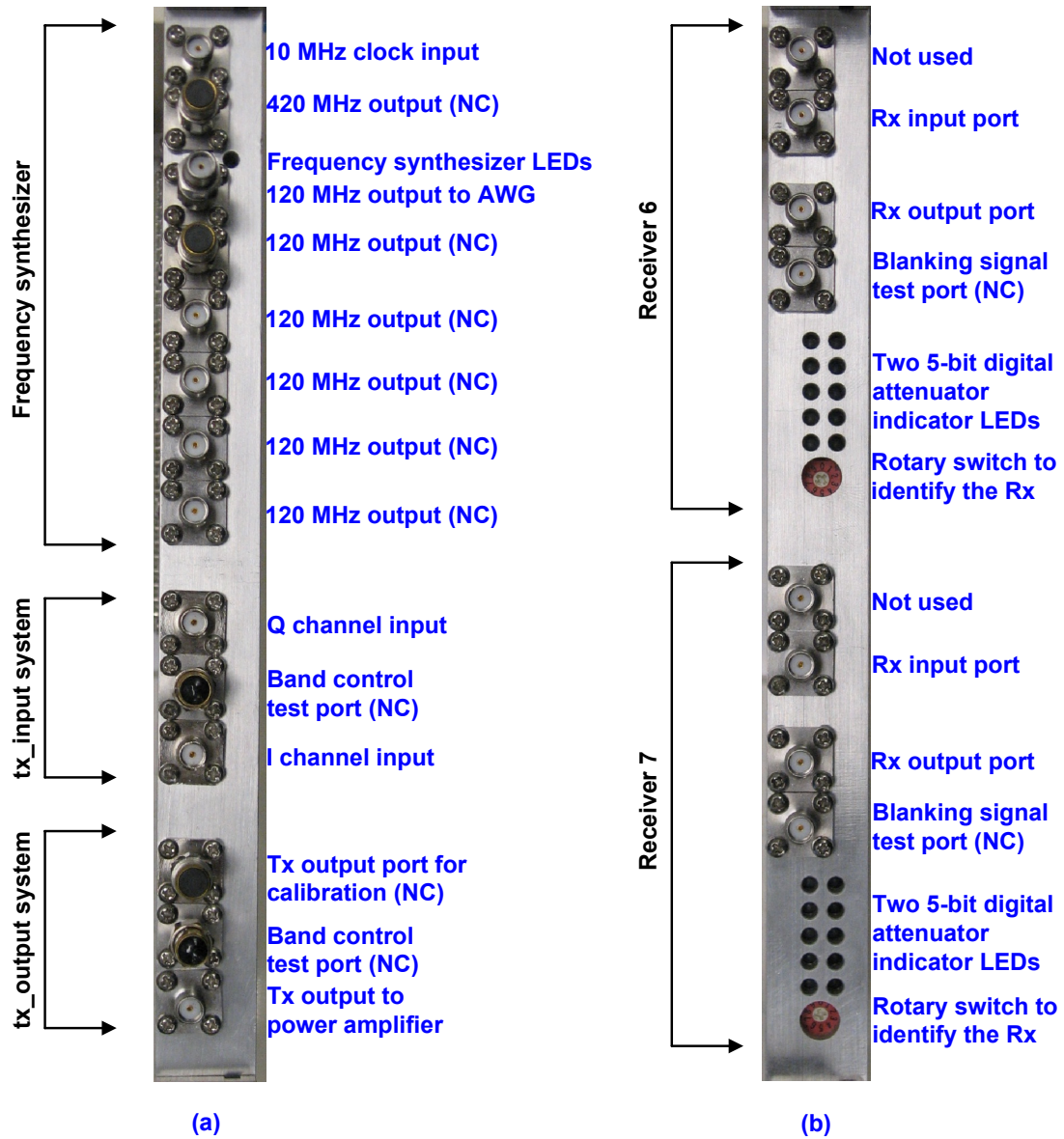


Figure 2.14. (a) Transmitter chassis ports (b) Receiver chassis ports

Chapter 3

Laboratory Testing and Results

This chapter discusses various tests performed in order to validate the proper functionality and performance of the sub-systems developed in this thesis. The different laboratory set-ups employed are described.

A detailed list of equipment required and complete system testing procedure can be found in the project test plan document [24].

3.1 Receiver testing

The receiver testing was performed to verify the following important parameters: receiver gain, input/output return loss, noise figure and P1-dB compression point. All the measurements are completed in a 50 ohm system. The receiver boards were tested for the parameters as listed in table 3.1

Table 3.1. Receiver test parameters

Parameter	Condition/Description
Full 2-port s-parameters	System gain ($ S_{21}(\omega) ^2$), Reverse isolation ($ S_{12}(\omega) ^2$), Input return loss ($ S_{11}(\omega) ^2$), Output return loss ($ S_{22}(\omega) ^2$)
Receiver selection	Ranging between 0 to 5
Band control	150 MHz or 450 MHz
Digital attenuation	Up to 31 dB in steps of 1 dB
Blanking control	ON or OFF

Receiver selection control enables to set any specific parameters (gain, blanking duration) to a particular receiver based on the experiment conditions. Since there are maximum of 6 receivers in the system the identifier values range from 0 through 5. Blanking ON implies that the receivers are blanked and they provide high isolation for any input signal and OFF indicates the opposite scenario.

The following section provides the testing procedure and results for a full 2-port s-parameter measurement analysis.

3.1.1 S-parameter measurement

In order to validate the design, the transmitter and receiver modules were tested both outside the chassis and inside the chassis as an integrated system. Even though most of the procedure holds good for testing either the transmitter or the receiver, there are few differences which are highlighted appropriately.

It is necessary to perform the test outside the chassis to verify that the board was indeed working before integrating with other sub-systems. The receiver PCB is controlled by a laptop computer and a network analyzer (Agilent 8753D) is used to perform the s-parameter measurement.

Figure 3.1.(a) shows the general block diagram for testing either a transmitter or receiver external to the chassis. As an example, the receiver PCB with the multi-pin receiver test cable with a 8x2 header connected is shown to demonstrate the test set-up in figure 3.1.(b). The detailed color combination and the corresponding Matlab code can be located in the appendix B.

Similar procedure holds good for the transmitter testing. But the major difference is that only the transmitter output section is subjected to full 2-port s-parameter analysis since the input section has a frequency up-conversion device which is a 4 port (LO, RF, I and Q inputs) circuit. Further, both input and output sections are tested for the band control operation manually by inserting or removing the jumper connection on the board. Hence for the transmitter analysis, there does not exist a multi-pin test cable in

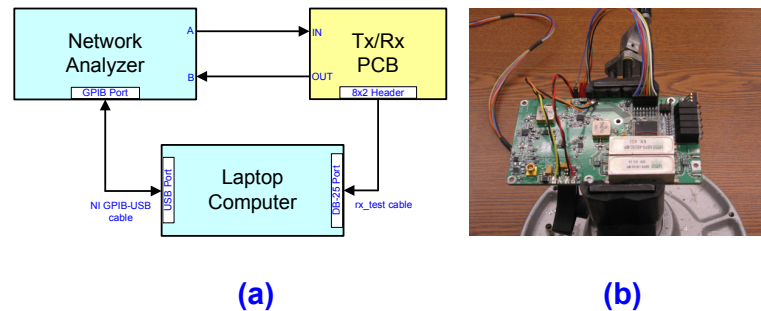


Figure 3.1. Preliminary receiver validation outside the chassis

the loop which is used in the receiver.

Figure 3.2.(a) shows the general block diagram for testing the transmitter or receiver internal to the aluminum chassis. As an example the transmitter chassis inserted in to

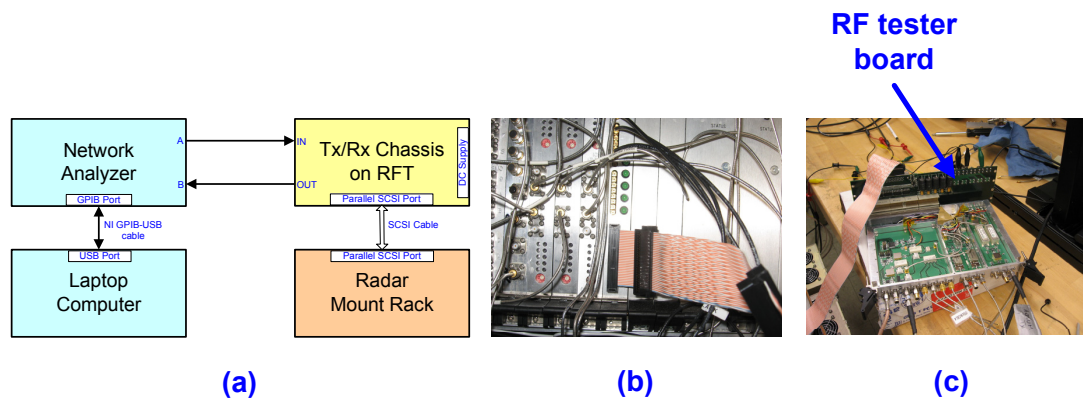


Figure 3.2. Transmitter validation using a RF tested board

the RF tester board is shown in figure 3.2.(c) and the same set-up holds good for the receiver. One end of the small computer system interface (SCSI) cable is connected to the RF tester board and the other end to the timing front panel on the radar rack (3.2.(b)). Power supply is provided to the RF tester board externally. The user has same level of control as before but now exercised through the radar GUI and thus the laptop computer controls only the network analyzer. In this procedure the complete parameter setting is done from the radar GUI and no manual intervention (jumper replacement) is required. Finally, as mentioned before, only the transmitter output section can be

subjected to a full 2-port s-parameter analysis. A detailed discussion on transmitter test results and analysis is covered in section 3.3.

Wherever a laptop computer is used to control the system, the data is stored as s-parameter .mat files using the matlab program listed in the appendix B. Sample results for the receiver channel 0 for 150 MHz and 450 MHz systems are shown in figure 3.3. For both systems, the measured system gain is approximately 50 dB and a minimum return loss of 15 dB. Similar results are expected for 5 other receiver channels. The receiver settings are given in table 3.2 relating to the results shown in figure 3.3.

Table 3.2. Receiver settings for the s-parameter measurements of 150 MHz and 450 MHz systems

Parameter	Value
Receiver selection	0
Band control	150 MHz or 450 MHz
Digital attenuator 1	10 dB
Digital attenuator 2	10 dB
Blanking control	OFF
Input power	-50 dBm

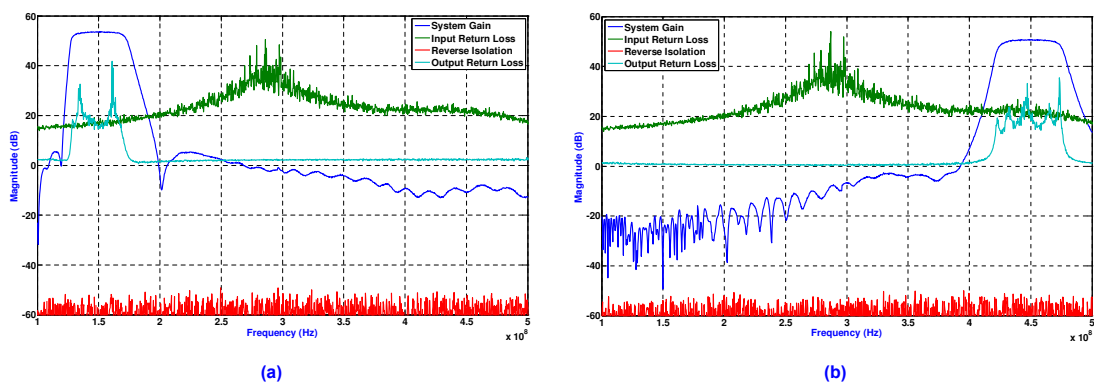


Figure 3.3. Measured s-parameters for receiver channel 0 for (a) 150 MHz system and (b) 450 MHz system

3.1.2 Noise floor measurements

The minimum detectable signal or the weakest signal that the receiver can detect intelligibly is limited by the noise floor of the receiver system. Noise in this case is

internally generated due to the electronic components used for implementation. A spectrum analyzer can be used to measure the noise floor of the receiver, but it should be noted that the the analyzer is also a receiver and thus inherently limited by its own noise. The first step is to measure the noise floor of the spectrum analyzer (Agilent E4407B in this case) and verify that it is sufficiently low so as to detect the receiver noise floor.

The noise power displayed on the analyzer corresponds to the effective noise power. To determine the noise floor, the noise power is normalized to 1 Hz bandwidth. The noise floor of the receiver was experimentally determined on the spectrum analyzer. Table 3.3 summarizes the measured noise floor values for the spectrum analyzer and the receiver channel 0 both for 150 MHz and 450 MHz systems. The other 5 receiver channels are expected to have comparable results. Figure 3.4 shows the recorded noise power spectrum of the spectrum analyzer and the 150 MHz and 450 MHz receiver systems.

Table 3.3. Measured noise floor values with noise power normalized to 1 Hz bandwidth

System	Noise Floor (dBm/Hz)
Spectrum analyzer	-137.37
150 MHz receiver	-118.39
450 MHz receiver	-116.30

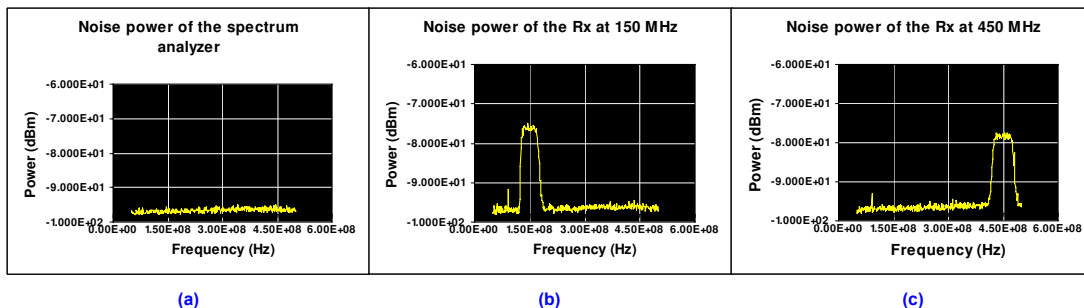


Figure 3.4. Measured effective noise power spectrum of (a) Spectrum analyzer (b) Receiver at 150 MHz and (c) Receiver at 450 MHz

3.1.3 Receiver noise figure measurements

Noise figure is an important receiver parameter and not much of the concern for the transmitter since transmitter operates generally at very high powers than compared to the noise power.

The noise figure measurements were performed using the standard Y-factor technique, which involves measuring the change in output noise power when two different known noise power levels are injected at the input of the receiver. In this case the two noise power levels are provided by a matched load at two significantly different temperatures: room temperature (290 K) and temperature of liquid nitrogen (77 K).

To measure the receiver output noise power at room temperature, firstly, the receiver input is terminated with a 50 ohm load and the output is connected to the power meter and the 'hot' noise power value is recorded. Next, the input termination is completely immersed in liquid nitrogen and now the 'cold' output noise power is recorded. The difference gives the relative noise power which can be used to calculate the corresponding noise figure values.

Consider a receiver specified by gain (G) and bandwidth (BW). Let the input noise temperature (T_{in}) and output noise power (N_o) be identified. Let T_e be the equivalent noise temperature of the receiver and k , the standard Boltzmann's constant.

$$T_{out} = G(T_{in} + T_e) \quad (3.1)$$

$$T_e = (F - 1)T_o \quad (3.2)$$

where T_{out} is obtained when T_{in} is 290 K (hot measurement) or when T_{in} is 77 K (cold measurement). F is the noise figure in linear units. The total noise power generated by the amplifier and from the input termination is

$$N_o = GkBW(T_{in} + T_e) \quad (3.3)$$

The Y-factor is defined as

$$Y = \frac{N_o|_{T_{in} = T_{hot}}}{N_o|_{T_{in} = T_{cold}}} = \frac{T_{hot} + T_e}{T_{cold} + T_e} > 1 \quad (3.4)$$

Solving for T_e ,

$$T_e = \frac{T_{cold} - YT_{hot}}{Y - 1} \quad (3.5)$$

$$F = \frac{T_o}{T_e} + 1 \quad (3.6)$$

where T_o is 290 K and noise figure in dB is

$$NF = 10\log_{10}(F) \quad (3.7)$$

Table 3.4 shows the values measured from the Y-factor method and calculated using the above equations for 2 receiver channels both for 150 MHz and 450 MHz systems. Similar results are expected from other 4 receiver channels.

Table 3.4. Measured and calculated noise figure values for 2 receiver channels both for 150 MHz and 450 MHz systems

Rx system frequency (MHz)	BW (MHz)	Hot power (dBm)	Relative power (dBm)	NF measured (dB)	NF calculated (dB)
150 (Rx 0)	40	-22.60	-2.32	2.5	2.49
450 (Rx 0)	50	-25.27	-1.82	3.3	3.31
150 (Rx 4)	40	-22.40	-2.33	2.5	2.47
450 (Rx 4)	50	-24.76	-1.81	3.3	3.35

3.1.4 Compression point measurements

The P1-dB compression point of a receiver is defined as the particular input power at which the output power is 1 dB less than the ideal linear 2-port output. The compression point of the receiver is calculated by providing known input power signal to the receiver and recording the output power on a spectrum analyzer. From table 2.5 in section

2.4.2, the minimum theoretical input power to saturate the receiver is -67 dBm. For the following measurements a range of input powers from -80 dBm to -50 dBm in steps of 2 dBm was provided. Further, the maximum input power to the receiver is set well below +30 dBm, which is the maximum safe continuous wave (CW) input power to the LNA. The input test signal is a single tone at 150 MHz for the lower operating band of the radar and 450 MHz signal for the 450 MHz system. Finally, the test conditions included 0 dB attenuation for both digital attenuators and blanking switch in OFF state. Figure 3.5 depicts the approximate 1 dB compression points for the receiver channel 0. The input and output P1-dB points for the 150 MHz system are -68 dBm and 1.5 dBm respectively. The input and output P1-dB points for the 450 MHz system are -64 dBm and 1.1 dBm respectively. Exact P1-dB points were not noted due to the measurement resolution and they are interpolated from the above graphs. Similar results are expected for the other receiver channels.

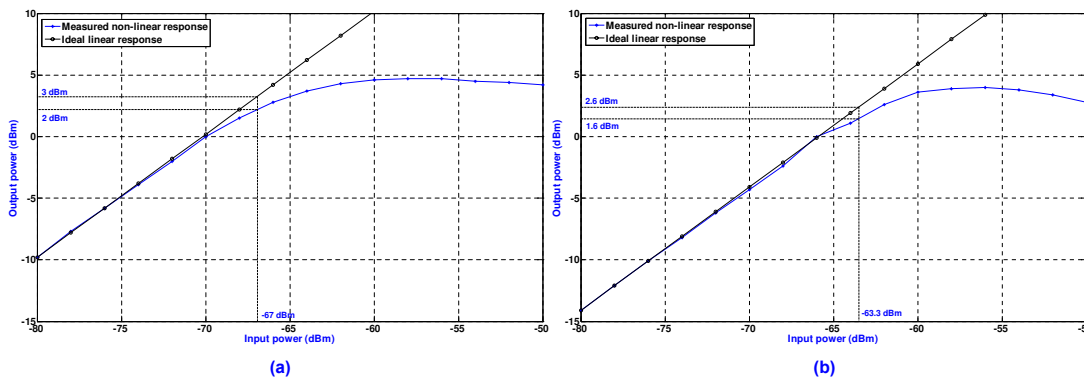


Figure 3.5. Measured compression point values for receiver channel 0 at (a) 150 MHz and (b) 450 MHz

3.2 Arbitrary waveform generation spectra

Prior to the actual testing of RF transmitter section, the spectral characteristics of the baseband signal were determined. For this purpose, the spectrum analyzer was used to record the spectra of waveforms generated in the digital sub-system. The I channel output from AWG at 0 dBm is fed in to the spectrum analyzer for analysis.

Typical parameters are 150MHz with 20 MHz bandwidth (20 MHz to 40 MHz) and 450 MHz with 30 MHz bandwidth (15 MHz to 45 MHz). The output is recorded using a laptop computer with the IntuiLink utility from Agilent Technologies which can capture the spectrum analyzer results on a Microsoft Excel spread sheet. Figure 3.6 shows the the 20 MHz and 30 MHz bandwidth chirp signals captured on the Agilent spectrum analyzer E4407B. As observed, these chirp waveforms are accompanied by harmonics which if not suppressed will leak in to the transmitter. Thus, the first device on the transmitter is an anti-imaging low pass filter to remove these high frequency unwanted signals. Alternatively this experiment is also repeated for the Q channel and similar results were observed.

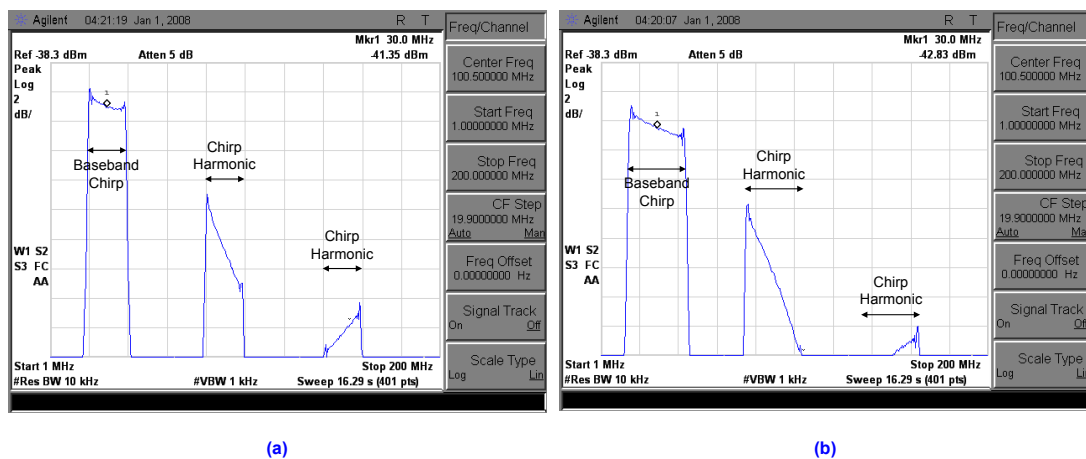


Figure 3.6. Measured AWG output spectrum with (a) 20 MHz bandwidth and (b) 30 MHz bandwidth

An important observation is that the chirp signals have an amplitude droop as the chirp sweeps from low to high frequency due to the sinc frequency roll-off effect. The output signal amplitude is affected by a *sinc* function [15] resulting in an amplitude which is frequency dependent. To overcome the problem of amplitude imbalance over the chirp bandwidth the input signal is pre-distorted such that it is precompensated for the roll-off effect during sampling. Figures 3.7.(b) and 3.8.(b) show the pre-distorted waveforms.

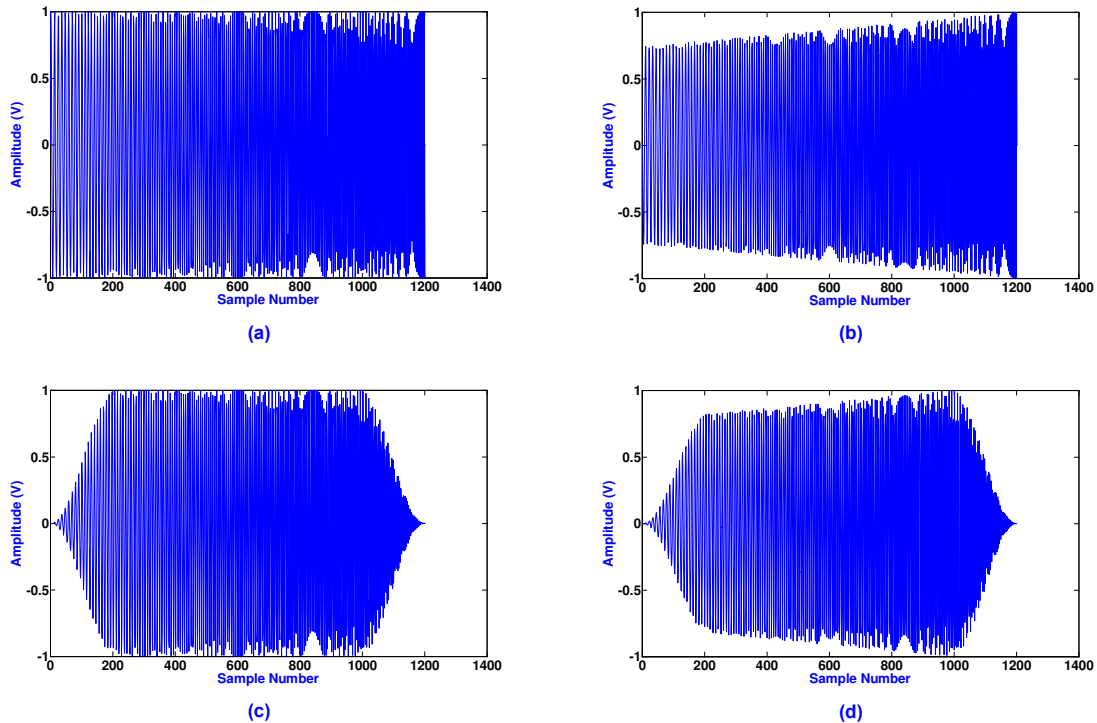


Figure 3.7. Simulated time domain 10 MHz to 30 MHz chirp signal: (a) Ideal rectangular chirp (b) Pre-distorted chirp (c) Amplitude tapered chirp (d) Pre-distorted and amplitude tapered chirp

Another effect in time domain is the Gibb's phenomenon which occurs when a chirp waveform is tapered (window operation) abruptly to produce a time domain rectangular pulse. Thus at the band edges, ringing effects can be observed which manifests as rapidly varying amplitude in frequency domain (3.8.(a)). To overcome the problem, the chirp signal is amplitude tapered (3.7.(c)), such that the skirts in time domain are smooth transitions from high to low amplitude which results in reduced ringing effects (3.8.(c)). Tapering the waveform has the advantage of reduced range side lobes after pulse compression and thus better signal to clutter ratio.

It should be noted that, amplitude tapering the waveform by applying a window involves penalty in terms of bandwidth. It has been observed that for a chirp with 30 MHz bandwidth and a 0.35 factor weighting in time domain reduces the bandwidth by 4% [25] which deteriorates the radar range resolution since range resolution is inversely

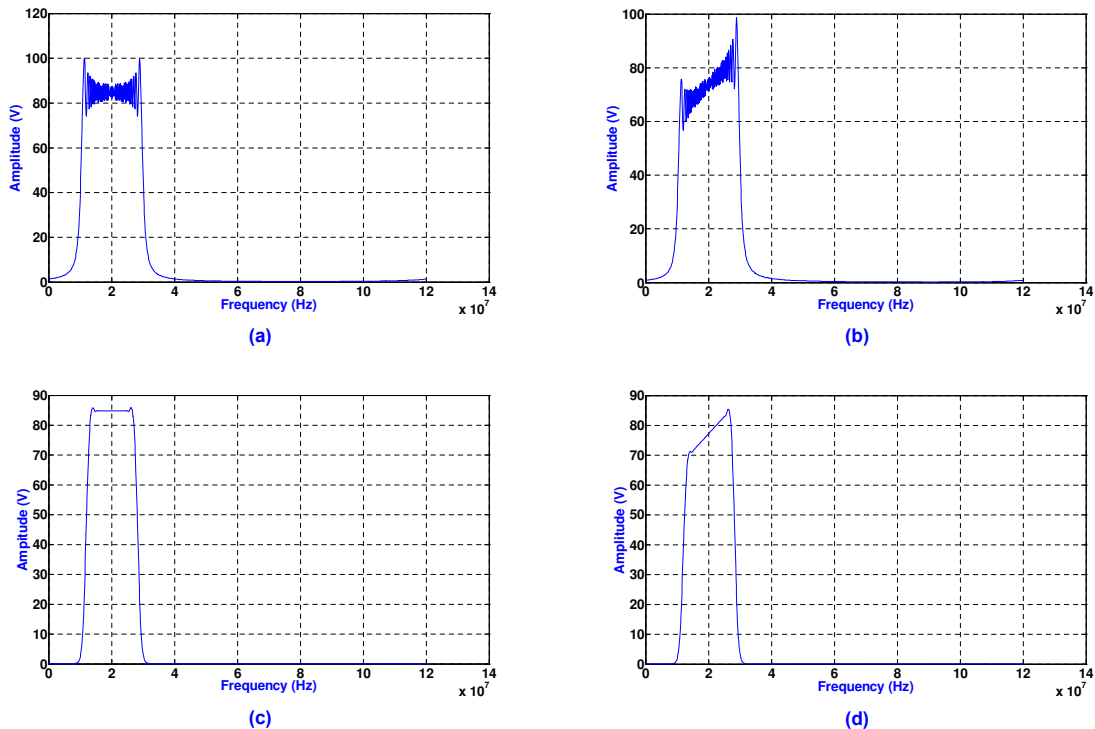


Figure 3.8. Simulated frequency domain 10 MHz to 30 MHz chirp signal:
 (a) Ideal rectangular chirp (b) Pre-distorted chirp (c) Amplitude tapered chirp (d) Pre-distorted and amplitude tapered chirp

proportional to bandwidth. Further, amplitude tapering also implies that less energy is put on the target which will affect the SNR of the received signal. Since the advantages are superior compared to the tolerable disadvantages tapering is a necessary operation in the current project.

3.3 Transmitter testing

As indicated in section 2.2.1 the radar transmitter is composed of a low power up-conversion stage followed by high power amplifiers. The low power section of the transmitter (tx_input and tx_output stages) was tested in terms of its up-conversion gain, system gain, carrier rejection and spectral purity.

3.3.1 tx_input testing

The low power tx_input section is mainly an up-conversion module. For testing the 150 MHz system, a CW signal of 120 MHz at 13 dBm is provided to the LO port from a RF signal generator (Agilent 8648D). The I and Q signals spanning a bandwidth of 20 MHz to 40 MHz with a power level of 0 dBm are provided to the I and Q ports of the transmitter. For the 450 MHz system, a CW 420 MHz LO signal with 10.3 dBm power is provided. The I and Q signals have a bandwidth of 15 MHz to 45 MHz with a power level of 0 dBm. Figure 3.9 shows the up-converted output of the tx_input section, recorded on the Agilent spectrum analyzer E4407B. In both the systems clearly the LO leakage (120 MHz and 420 MHz) can be observed. Compared to the output chirp signal, the LO power is approximately 57 dB higher for 150 MHz system and 23 dB for the 450 MHz system. This can be attributed to two reasons. Firstly, the chirp has band of frequencies and the total energy within the 3 dB bandwidth corresponds to 0 dBm power, but when displayed on the analyzer the individual components show a lower power level due to detector averaging [26]. Secondly, suitable narrow bandpass filtering is required to remove the LO leakage during the up-conversion process. The bandpass filters (40 MHz for 150 MHz system and 50 MHz for 450 MHz system) used in the current design were not sufficiently narrow band to suppress the LO leakage at the mixer output, since the baseband signal bandwidth was only 20 MHz and 30 MHz for 150 MHz and 450 MHz systems respectively.

3.3.2 tx_output testing

The s-parameters of the transmitter output section were recorded as explained in section 3.1.1. The primary parameters for this section are pass-band system gain ($|S_{21}(\omega)|^2$), input return loss ($|S_{11}(\omega)|^2$), output return loss ($|S_{22}(\omega)|^2$) and reverse isolation ($|S_{12}(\omega)|^2$). Figure 3.10 shows the s-parameters plotted for 150 MHz and 450 MHz systems which were recorded on the Agilent 8753D network analyzer.

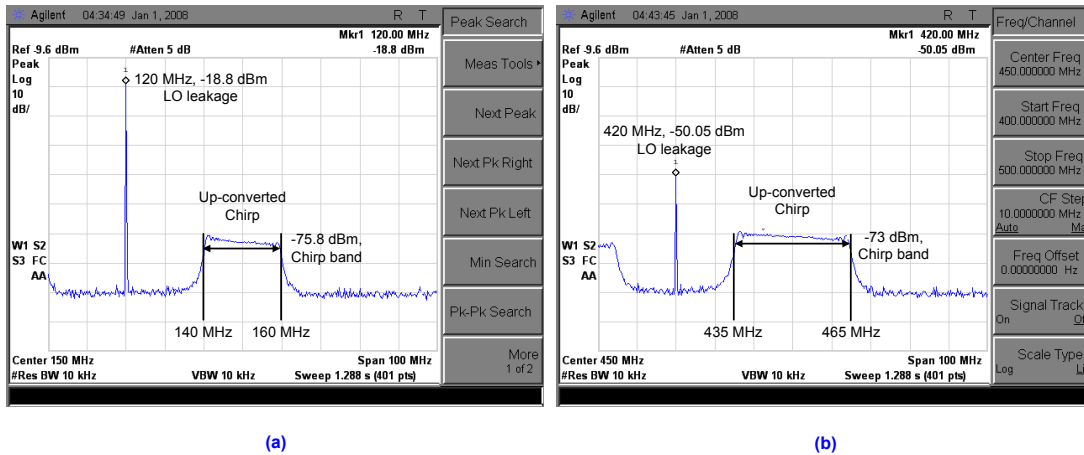


Figure 3.9. Measured output spectrum of transmitter input section for (a) 150 MHz system and (b) 450 MHz system

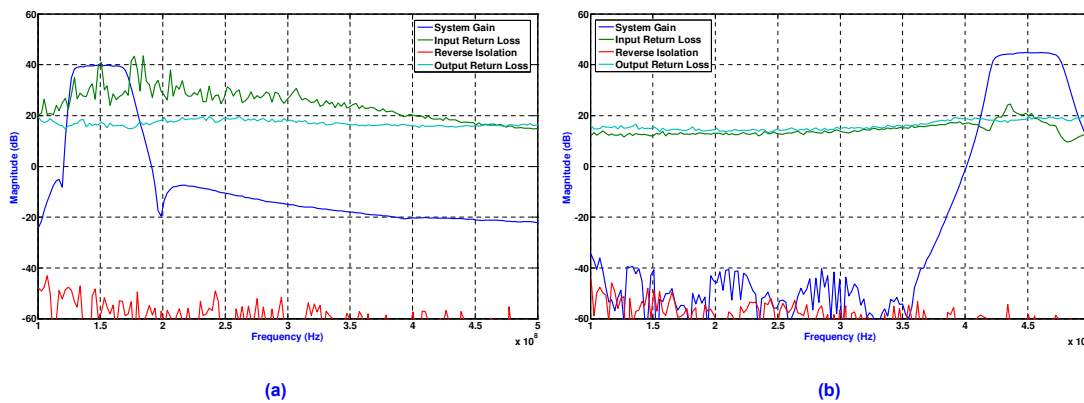


Figure 3.10. Measured s-parameters for tx_output for (a) 150 MHz system and (b) 450 MHz system

The measured system gain at 150 MHz is approximately 39.6 dB and at 450 MHz the gain is 44.6 dB. The measured input and output return loss for both systems is approximately 20 dB. From section 2.4.1, the theoretical system gains at 150 MHz and 450 MHz is 32.6 dB and 38.6 dB respectively. The discrepancy can be attributed to using the worst case values for theoretical calculations (least amplifier gain and highest possible insertion loss for filters) resulting in lower system gain values.

3.3.3 Transmitter output spectrum

Both input and output sections of the transmitter were integrated together and tested. For testing the 150 MHz system, a CW signal of 120 MHz at 13 dBm is provided to the LO port from a RF signal generator (Agilent 8648D). I and Q signals with a bandwidth of 20 MHz to 40 MHz and a power level of 0 dBm are provided to the I and Q ports of the transmitter. For the 450 MHz system, a 420 MHz CW LO signal with 10.3 dBm power is provided. The I and Q bandwidth in this case is 15 MHz to 45 MHz with 0 dBm power level. The complete low power transmitter output comprising both transmitter input and output sections is shown in figure 3.11 as recorded on the Agilent spectrum analyzer E4407B.

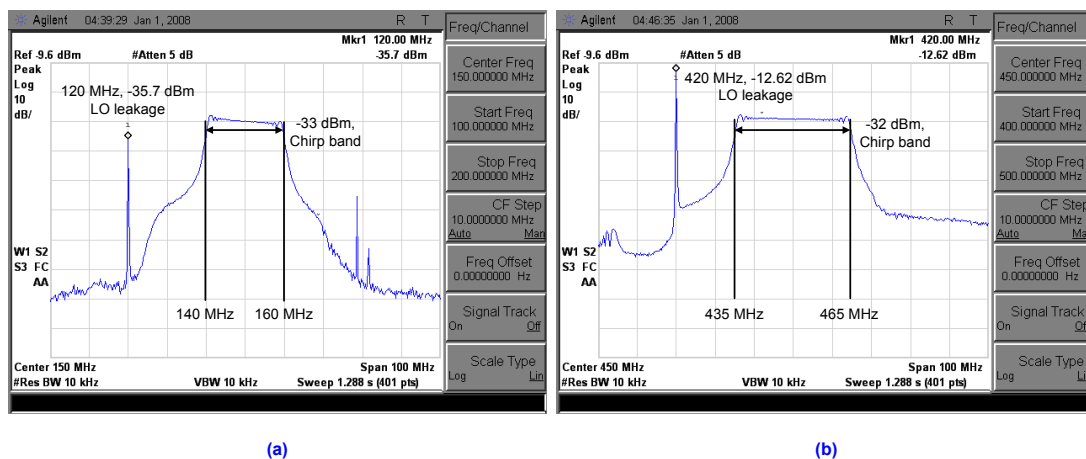


Figure 3.11. Measured output spectrum of integrated transmitter section for (a) 150 MHz system and (b) 450 MHz system

As mentioned before, the spectrum analyzer reading for a chimp waveform is not very useful in determining the exact power level of the signal. Hence the output waveform is observed on an oscilloscope to read the rms voltage of the chimp signal over the pulse duration ($10 \mu\text{s}$ or $3 \mu\text{s}$) from which power in dBm for a 50 ohm load can be calculated. A typical recorded rms voltage value at the integrated transmitter output for a 150 MHz system (bandwidth of 140 MHz to 160 MHz), with $3 \mu\text{s}$ pulse is 800 mV. This corresponds to power of 11 dBm. For a 450 MHz system (bandwidth of 435 MHz to 465

MHz), with 10 μ s pulse is 500 mV. This corresponds to power of 7 dBm. As discussed in section 2.4.1 and corresponding table 2.4, the P1-dB input power to the power amplifiers is -6 dBm (150 MHz) and 13 dBm (450 MHz). To operate in the linear region of the amplifier the input power should be backed-off by a minimum of 10 dB. This implies inserting at least 27 dB pad at the integrated transmitter output for 150 MHz and at least 10 dB for the 450 MHz system. Further, these attenuator values can also be used to control the required output power from the high power amplifiers by varying the input power level.

It can be observed that after suitable bandpass filtering and amplification, the 120 MHz LO is suppressed significantly for the 150 MHz system, whereas the 420 MHz LO is not suppressed as well. The latter situation can be explained as follows.

1. The difference between LO (420 MHz) and lower chirp frequency (435 MHz) is 15 MHz whereas it is 20 MHz in the case of the 150 MHz system. The bandpass filter passband and stopband attenuation are of prime importance for carrier suppression. Lorch Microwave bandpass filter specifications are tabulated in table 3.5. Clearly the specifications for 150 MHz are better in terms of out-of-band signal rejection and in-band insertion loss compared to 450 MHz.

Table 3.5. Typical Lorch Microwave bandpass filter specifications used in the transmitter and receiver

Frequency (MHz)	Insertion Loss (dB)	Return Loss (dB)
120	40	1
140	4	16
160	4	16
420	10	5
435	3	27
465	3	31

2. The above mentioned bandpass filters used in the design had a 3-dB passband (approximately) of 40 MHz for 150 MHz system and 50 MHz for 450 MHz system. But the chirp bandwidth used in the actual field experiment is 20 MHz and 30 MHz

respectively. Thus the LO and out-of-band signal suppression is not significantly high as desired.

3.4 Thermal stress testing

The transmitter and receiver boards were subjected to extreme temperature cycling to test for robustness. The boards were placed inside Envirotronics Systems PlusTM temperature chamber for more than an hour at three different temperatures: -40 °C, 0 °C and +60 °C. After each temperature setting the boards are allowed to return to room temperature before going for the next temperature value. The response of the circuit boards were collected after each cycle and no significant performance variations were observed.

3.5 System loopback and calibration testing

The entire system was integrated and tested in a loopback mode. Figure 3.12 shows the calibration set-up block diagram. This is the general set-up and is used to test the functionality of both 150 MHz and 450 MHz systems. This includes the complete system including high power amplifiers but excluding the antennas.

The low power attenuators before the power amplifiers were inserted to avoid saturation of the high power amplifiers and to control the output power of the radar (actual transmit power during operation). A fiber optic delay line is selected to provide a two-way delay of at least twice the pulse duration of the transmit signal. A delay of 20 μ s was typically used. Figure 3.13 shows the loopback connections and inset shows the fiber optic spools used for loopback testing.

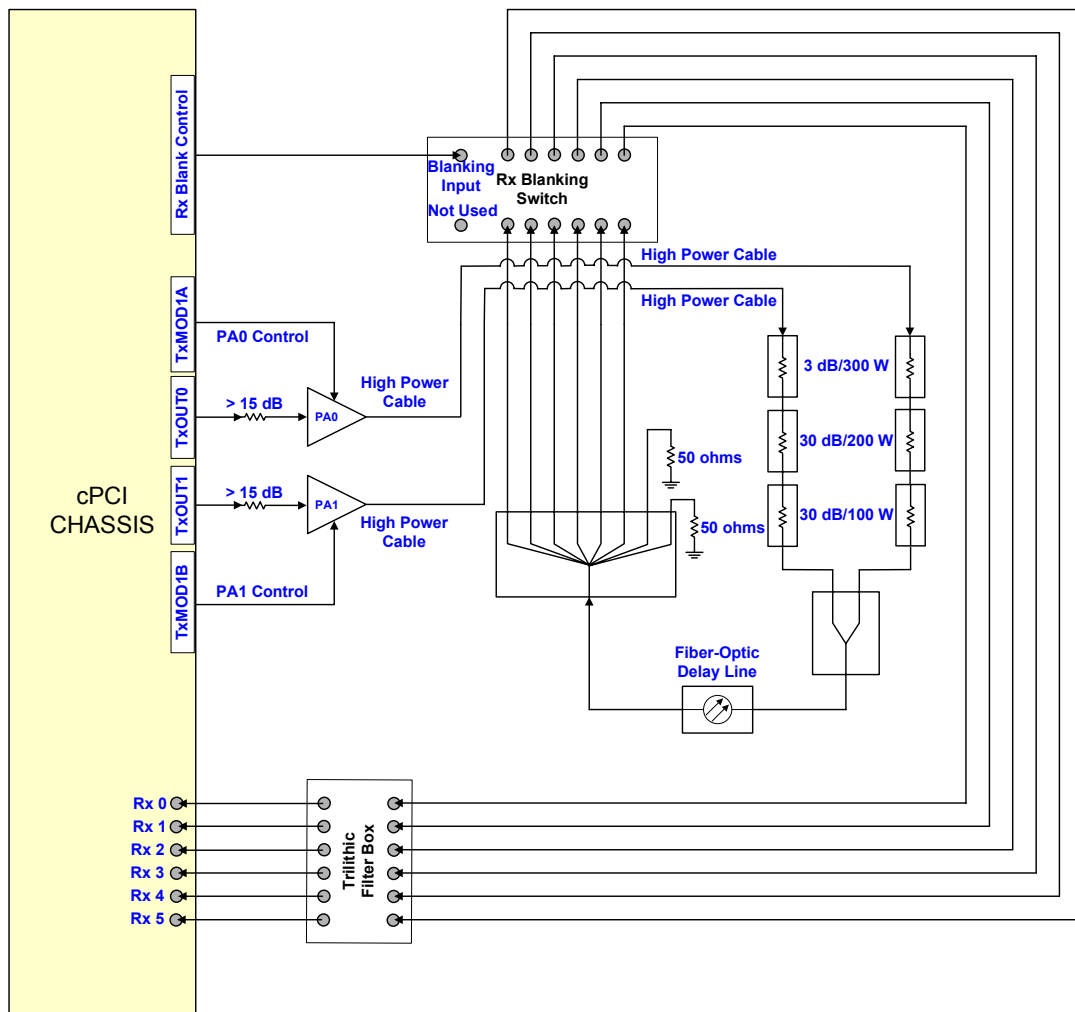


Figure 3.12. System loopback and calibration block diagram

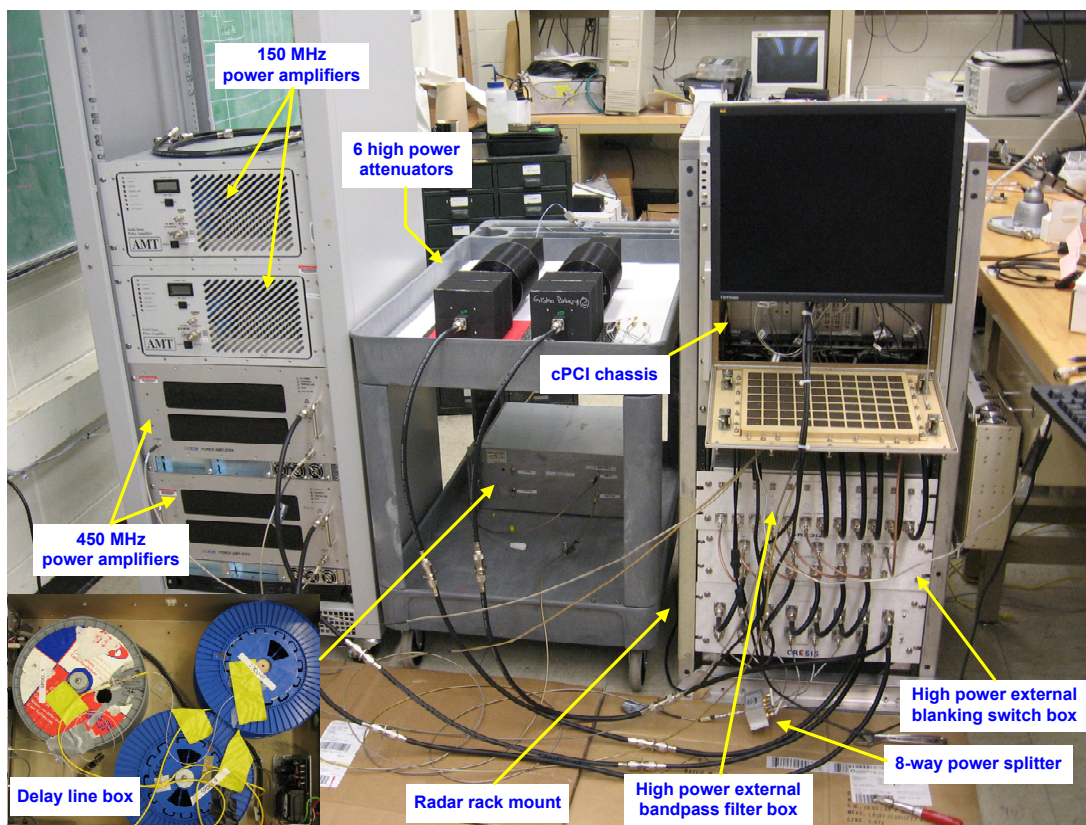


Figure 3.13. System loopback set-up and the optical fiber spools (inset)

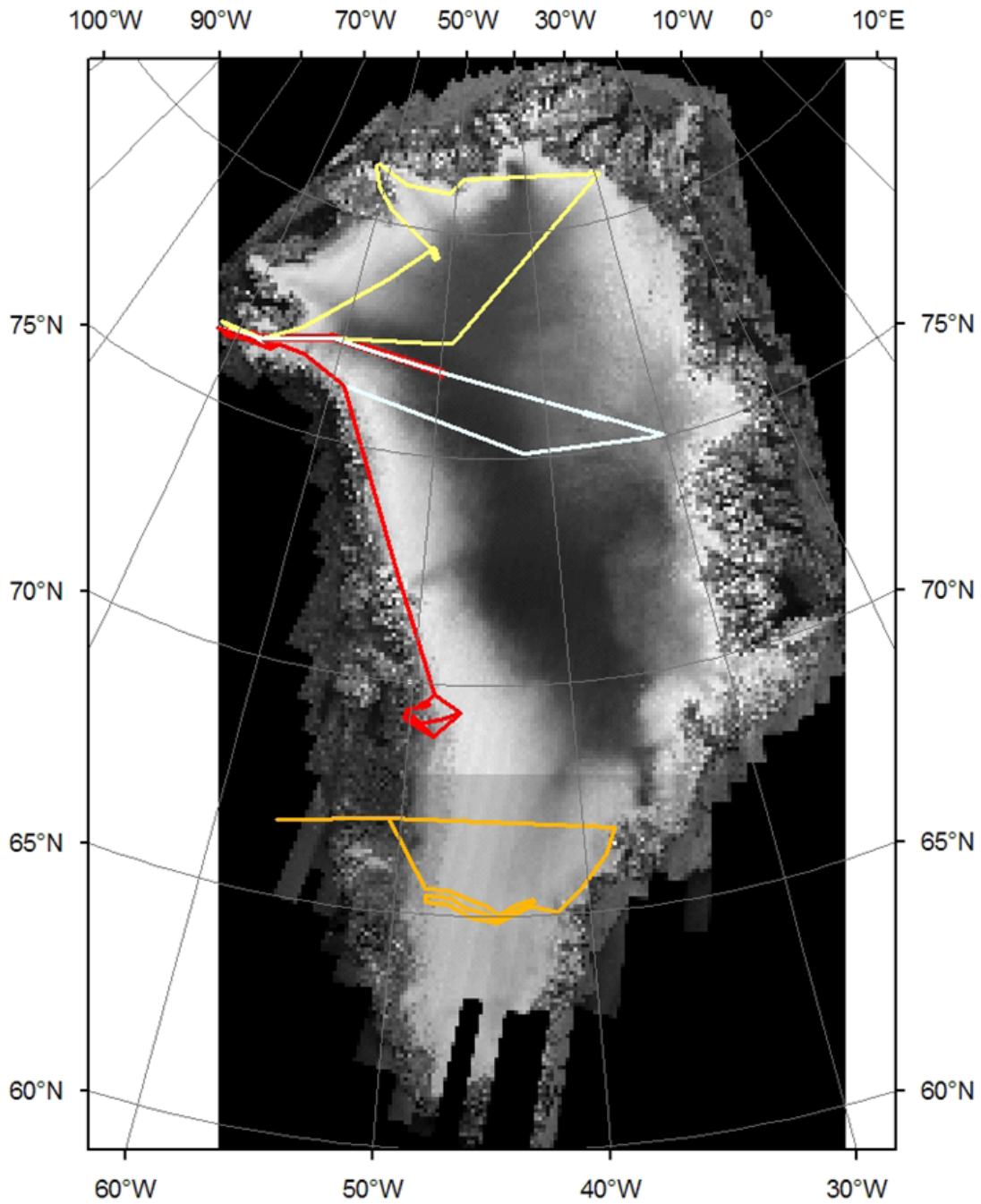
Chapter 4

Field Experiment and Results

This chapter discusses the field experiment in brief and analysis of sample field data. The radar was deployed in September 2007 to collect data over several parts of Greenland. Flights were conducted at altitudes ranging from 500 m up to 6700 m above the ice sheets. The flight lines for the experiment are shown in figure 4.1. A detailed discussion of the logistics for this campaign can be found in [27]. Figure 4.2 shows the system mounted on the metal racks and installed inside NASA P-3 aircraft.

4.1 Field experiment description

The field experiment was conducted on pre-determined flight lines as shown in figure 4.1. The primary operating modes were termed as interferometric mode (also called ping-pong mode) and depth sounder mode. The modes were decided based on a two 4-element dipole antenna array transmit-receive configuration. Each 4-element array is placed beneath each wing of the aircraft as shown in figure 4.3. In the interferometric mode the in-board elements on each wing are used for transmitting and the other out-board elements are used to receive. In depth sounder mode one 4-element antenna array is used for transmitting and the 4 dipoles on the other wing for receiving. Thus only 4 of the 6 receivers are used for data collection in this mode. The advantage of using ping-



Legend for flight lines






GISMO flight 1: 8, 10, 11 Sep 08	
GISMO flight 1R (overlapping white line): 12 Sep 08	
GISMO flight 2: 7 Sep 08	
Jakobshavn from Thule: 14, 15 Sep 08	
GISMO flight 4: 18 Sep 08	

Figure 4.1 Flight lines for Greenland 2007-2008. Color-coded flight lines



Figure 4.2. System installed on NASA P-3 aircraft

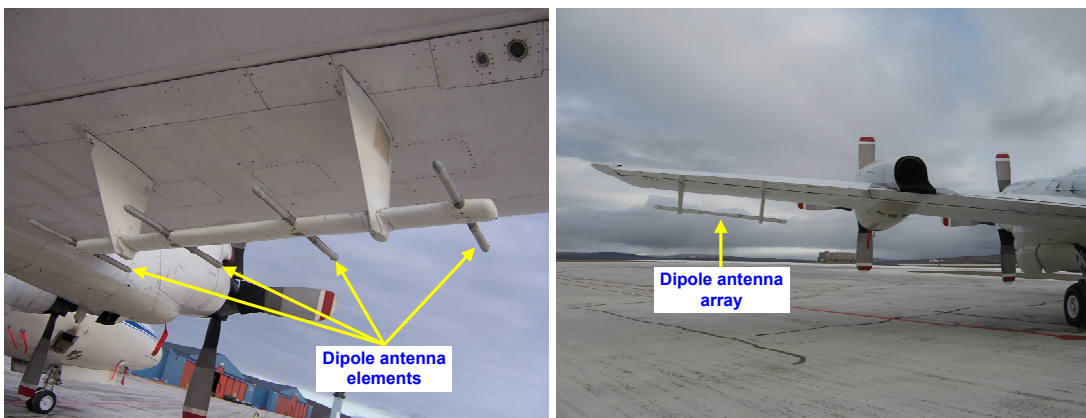


Figure 4.3. Dipole antenna array installed beneath the aircraft wings

pong mode is to have comparable interferometric images to a system with large physical baseline and a system with smaller physical baseline and ping-pong configuration [28].

4.2 Sample results and discussion

Few sample results from the field experiment are given in this section. Most of the data are still being processed. The preliminary results presented here attest the satisfactory performance of the hardware developed for this thesis project.

Figure 4.4 depicts the locations for the results pertaining to table 4.1. Information for the results collected is summarized in table 4.1

Table 4.1. Parameters for September 2007 field mission sample results

Fig No.	Date	Mission plan	Freq (MHz)	Mode	Altitude (m)	Pulse duration (μ s)
4.5	Sep 08, 2007	East of Thule including North Ice Stream	450	Interferometric	6800	3 and 10
4.6	Sep 10, 2007	East of Thule including North Ice Stream	450	Depth sounder	3100	3 and 10
4.7	Sep 11, 2007	East of Thule including North Ice Stream	150	Interferometric	6700	3 and 10
4.8	Sep 21, 2007	Jakobshavn, perpendicular to channel flow	150	Depth sounder	1000 to 7000	3 and 10

Figures 4.5 to 4.8 represent the results collected with the details mentioned in table 4.1.

From the sample echogram results it can be concluded that at higher altitudes (figures 4.5 and 4.7) the performance for both 150 MHz and 450 MHz is degraded due to the clutter from the surface. Further at 450 MHz, the attenuation loss was more than predicted by the existing models. This data will be used to test the clutter rejection concepts which can be used in the later projects for sounding the ice-bed from higher

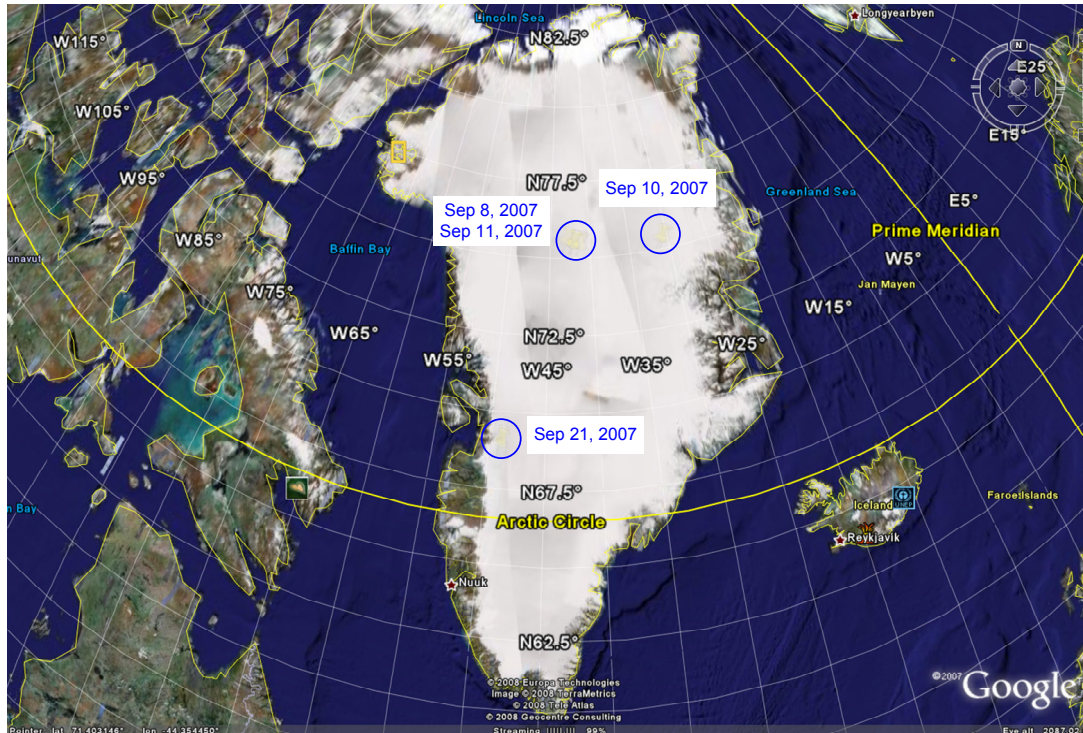


Figure 4.4. Locations of the field experiment for the presented sample data results

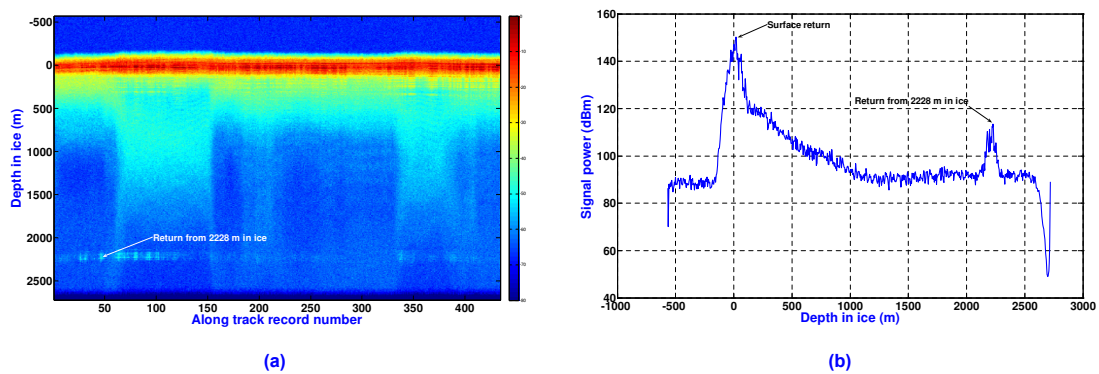


Figure 4.5. (a) Echogram and (b) A-scope of data collected for 450 MHz system at high elevation in interferometric mode

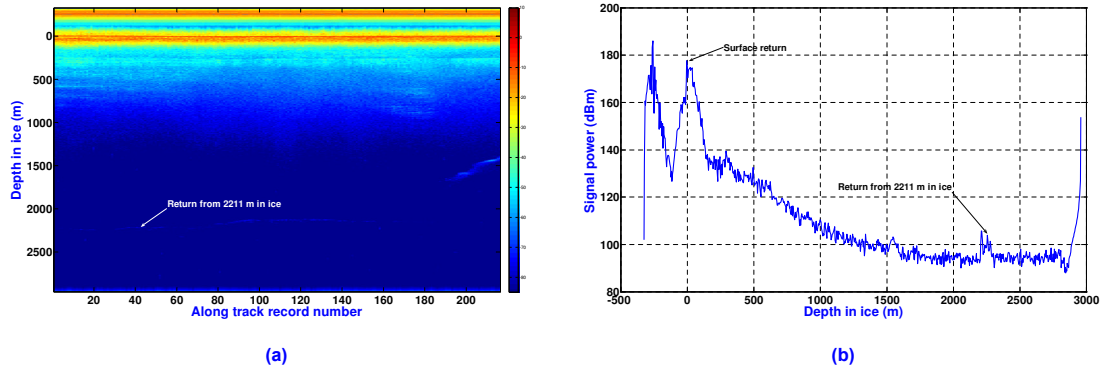


Figure 4.6. (a) Echogram and (b) A-scope of data collected for 450 MHz system at low elevation in depth sounder mode

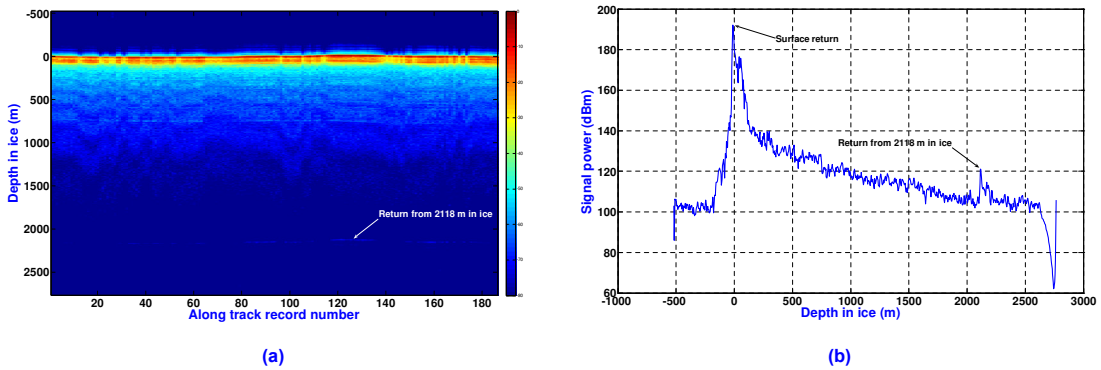


Figure 4.7. (a) Echogram and (b) A-scope of data collected for 150 MHz system at high elevation in interferometric mode

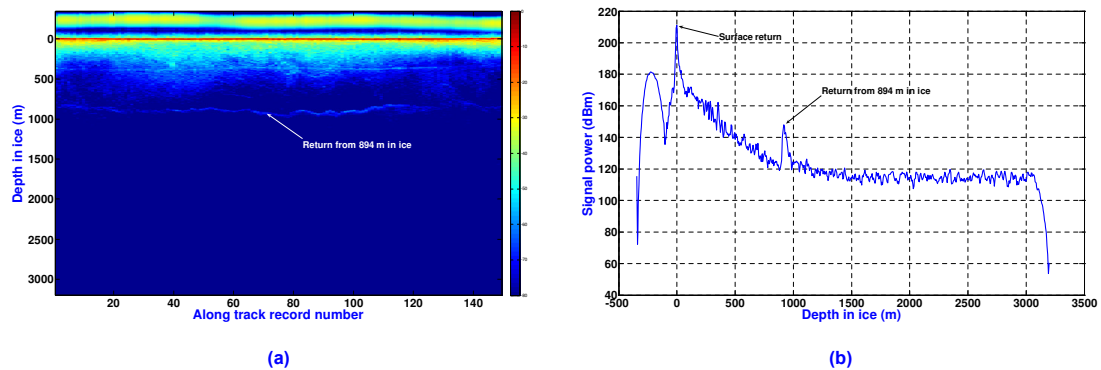


Figure 4.8. (a) Echogram and (b) A-scope of data collected for 150 MHz system at an elevation of 1700 m in depth sounder mode

altitudes. There is a need to develop or improvise better clutter cancellation algorithms for transitioning the current system on to a spaceborne platform. Further, it can be concluded that any future high altitude experiments will substantially require higher power and more directional antennas [29].

As documented in the data review document [29], it is observed that the accelerometers emitted a strong noise signal that corrupted the 150 MHz radar data. Further, this noise was identified early on September 8. But a detailed analysis of September 7 data did not reveal any such interference. Thus, the EMI effect of accelerometers need to be verified before the next field experiment to make sure that they are not acting as a noise source. Another observation revealed that better shielding may be required for future experiments to suppress the laser noise affecting the signal of interest.

Chapter 5

Future Improvements

There is always room for improvement in any system design and this project is not an exception. Based on laboratory test results, practical observations during the experiment which are outside the 'ideal' laboratory conditions and also based on the analysis of experimental data it can be concluded that several aspects of the radar can be improved for better performance. This section highlights few improvements relating to the transmitter and receiver systems.

5.1 EMI testing

During the September 2007 field experiment and the subsequent data analysis revealed that the collected data were affected by unwanted electromagnetic emissions and thus it was imperative to detect the sources of such interference. Electromagnetic interference (EMI) tests were performed to determine any electromagnetic disturbances that could result in reduced performance of the system. The system was tested at the Sprint anechoic EMI testing facility located at Olathe, Kansas, USA. The basic idea of this test was to monitor the noise spectrum with several parts of the system turned ON independently and also to record the data from the receiver while these parts are ON. A list of sample test cases is given in the table 5.1. The \checkmark indicates that the particular

equipment is switched ON. Figure 5.1 depicts the system set-up for the EMI testing.

Table 5.1. Sample test cases for the study of EMI effect on the system response

Equipment	Test 1	Test 2	Test 3	Test 4	Test 5	Test 6	Test 7	Test 8
Power switch	√	√	√	√	√	√	√	√
Power amplifier	√							
Ethernet switch		√						
Laptop computer			√					
Wi-fi				√				
Bluetooth					√			
NI accelerometer DAQ system						√		
UPS							√	

Power switches were used to provide power supply to the radar system and other equipment (delay line box, blanking switch box, spectrum analyzer, oscilloscope) and they can be a transient noise source. Ethernet switch was used as a medium to connect the radar system to external memory and control devices to transfer the recorded data and can contribute unwanted signals due to continuous switching transients. Laptop computer was used as an alternative to the radar controller to control the radar system. Further, the computer was also equipped with wi-fi and bluetooth features and it was important to determine the effect of these wireless devices on the radar performance. The National Instruments (NI) accelerometer DAQ system used in measuring the vibrations during flight can also generate noise being an active device. The above tests were performed with following other combinations of radar in ON/OFF mode, with 1 or 32 coherent integrations and '0/pi' mode in ON/OFF conditions. For each test case, an 8-element tear-drop antenna was used to monitor the system EMI response. Further, a wideband Vilvaldi antenna was also used for twin purposes. Firstly, to monitor the spectrum inside the chamber when each equipment was turned ON successively

with the spectrum analyzer outside the chamber recording the results. Secondly, it was disconnected from the external spectrum monitoring cable connected to the spectrum analyzer and now connected to the 'open-circuit' channel of high power blanking switch box as shown in figure 5.1. In the second role, the data from each receiver channel was recorded by the DAQ system for analysis. This procedure is repeated for every test case in table 5.1. Figure 5.2 shows sample results for particular test cases. It can be

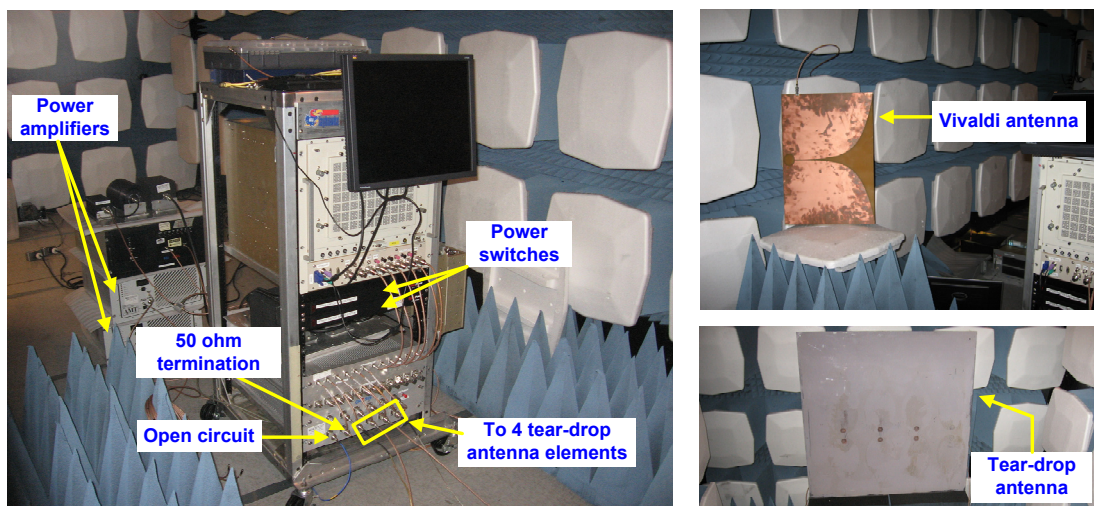


Figure 5.1. Sprint anechoic chamber test set-up

observed that with the ethernet switch ON, the noise floor increases approximately by 15 dB within the operating bandwidth which results in degraded SNR. As observed, few spikes peak up to 18 dB above the system noise floor in the operating bandwidth.

5.2 High power amplifier characterization

The output power of the two power amplifier modules was measured for both 150 MHz and 450 MHz amplifiers for different levels of input power. These tests were intended to obtain a calibrated measurement of amplifier output power as well as the linear operating region of the modules.

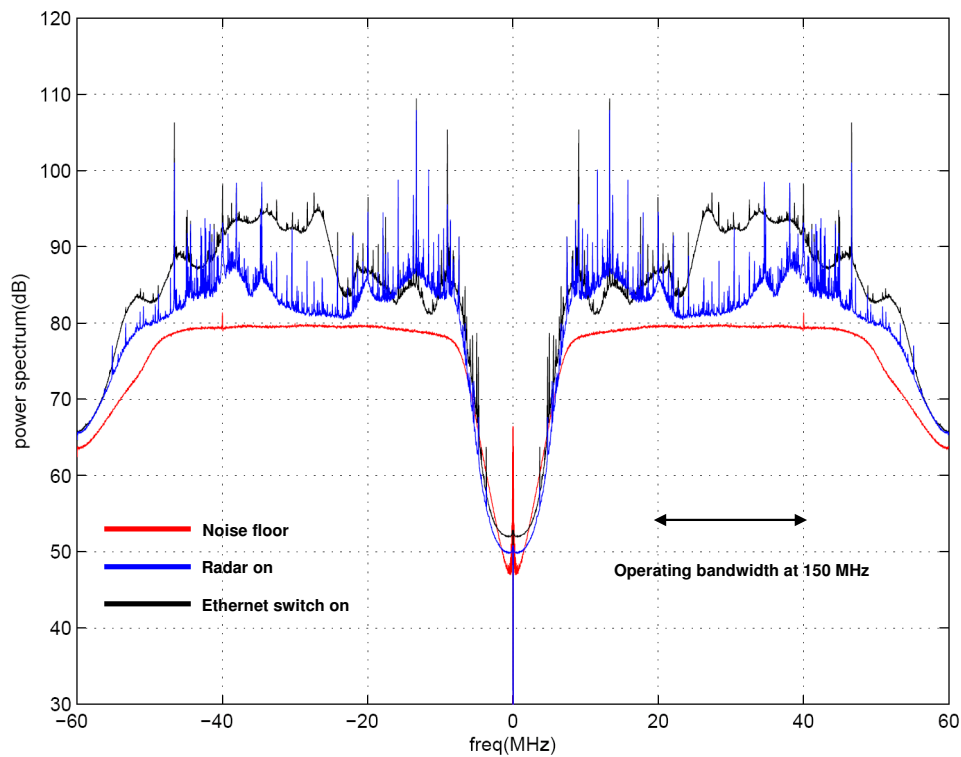


Figure 5.2. Measured EMI test results

5.2.1 150 MHz amplifier

The test set-up is illustrated in figure 5.3. A single tone baseband $10 \mu\text{s}$ pulsed signal

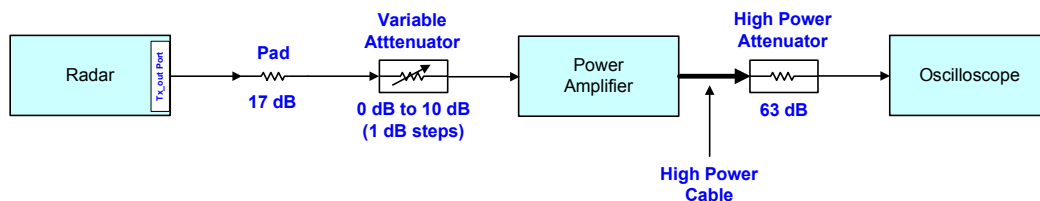


Figure 5.3. 150 MHz power amplifier P1-dB characterization test set-up

at 150 MHz was applied as the input to the amplifier. The input power to the power amplifier is varied by changing the variable attenuator value in 1 dB steps. The output power is recorded on the oscilloscope which includes cable losses (0.9 dB) between the power amplifiers and the oscilloscope and also 63 dB high power attenuators. These losses are removed and the output power values are tabulated in table 5.2 and 5.3. An

additional column indicating the power reading on the amplifier was added for reference.

Figure 5.4 shows the output power as a function on input drive level. It can be observed

Table 5.2. Measured output power for the 150 MHz power amplifier module PA 0

Input power (dBm)	Output power (dBm)	Output power (W)	Reading on PA display (W)
-19	47.54	56.75	23
-18	48.50	70.89	38
-17	49.57	90.77	61
-16	50.71	117.87	94
-15	51.87	153.95	139
-14	52.89	194.85	202
-13	54.05	254.50	283
-12	54.97	314.20	382
-11	55.89	388.87	495

Table 5.3. Measured output power for the 150 MHz power amplifier module PA 1

Input power (dBm)	Output power (dBm)	Output power (W)	Reading on PA display (W)
-19	47.74	59.45	39
-18	48.50	70.89	55
-17	49.57	90.77	77
-16	50.53	113.11	108
-15	51.71	148.50	149
-14	52.75	118.71	204
-13	53.81	240.56	272
-12	54.86	306.39	355
-11	55.80	380.18	450

that the amplifier is linear up to 400 W of output power at which the deviation from the ideal response is approximately 0.15 dB. The amplifier could not be driven in to compression to estimate the P1-dB to prevent damage since input power levels greater than -11 dBm result in an 'overdrive' fault condition. Further the gain of the amplifier is noted to be about 66.5 dB.

For comparison, the response of both amplifiers is plotted in figure 5.5. The maximum difference in output power for the two amplifiers is observed to be 0.24 dB for

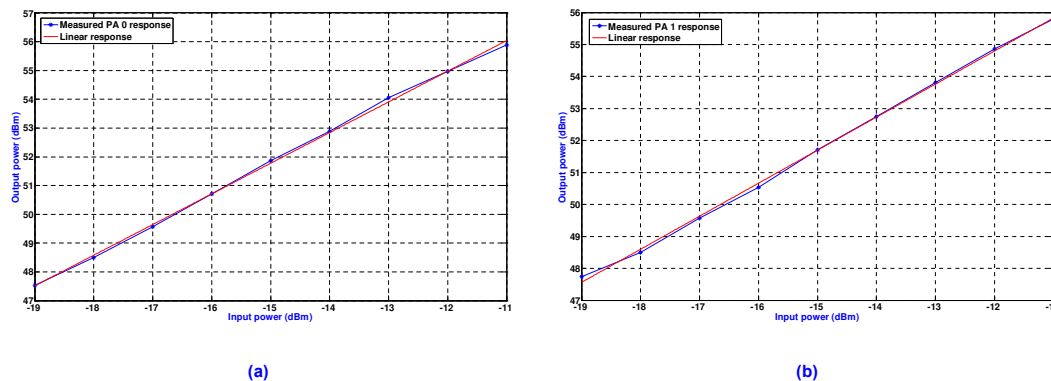


Figure 5.4. Measured response of (a) PA 0 for 150 MHz tone as input and (b) PA 1 for 150 MHz tone as input

the input drive level of -13 dBm. The linear response is the interpolation of the PA 0 amplifier response.

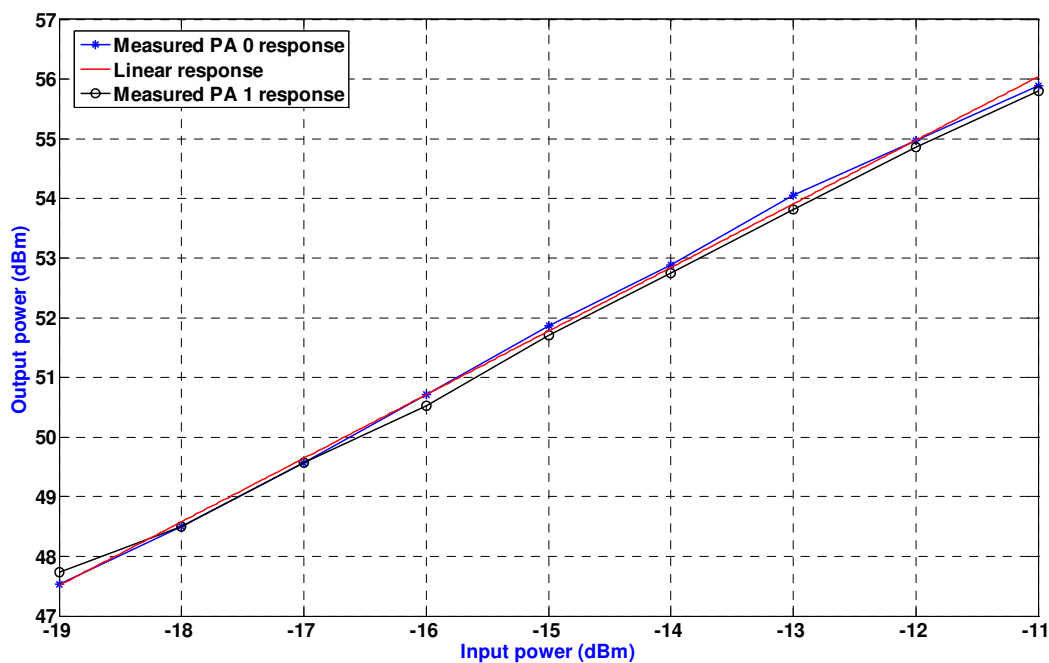
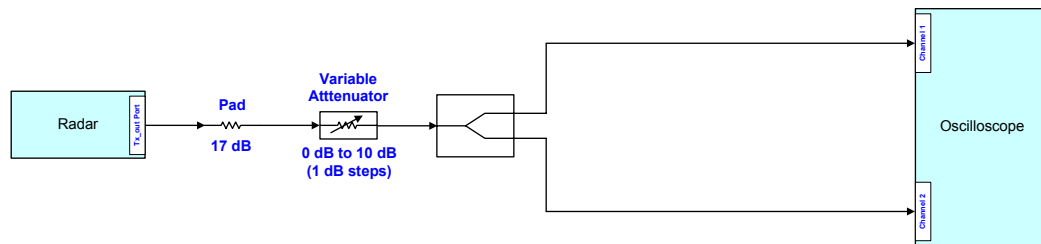


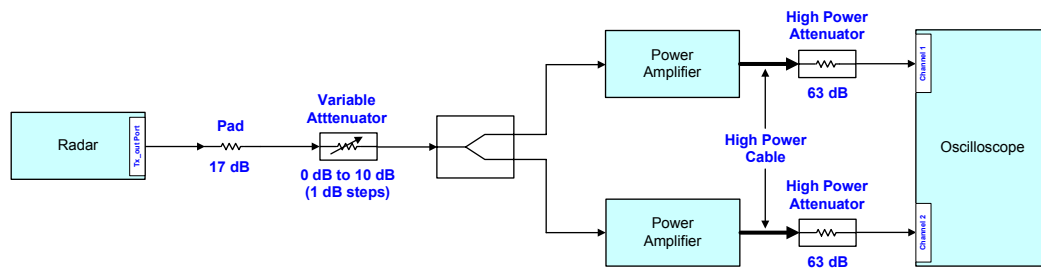
Figure 5.5. Measured response of PA 0 and PA1 for 150 MHz tone as input for comparison

The 150 MHz high power amplifiers were also subjected to amplitude and phase imbalance measurements. A single tone baseband 10 μ s pulsed signal at 150 MHz was applied as the input to the amplifier. Figure 5.6.(a) depicts the set-up procedure for

measuring imbalance in the 3-dB power splitter (Mini-Circuits ZFSC-2-1) used in the experiment. It was observed that the values of amplitude and phase difference were smaller than 0.5 dB and 1° as per the data sheets. Figure 5.6.(b) shows the lab setup



(a)



(b)

Figure 5.6. Calibration test set-up for the (a) 3-dB power splitter and (b) high power amplifiers

for measuring the amplitude and phase imbalance of the power amplifiers. The input power is varied by using a variable attenuator and the output of the transmitter is fed in to the previously calibrated 3-dB power splitter which creates 2 paths for providing the input to amplifiers. The amplitude imbalance between 2 power amplifiers is calculated by recording the rms voltage difference between 2 channels of the oscilloscope. The amplitude difference values in the table 5.4 are normalized to the minimum difference value. The phase imbalance is calculated by considering the difference in time scale values (Δt) between 2 channels when observed on the scope. Since the frequency of

operation is 150 MHz, the wavelength corresponds to 2 m. Thus the phase difference is given by $\text{Phase difference} = 360^\circ * \Delta t * \text{frequency}$. Figure 5.7 depicts the amplitude

Table 5.4. Measured amplitude and phase imbalance values for the two 150 MHz power amplifiers

Input power (dBm)	Amplitude Difference (dB)	Phase Difference (deg)
-22	0	0
-21	0	0
-20	0	0
-19	0.66	0
-18	0.66	2.7
-17	1.24	2.59
-16	1.24	2.80
-15	2.21	4.32
-14	3.35	4.86
-13	4.26	4.05
-12	4.77	3.51

and phase imbalance as a function of amplifier output power. Clearly with high output powers the amplitude and phase difference are higher than at lower output powers, since higher powers imply moving away from the linear region towards the non-linear regime of the amplifier.

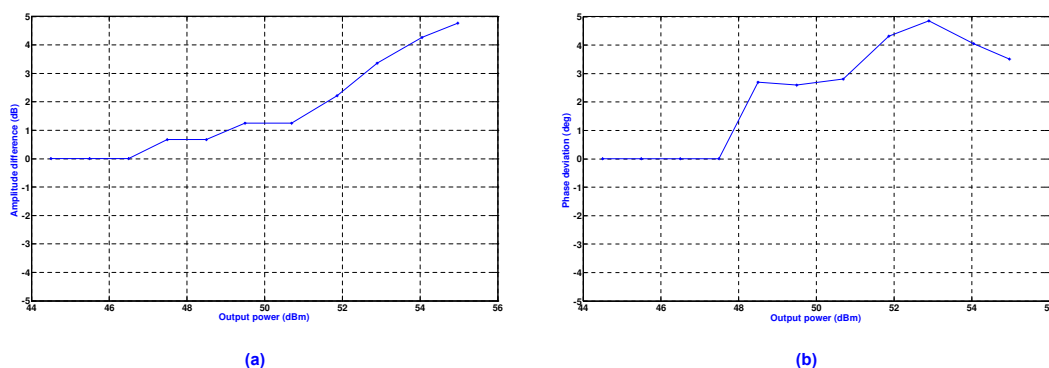


Figure 5.7. Measured amplitude and phase difference response between 150 MHz PA 0 and PA 1 high power amplifier modules

5.2.2 450 MHz amplifier

The 450 MHz power amplifier was also subjected to P1-dB characterization and details can be obtained in [30]. A plot of the output power as a function of input power for the amplifiers appears in 5.8. The effect of the attenuator chain placed at the output

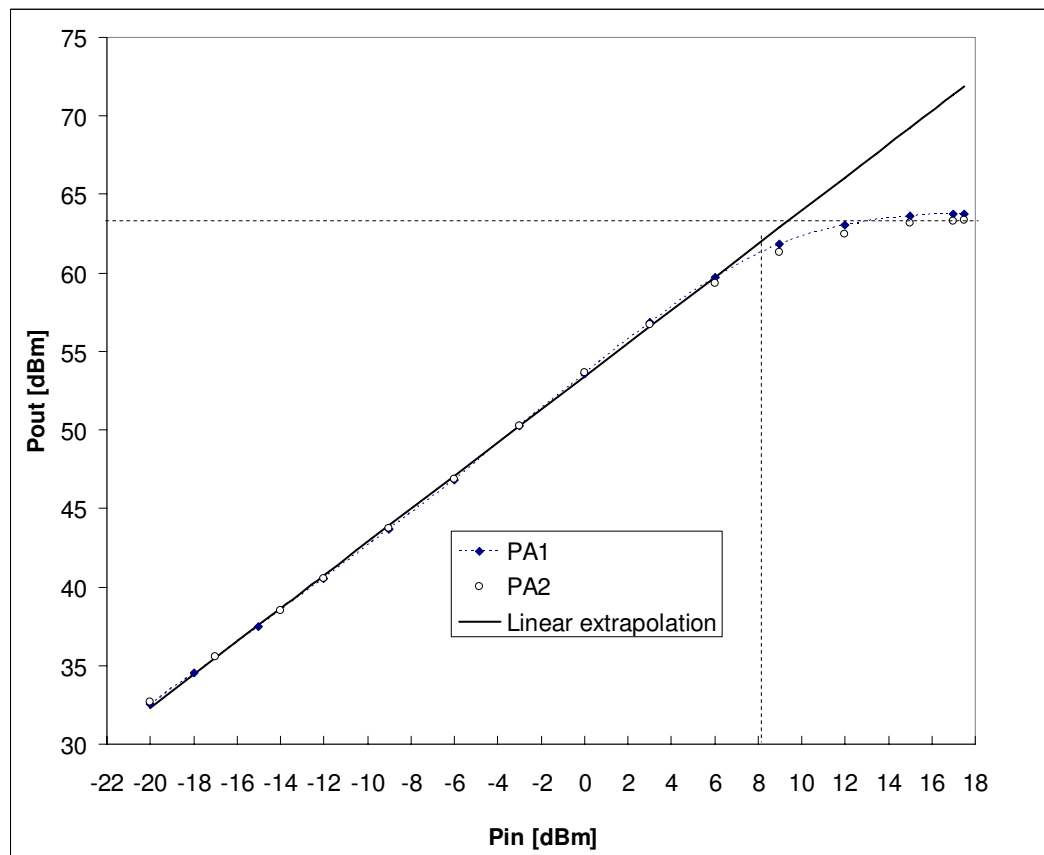


Figure 5.8. Measured response for the 450 MHz high power amplifier

of the amplifiers, as well as cable losses were calibrated out of the measurement. Both units (designated PA1 and PA2, respectively) are linear up to about 8 dBm of input power, after which saturation effects are noticeable. The measured values of output power for an input power of +17 dBm are 63.7 dBm and 63.3 dBm for PA1 and PA2 respectively. These figures agree with the settings reported by Delta-Sigma (slightly larger than 63 dBm for both units).

5.3 Transmitter design

5.3.1 AWG improvements

The output from the AWG are I and Q signals with a bandwidth specified by the user. It was observed that for bandwidths greater than 30 MHz the spectral content at the AWG output was not pure as expected. It had harmonics of the baseband signal, harmonics of LO signal (120 MHz) and also other spurious products. This is attributed to having a different part (differential amplifier) at the AWG output board for various designs.

Further, not any bandwidth can be used as baseband signal. For certain bandwidth combinations (example: 5 MHz to 25 MHz) the output of the receiver after under-sampling does not result in the required baseband signal. As discussed in section 2.6 the sampling rate of the ADC is a very important factor determining the proper working of under-sampling concept. If the sampling rate can be made variable, then any bandwidth (within the limitations of sinc roll-off effect) can be selected and yet the signal be recovered through under-sampling. For example, with 420 MHz as the LO, a chirp bandwidth of 15 MHz to 55 MHz cannot be selected. This is because when sampling at 120 MHz, the up-converted 435 MHz to 475 MHz band would not fold into any of the Nyquist zones, whereas if the sampling rate is varied to 140 MHz, then it would fold into 7th Nyquist zone.

A future enhancement in the GUI is to have an independent command over the receiver and transmitter control signals, thus enabling the transmitter or receiver based on the operating duration of the PRT.

5.3.2 IQ modulator

One of the important components of the transmitter is the IQ modulator. For 150 MHz system the modulator was an off-the-shelf part from Synergy Microwave, but for the 450 MHz system, a suitable modulator was not available. A IQ modulator was

designed and developed in-house as depicted in appendix A. This mixer was tested and results were noted for conversion loss and sideband suppression which are reported to be 8 dB (maximum) and 30 dB (maximum) respectively. Even though phase and amplitude matched double balanced mixers were ordered from Mini-Circuits for constructing this IQ modulator, it was assumed that they were matched and hence no measurements were taken for any imbalance in phase and amplitude. Thus a new circuit with lumped component network can be designed for controlling the output amplitude and phase. An example design is to add a capacitor network to the LO branch which improves the sideband rejection specification [31].

A totally new approach was employed to design the IQ modulator using Analog Devices AD8345 quadrature modulator which is an active mixer circuit. Even though active mixers have their own advantages and limitations [32] [33], the current design requires few modifications.

AD8345 has a differential LO and differential baseband (I and Q) inputs, but the current transmitter has a single LO, I and Q inputs. Thus the AD8345 was used in conjunction with two AD8132 differential amplifiers to provide a differential input to the modulator [34] [35]. The sideband (405 MHz) suppression of at least 30 dB was observed when a single tone input was provided (15 MHz input with 420 MHz as LO). The hardware circuit connections for this method are shown in figure 5.9.(a). Further, as an alternative to the AD8132, a suitable biasing circuit which converts single to differential inputs was implemented in-house which is shown in figure 5.9.(b).

The active mixer implementation has extra circuitry compared to the existing passive mixer design in addition to requiring a +5V and -5V supply thus increasing the complexity of the design. But to overcome this problem and to make room for the increased circuitry, the SMS206 IQ modulator can be completely removed and the AD8345-AD8132 combination can be used both for 150 MHz and 450 MHz systems due to the wideband operation of these components.

Another option was explored using the IQ modulator SKY73010 from Skyworks

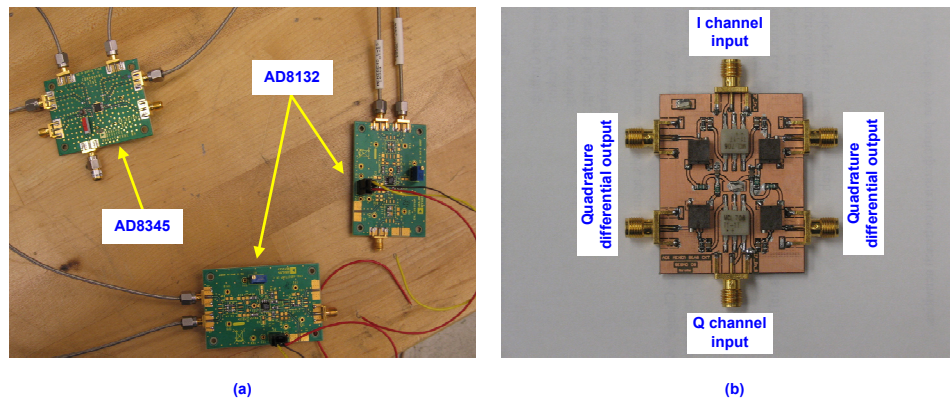


Figure 5.9. (a) Analog Devices IQ modulator circuit. (b) In-house designed bias circuit

Solutions, Inc. This option was not pursued much due to the same reasons of enhanced circuitry being an active mixer and requiring differential inputs. Further it works from 300 MHz to 2500 MHz and thus it is not a good choice for the 150 MHz system as per the specifications [36].

Finally a Synergy Microwave SMS A49 IQ modulator was tested. Even though this mixer was an unreleased product, it was tested based on the vendor's suggestion. Its performance was worse and did not meet the input baseband frequency specifications (operated over DC to 20 MHz only) for the system.

It can be concluded that several options for the IQ modulator were explored and it was observed that the active mixers provide a low sideband conversion loss and a high sideband and carrier suppression but at the expense of increased board real estate and power supply. The passive mixers are a good alternative for the current system and existing mixer can be improved by introducing the tuning circuit to reduce the amplitude and phase imbalance at the I and Q outputs.

5.3.3 Lowpass and bandpass filters

The current design uses a custom built Bree Engineering lowpass filter (801783) which has a 1.7 dB cut-off frequency at 55 MHz. But, due to the sinc roll-off effect, the

highest usable frequency is 48 MHz and hence a 55 MHz filter is redundant. Another option was explored from KR Electronics (KR2740) which has a 0.5 dB cut-off frequency at 44 MHz. This filter works satisfactorily and is used as the front-end lowpass filter in the spare transmitter system.

One more option for the lowpass filter was to design a lowpass filter in-house using lumped components as a learning exercise. This filter has a comparable performance as with the commercially available filters and figure 5.10 shows the designed filter with its s-parameters. This filter was designed on Agilent ADS filter design guide.

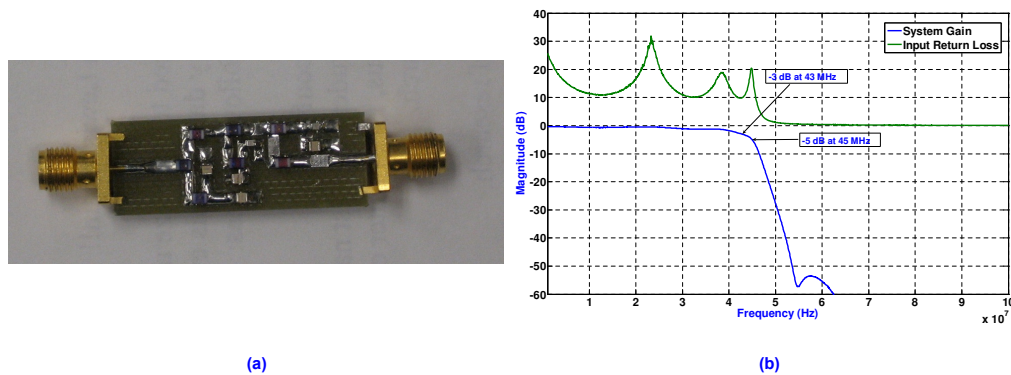


Figure 5.10. (a) Lowpass filter designed at CReSIS. (b) Measured s-parameters of the filter

Finally, regarding the bandpass filters in the transmitter, as mentioned in the section 3.3.3, the bandwidth needs to be reduced to 20 MHz for the 150 MHz system and 30 MHz for the 450 MHz system. Since the base design of the transmitter PCB is already in place, the best option is to order new filters from the vendors which match the current PCB footprint.

5.4 Receiver modifications

5.4.1 Blanking switches

The blanking switches included in the original design had several shortcomings. As discussed in section 2.2.2, a large box is needed to accommodate these high power

blanking switches since they are bulky in size. The switching speed is limited to $10 \mu\text{s}$ which made it less viable for use in low-altitude flights. In such cases the switching speed is desired to be less than $3 \mu\text{s}$ based on the two-way travel time. Finally, the switches are much more expensive than other solid state alternatives (example: HMC646LP2).

The main reason for the selection of these switches is the high power handling capability. But the necessity of using high power switches is not evident and the hypothesis follows. The peak power in either of the modes described in section 4.1 is only 62 dBm (1.6 kW) with 2 power amplifiers operating simultaneously. Thus, each amplifier outputs 59 dBm (800 W) and in the ping-pong mode scenario only 1 element may receive this power. From the antenna characterization results, it has been observed that a minimum of 20 dB isolation exists between the adjacent antenna elements and thus the worst case power reaching the immediate next element is about 39 dBm (8 W). Before it reaches the switches there are cable losses of about 1.5 dB approximately which reduces the power to 37.5 dBm (5.6 W). But currently the high power switches can handle a peak power of 63 dBm (2 kW) and thus from the analysis it can be concluded that these switches are over-rated. A new design was explored with blanking switches on the receiver PCB before the LNA which can handle peak power ranging from 39 dBm (8 W) to 40 dBm (10 W). Thus, even the blanking switches (Analog Devices ADG901) after the LNA can be completely eliminated.

A switch from Skyworks Solutions, Inc AS216-339, which has a very low insertion loss of 0.7 dB and a peak power handling capacity up to 40 dBm (10 W) over a frequency range of 300 kHz to 2.5 GHz [37] was experimented. The switch was characterized on a network analyzer and the insertion loss and isolation values were found to be matching with the data sheet specifications. Figure 5.11 shows the switches introduced on the new receiver front-end PCB for analysis.

Figure 5.11 depicts 2 designs, the first one with the Trilithic bandpass filter to determine the response at 150 MHz. This path cannot be chosen for the final implementation since the bandpass filter has very high insertion loss of ~ 2.5 dB, which degrades the

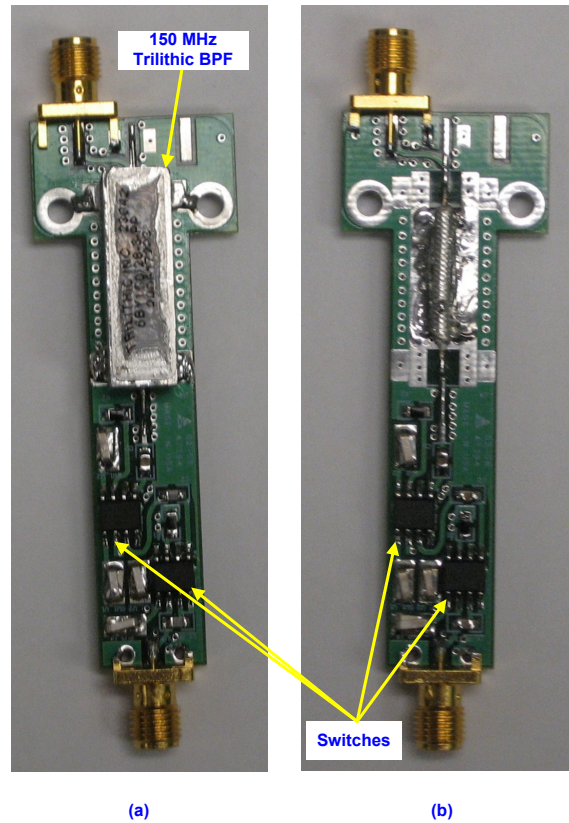


Figure 5.11. Skyworks switches (a) with bandpass filter and (b) without bandpass filter in the receiver path

receiver noise figure significantly. The second design has a shorted filter path and this was to determine the combined insertion loss of both switches in tandem. A maximum insertion loss of 1.1 dB and a minimum isolation of 80 dB was observed in this case and hence the preferred method.

5.5 General improvements

Some general improvements are suggested in the following section.

1. The tx_input and tx_output boards are accommodated in a single chassis as discussed in the previous sections. Currently there is no provision to view the mixer output during debugging. The design can be modified to have an output SMA connector to view the modulator output. This requires modification both in the

transmitter PCB and the chassis design.

2. Documenting the conducted research and results is extremely important. As a part of this project, documents for most of the tasks have been created and this can be continued and improved as a best practice.
3. Thermal stress testing can be automated so as to test the system continuously while recording the s-parameters on the network analyzer.

Chapter 6

Conclusion

We have developed a dual-band multistatic multi-channel airborne radar system for bed characterization and imaging of the polar ice sheets. We have described the radar design and the performance for 150 MHz and 450 MHz cases which validates that the system can detect the weak bed signals overcoming the path attenuation and the inherent system losses. We deployed the system for data collection during the fall 2007 Greenland experiment and accumulated data from high and low elevation flight paths at both frequency bands. This is the first time ever to map and collect the ice bed data successfully with a 450 MHz airborne system. Further we have presented the results both from our laboratory and the actual experiment. The lab results enabled us to improve the transmit waveform by performing pre-distortion and amplitude tapering which improved the range sidelobe reduction before going for the actual field exploration. From the field experiment results, we have observed that there are high losses in the signal returns at 450 MHz than predicted by the current models. Further, the 450 MHz system requires more transmit energy than the 150 MHz system to match the performance with each other.

Appendix A

Schematic and PCB Layout

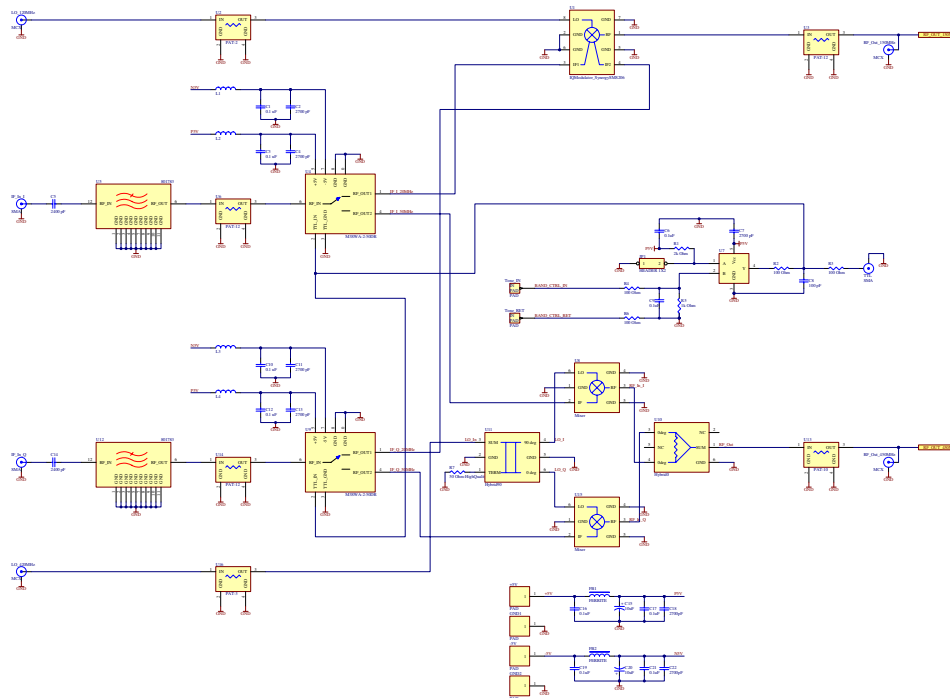


Figure A.1. Transmitter input schematic

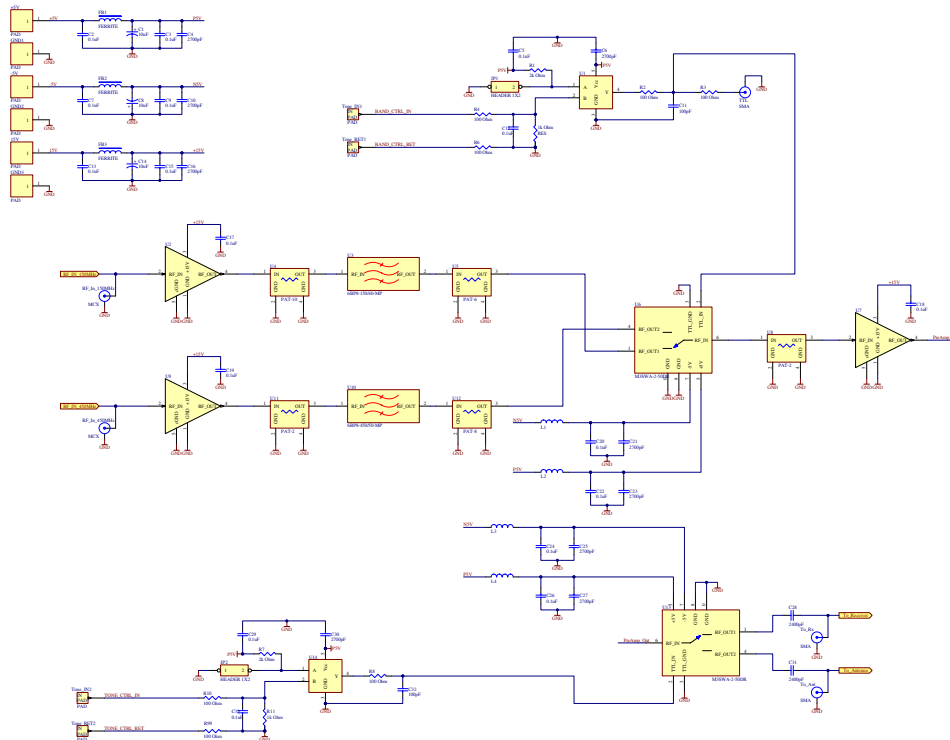


Figure A.2. Transmitter output schematic

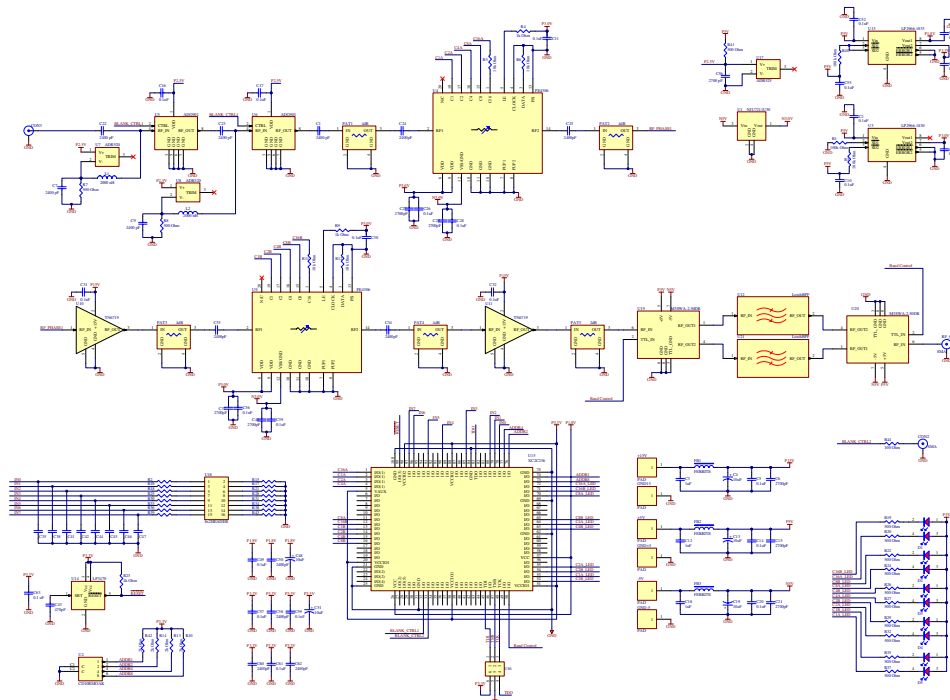


Figure A.3. Receiver output schematic

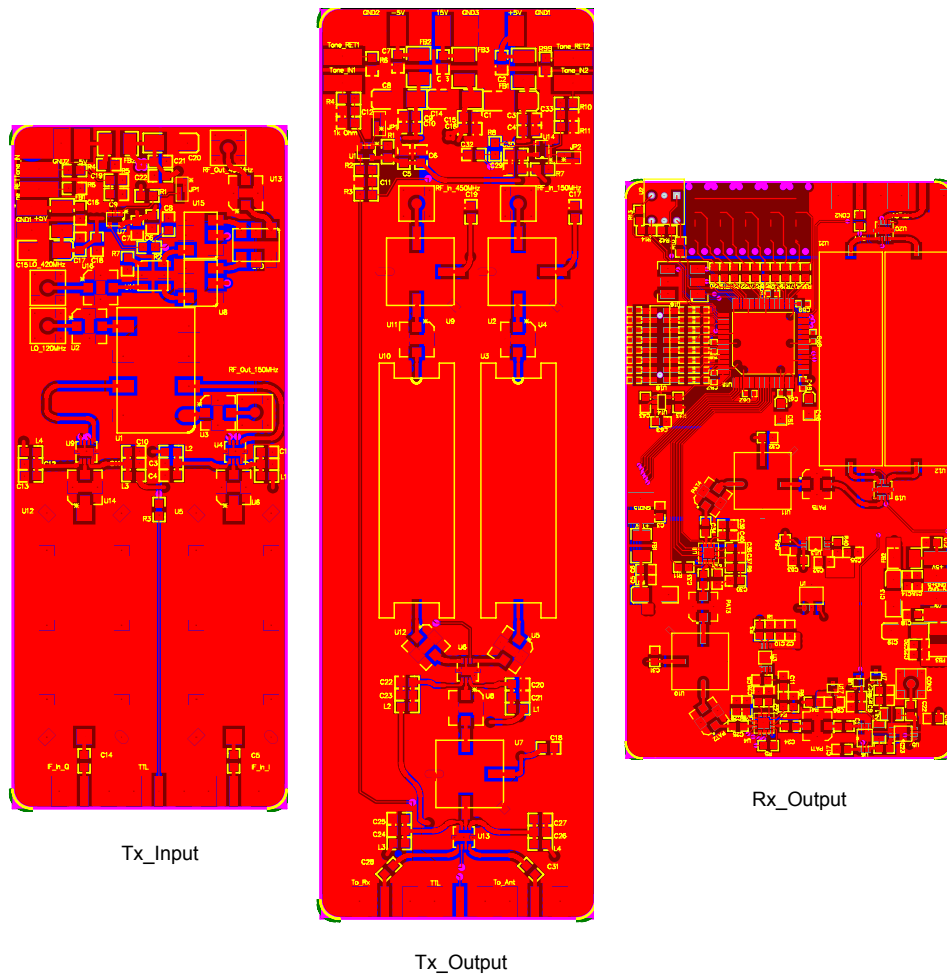


Figure A.4. Transmitter and receiver PCBs

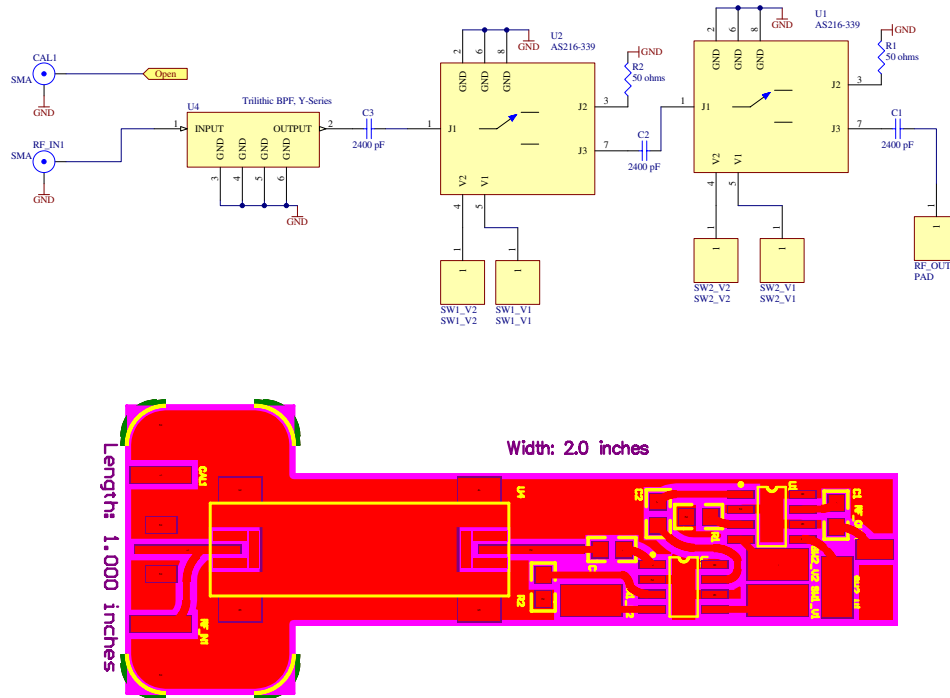


Figure A.5. Receiver input with Skyworks AS216-339 switch introduced between Trilithic band-pass filter and Miteq LNA

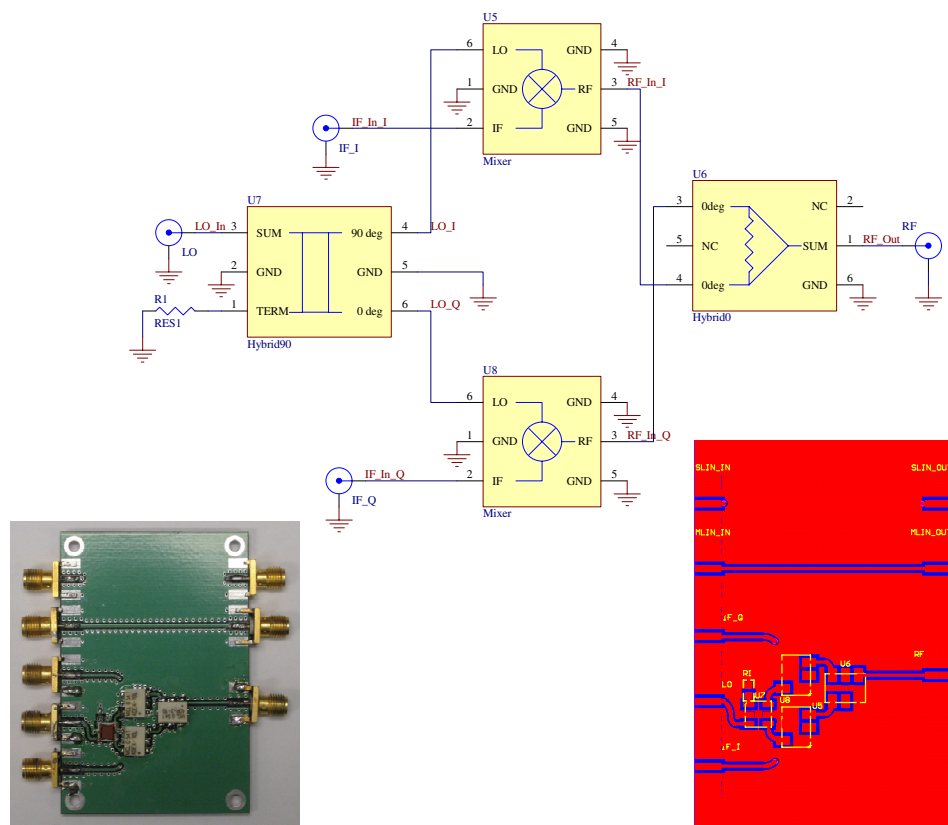


Figure A.6. In-house developed CReSIS-MiniCircuits IQ modulator

Appendix B

Matlab Listing

B.1 Program listing 1

```
% Function to get the s parameters
% Author: John Paden
% Modified by: Sahana Raghunandan, Kiran C Marathe

function gismo_getNAdata(numAve,numMeas, addr, atten1, atten2, blank, band)
% getNAdata(numAve,numMeas)
% numAve = hardware averages in NA
% numMeas = separate measurements stored to file
%
% Typical usage:
% getNAdata(1,1);
% putNAsettings(NA)
% putNAcal(NA.calArray)
%
% NOTE: If the program crashes, it will not close the gpib
% object. The GPIB object must be closed before running the
```

```
% program again. The GPIB object is "obj" and is set to be
% a global variable in this program. So from command line:
% global obj; fclose(obj);

format compact; format long;
% Hewlett Packard (Agilent) 8722C, 8722D, and 8753D all appear to work

global obj;
% Open 'ni' National Instrument card, board 0, GPIB interface 16
% Verify that your NA is set to address 16 (under "Local" button on NA)
obj = gpib('ni',0,18);
% Need to increase input buffer size:
% Maximum number of points = 1601 points
% Real + Imag = 2 doubles per point
% 8 bytes per double
set(obj,'InputBufferSize',2*1601*8);
% Increase time out to allow the instrument a long time to take data
% (for really slow datasets, you may have to increase this more)
set(obj,'Timeout',100);

fopen(obj);

fprintf(obj,'CORR ON');
fprintf(obj,'AVEROON');
fprintf(obj,sprintf('AVERFACT %.0d',numAve));
% The following settings should be set by the user already
% (left here only for future reference)
```

```

% fprintf(obj,'POIN 1601');
% fprintf(obj,'STAR 300e6');
% fprintf(obj,'STOP 2e9');
% fprintf(obj,'IFBW 1000');
% fprintf(obj,'POWE -10');

for ind = 1:numMeas

fprintf('Measurement %.0d of %.0d\n',ind,numMeas);
fprintf(obj,sprintf('NUMG %.0d',numAve));

fprintf(obj,'S11;');
fprintf(obj,'FORM5;');
fprintf(obj,'OUTPDATA;');
hdr = char(fread(obj,2,'char')).';
if ~strcmp(hdr,'#A')
    fprintf('Error in header\n');
end
len = fread(obj,1,'ushort')/8;
tmp = fread(obj,2*len,'float');
tmp = reshape(tmp,[2 len]).';
S11(:,ind) = tmp(:,1) + j*tmp(:,2);
fprintf(obj,'S21;');
fprintf(obj,'FORM5;');
fprintf(obj,'OUTPDATA;');
char(fread(obj,2,'char'));
len = fread(obj,1,'ushort')/8;
tmp = fread(obj,2*len,'float');

```

```

tmp = reshape(tmp,[2 len]).';
S21(:,ind) = tmp(:,1) + j*tmp(:,2);
fprintf(obj,'S12;');
fprintf(obj,'FORM5;');
fprintf(obj,'OUTPDATA;');
char(fread(obj,2,'char'));
len = fread(obj,1,'ushort')/8;
tmp = fread(obj,2*len,'float');
tmp = reshape(tmp,[2 len]).';
S12(:,ind) = tmp(:,1) + j*tmp(:,2);
fprintf(obj,'S22;');
fprintf(obj,'FORM5;');
fprintf(obj,'OUTPDATA;');
char(fread(obj,2,'char'));
len = fread(obj,1,'ushort')/8;
tmp = fread(obj,2*len,'float');
tmp = reshape(tmp,[2 len]).';
S22(:,ind) = tmp(:,1) + j*tmp(:,2);

end

% Get NA settings and create log file
NA = getNASettings(obj);
NA.ave = numAve;
NA.calArray = getNACal(obj);
fprintf(obj,'*IDN?');
NA.idn = fscanf(obj)
fclose(obj);

```



```

% Save s-parameters
rx_num = num2str(addr);
atten_1 = num2str(atten1);
atten_2 = num2str(atten2);
blnk = num2str(blank);
bandctrl = num2str(band);

filename = strcat('gismorx','_',rx_num,'_',atten_1,'_',atten_2,'_',blnk,...
'_',bandctrl)
save(['C:\gismo\sparams\rx\' filename'],'S11','S21','S12','S22','NA');

return;

```

B.2 Program listing 2

```

% Function to set the GISMO receiver parameters
% Author: Torry Akins
% Modified by: Sahana Raghunandan, Kiran C Marathe

function gismo_attenblnkband(addr, atten1, atten2, blank, bandctrl)

parport = digitalio('parallel','LPT1');
% hwinfo = daqhwinfo(parport)
% Port 0, Lines 0:2
hline = addline(parport, 0:7, 0, 'Out')

```

```
dataWord = [];  
% Allocate software values  
addr = mod(addr,8);  
if floor(addr/4),  
    dataWord = 1;  
else,  
    dataWord = 0;  
end;  
addr = mod(addr,4);  
if floor(addr/2),  
    dataWord = [dataWord 1];  
else,  
    dataWord = [dataWord 0];  
end;  
addr = mod(addr,2);  
if floor(addr/1),  
    dataWord = [dataWord 1];  
else,  
    dataWord = [dataWord 0];  
end;  
  
dataWord = [dataWord 0 0 0 0];  
  
atten1Word = [];  
% Allocate software values  
atten1 = mod(atten1,32);  
if floor(atten1/16),  
    atten1Word = 1;
```

```
else,
    atten1Word = 0;
end;
atten1 = mod(atten1,16);
if floor(atten1/8),
    atten1Word = [atten1Word 1];
else,
    atten1Word = [atten1Word 0];
end;
atten1 = mod(atten1,8);
if floor(atten1/4),
    atten1Word = [atten1Word 1];
else,
    atten1Word = [atten1Word 0];
end;
atten1 = mod(atten1,4);
if floor(atten1/2),
    atten1Word = [atten1Word 1];
else,
    atten1Word = [atten1Word 0];
end;
atten1 = mod(atten1,2);
if floor(atten1/1),
    atten1Word = [atten1Word 1];
else,
    atten1Word = [atten1Word 0];
end;
```

```
atten2Word = [];  
% Allocate software values  
atten2 = mod(atten2,32);  
if floor(atten2/16),  
    atten2Word = 1;  
else,  
    atten2Word = 0;  
end;  
atten2 = mod(atten2,16);  
if floor(atten2/8),  
    atten2Word = [atten2Word 1];  
else,  
    atten2Word = [atten2Word 0];  
end;  
atten2 = mod(atten2,8);  
if floor(atten2/4),  
    atten2Word = [atten2Word 1];  
else,  
    atten2Word = [atten2Word 0];  
end;  
atten2 = mod(atten2,4);  
if floor(atten2/2),  
    atten2Word = [atten2Word 1];  
else,  
    atten2Word = [atten2Word 0];  
end;  
atten2 = mod(atten2,2);  
if floor(atten2/1),
```

```

        atten2Word = [atten2Word 1];
else,
        atten2Word = [atten2Word 0];
end;

dataWord = [dataWord atten2Word atten1Word atten2Word atten1Word ...
            atten2Word atten1Word atten2Word atten1Word];

dataWord = logical(dataWord);
writeDataWord(parport, dataWord, blank, bandctrl);

% bvdata = logical([0]);
% putvalue(parport.Line(2),bvdata)
% portval = getvalue(parport)

delete(parport);
clear parport;

return;

%-----
function [LE, CLK, Data, RxMode1, RxMode0, RxBlank1, RxBlank0,...
        RxBand] = getConfig()
% white - grey - yellow
white = 1;          % IN0
grey = 2;          % IN1
yellow = 3;        % IN2
orange = 4;        % IN3

```

```

red = 5;           % IN4
green = 6;        % IN5
blue = 7;         % IN6
purple = 8;       % IN7
LE = yellow;
CLK = white;
Data = grey;
RxMode1 = blue;
RxMode0 = green;
RxBlank1 = red;
RxBlank0 = orange;
RxBand = purple;
return;

%-----
function writeDataWord(parport, dataWord, blank, bandctrl)

[LE, CLK, Data, RxMode1, RxMode0, RxBlank1, RxBlank0,...
 RxBand] = getConfig;

delay = 0;

% Latch enable low

bvdata([LE CLK Data RxMode1 RxMode0 RxBlank1 RxBlank0 RxBand])...
 = logical([0 0 0 0 0 blank blank bandctrl]);
putvalue(parport, bvdata);
pause(delay);

```

```

% fprintf('Latch low\n');
for ind = 1:length(dataWord)
    % Set data line and clock data in
    dataBit = dataWord(ind);
    % fprintf('Writing bit %.0f: %.0f\n',ind,dataBit);
    bvdata([LE CLK Data RxMode1 RxMode0 RxBlank1 RxBlank0])...
    = logical([0 0 dataBit 0 0 blank blank]);
    putvalue(parport,bvdata);
    pause(delay);
    bvdata([LE CLK Data RxMode1 RxMode0 RxBlank1 RxBlank0])...
    = logical([0 1 dataBit 0 0 blank blank]);
    putvalue(parport,bvdata);
    pause(delay);
    bvdata([LE CLK Data RxMode1 RxMode0 RxBlank1 RxBlank0])...
    = logical([0 0 dataBit 0 0 blank blank]);
    putvalue(parport,bvdata);
    pause(delay);
end
% fprintf('Latch high\n');
% Latch enable high
bvdata([LE CLK Data RxMode1 RxMode0 RxBlank1 RxBlank0])...
    = logical([1 0 0 0 0 blank blank]);
putvalue(parport,bvdata);
pause(delay);

return;

```

B.3 Program listing 3

```

% Main function for GISMO Rx settings
% Author: Kiran C Marathe

clc;

clear all;

close all;

% Rx parameters

% Atten1, Atten2, Blank and Band Control

ATTEN_MAX = 0;
ATTEN_MIN = 0;

addr = 2;          % Rx number

blank = 1;        % 1 = No Blanking

freband = [150 450];

% NA parameters

avg_1 = 1;        % Number of averages
avg_2 = 1;        % Number of measurements

% 1 = 450 MHz band; 0 = 150 MHz band

for band = 0:1

    for atten_1 = ATTEN_MIN:ATTEN_MAX

        for atten_2 = ATTEN_MIN:ATTEN_MAX

            % Set Rx parameters

            gismo_attenblnkband(addr, atten_1, atten_2, blank, band);

            % Perform NA testing

            % Create log file with settings and also individual filenames

            % To change the file storage location, edit gismo_getNAdata.m

```



```

        gismo_getNAdata(avg_1, avg_2, addr, atten_1, atten_2, ...
            blank, freband(band+1));
    end
end
end
end

```

B.4 Program listing 4

```

% Program for chirp simulation
% Author: Anthony Hoch

addpath F:\WAVES\Waveform_Programs\GISMO_programs

clear all; close all; clc;

% DEFINE CHIRP SIGNAL
f0 = 10e6; % Linear chirp starting frequency,Hz
f1 = 30e6; % Linear chirp ending frequency,Hz
fc = (f0+f1)/2; % Linear chirp center frequency, Hz
BW = f1-f0; % Linear chirp bandwidth,Hz
pulseDuration = 10e-6; % linear chirp duration,sec
alpha = pi*BW/pulseDuration; % Chirp rate, Hz/Sec
wc = 2*pi*fc; % Angular center frequency
w0 = 2*pi*f0; % Angular starting frequency

% DEFINE SYSTEM PARAMETERS
Fs = 120e6; % Sampling Frequency, Hz
dt = 1/Fs; % Sampling Rate, sec

```

```

nt = 2*ceil(0.5*pulseDuration/dt); % number of time samples
time = (0:1:nt-1)*dt;           % time array for data acquisition

% DETERMINE WAVEFORMS IN TIME DOMAIN
signal_s_t = exp(j*w0*time+j*alpha*(time.^2)); % waveform in time domain
signal_w_t = signal_s_t.*tukeywin(nt,0.35).'; % amplitude tapering

FreqWeight = 1 + [0.0 : [0.35/length(signal_w_t(2:end))] : 0.35];
signal_w_t = [signal_w_t.*FreqWeight]./max([signal_w_t.*FreqWeight]);

% WRITE WAVEFORM FILES FOR RADAR INPUT
% EXAMPLE : writeWaveformFile(file_name,data,start_freq,stop_freq,...
pulse_length,sampling_freq,timeDelay,data_type)
%writeWaveformFile('AMH_R020_BW20_PD10_UP035.wf',conj([0 signal_w_t 0]),...
f0,f1,2*pulseDuration,Fs,0,'int16');

figure(1); plot(real(conj([0 signal_w_t 0]))); title('real');
figure(2); plot(imag(conj([0 signal_w_t 0]))); title('image');

df = 1/time(end); freq = [1:1:nt].*df;
figure(3); plot(freq,abs(fft((conj([ signal_w_t ])))))'; title('image');
figure(4); plot(freq,abs(fft(([ signal_w_t ])))))'; title('real');
grid on;

```

B.5 Program listing 5

```

% Plotting the echogram and A-scope
% Author: Kiran C Marathe

```

```
close all;
clear all;
clc;
load 'sar_September21_145-149.mat';
load 'September21_145-149range_stackIncohLG.mat';

idx = 1:839;
new_var = f_stackIncoh/max(max(f_stackIncoh));
imagesc([], xrangeLG((idx-1)*6+1)-h0, 20*log10(abs(new_var)), [-80 0]);
xlabel('Along track record number');
ylabel('Depth in ice (m)');
title('');
figure;
plot((xrangeLG((idx-1)*6+1)-h0), 20*log10(1000*abs(f_stackIncoh(:,70))),...
     'LineWidth', 2.5);
ylabel('Signal Power (dBm)');
xlabel('Depth in ice (m)');
title('');
grid on;
```

Appendix C

Bill of Materials

Receiver Front-end

Line #	Qty	Style	Description	Package	Ref Design	Manufacturer	Manufacturer P/N	Vendor	Vendor P/N	Price/Part	Notes
1	1	SMD	Capacitor : 470 pF	0805	C43	Panasonic	ECJ-2VC1H471J	Digi-Key	PCC471CGCT-ND	\$0.05	
2	9	SMD	Capacitor : 2400 pF	0805	C1, C7, C9, C22, C23, C24, C25, C33, C34	Murata Electronics	GRM2165C1H242JA01D	Digi-Key	490-1629-1-ND	\$0.19	
3	4	SMD	Capacitor : 2400 pF	0603	C50, C58, C60, C62	Murata Electronics	GRM1885C1H242JA01D	Digi-Key	490-3282-1-ND	\$0.16	
4	8		Capacitor : 2700 pF	0805	C6, C15, C21, C27, C29, C37, C40, C56	Panasonic	ECJ-2VC1H272J	Digi-Key	PCC2159CT-ND	\$0.21	
5	21	SMD	Capacitor : 0.1 uF	0805	C2, C5, C8, C10, C11, C14, C16, C17, C20, C26, C28, C30, C31, C32, C36, C39, C52, C53, C54, C55, C63	Panasonic	ECJ-2YB1H104K	Digi-Key	PCC1840CT-ND	\$0.16	
6	12	SMD	Capacitor : 0.1 uF	0603	C35, C38, C41, C42, C44, C45, C46, C47, C49, C57, C59, C61	Rohm	MCH185CN104KK	Digi-Key	511-1175-1-ND	Not Available	
7	3	SMD	Capacitor : 1 uF	0805	C3, C12, C18	Panasonic	ECJ-2FB1E105K	Digi-Key	PCC2319CT-ND	\$0.13	
8	2	SMD	Capacitor : 10 uF (Tantalum A)	Tant-A	C48, C51	Kemet	T494A106M016A1	Digi-Key	899-3824-1-ND	\$3.78	
9	3	SMD	Capacitor : 10 uF (Tantalum C)	Tant-C	C4, C13, C19	Kemet	T494C108K025A1	Digi-Key	899-3842-1-ND	\$1.43	
10	1	SMD	Resistor : 100 ohm	0805	R44	Rohm	MCR10EZHF1000	Digi-Key	RHM100CCT-ND	\$0.04	
11	16	SMD	Resistor : 100 ohm	0603	R2, R15, R16, R17, R18, R21, R25, R28, R30, R31, R33, R34, R36, R38, R39, R43	Rohm	MCR03EZPFX1000	Digi-Key	RHM100HCT-ND	\$0.06	
12	13	SMD	Resistor : 499 ohm	0805	R7, R8, R19, R20, R22, R24, R26, R27, R29, R32, R35, R37, R41	Rohm	MCR10EZPF4990	Digi-Key	RHM499CRCT-ND	\$0.04	
13	2	SMD	Resistor : 1 kohm	0805	R4, R9	Rohm	MCR10EZHF1001	Digi-Key	RHM1.00KCCT-ND	\$0.04	
14	4	SMD	Resistor : 2 kohm	0805	R10, R13, R14, R42	Panasonic	ERJ-BENF2001V	Digi-Key	P2.00KCCT-ND	\$0.05	
15	1	SMD	Resistor : 4.02 kohm	0805	R23	Rohm	MCR10EZHF4021	Digi-Key	RHM4.02KCCT-ND	\$0.04	
16	4	SMD	Resistor : 10 kohm	0805	R5, R6, R11, R12	Rohm	MCR10EZPF1002	Digi-Key	RHM10.0KCCT-ND	\$0.04	
17	3	SMD	Resistor : 100 kohm	0805	R1, R3, R40	Rohm	MCR10EZPF1003	Digi-Key	RHM100KCCT-ND	\$0.04	
18	3	SMD	Ferrite Bead Core Inductor	SMFB	FB1, FB2, FB3	Panasonic	EXC-CL4532U1	Digi-Key	P9812CT-ND	\$0.61	
19	1	SMD	Fixed Attenuators : 2 dB	PAT-X	PAT5	Mini-Circuits	PAT-2+	Mini-Circuits	PAT-2+	\$2.95	
20	4	SMD	Fixed Attenuators : 4 dB	PAT-X	PAT1, PAT2, PAT3, PAT4	Mini-Circuits	PAT-4+	Mini-Circuits	PAT-4+	\$2.95	
21	2	SMD	Blanking Switch	RM-8	U5, U6	Analog Devices	ADG901	Digi-Key	ADG901BDM-ND	\$2.43	
22	2	SMD	Voltage Regulator : 2 V	SC-70	U7, U8	Analog Devices	ADR520	Digi-Key	ADR520BKS-R2CT-ND	Not Available	
23	1	SMD	Voltage Regulator : 2.5 V	SC-70	U17	Analog Devices	ADR525	Digi-Key	ADR525BKS-R2CT-ND	\$2.43	
24	1	SMD	Voltage Regulator : N3 V	SOT-89	U1	NJR Co., Ltd	NJU7211U30	Mouser Electronics	513-NJU7211U30	\$0.42	
25	1	SMD	Dual Voltage Regulator : 1.8 V/3.0 V	MSOP-8	U3	National Semiconductor	LP2966	Digi-Key	LP2966IMM-1830CT-ND	\$2.33	
26	1	SMD	Dual Voltage Regulator : 1.8 V/3.3 V	MSOP-8	U13	National Semiconductor	LP2966	Digi-Key	LP2966IMM-1833CT-ND	\$2.33	
27	1	SMD	Power on Reset	SOT23-5	U14	National Semiconductor	LP3470	Digi-Key	LP3470IM5-2.63CT-ND	\$1.55	
28	1	TH	10 Position Rotary Switch		U2	ITT Industries	CD10RM0AK	Digi-Key	CKN3046-ND	Not Available	
29	2	SMD	Digital Attenuator	20 pin QFN	U4, U9	Peregrine Semiconductor	PE4306	Richardson Electronics	PE4306-51	\$2.53	
30	2	SMD	Band control switch	DL805	U19, U20	Mini-Circuits	M3SWA-2-50DR+	Mini-Circuits	M3SWA-2-50DR+	\$4.95	
31	1	SMD	Header 8x2		U18	Molex/Waldom electronics Corp	87759-1650	Digi-Key	WM18655-ND	\$2.42	
32	1	SMD	Header 3x2		U16	Molex/Waldom electronics Corp	15-91-0060	Digi-Key	WM17457-ND	\$0.77	
33	2	SMD	Amplifier	SM-3	U10, U11	Spectrum Microwave	TN6719	Spectrum Microwave	TN6719	\$268.00	
34	1	SMD	Bandpass Filter : 150 MHz	2-pin	U12	Lorch Microwave	6BP8-150/40-MP	Lorch Microwave	6BP8-150/40-MP	\$378.00	
35	1	SMD	Bandpass Filter : 450 MHz	2-pin	U21	Lorch Microwave	6BP8-450/50-MP	Lorch Microwave	6BP8-450/50-MP	\$276.00	
36	5	SMD	Bi-level LED		D1, D2, D3, D4, D5	Dialight	592-2222-002F	Allied Electronics	511-0642	\$4.28	
37	1	SMD	Xilinx CPLD	TQFP100	U15	Xilinx		New Horizons Electronics Corp	XC2C256-7VQ100C	\$12.35	
38	1	SMD	MCX connector		CON3			Mouser Electronics	530-133-3711-201	\$5.33	
39	1		Boards for assembly		CRESIS Design	Sierra Protoexpress					

Note SMD : Surface Mount Design
 TH : Thru Hole
 Common manufacturers for Capacitors, Inductors and Resistors are Panasonic, Murata Electronics, Kemet, AVX Corporation, Rohm and Vishay

Figure C.1. Receiver front-end board bill of materials

Frequency Synthesizer

Line #	Qty	Style	Description	Package	Ref Design	Manufacturer	Manufacturer P/N	Vendor	Vendor P/N	Price/Part	Notes
1	4	SMD	Capacitor : 560 pF	0805	C3, C10, C15, C16	Panasonic	ECJ-2VCH561J	Digi-Key	PC561CGTR-ND	\$0.01	Manufacturer/Vendor and P/N are flexible.
2	4	SMD	Capacitor : 2700 pF	0805	C21, C22, C23, C24	Panasonic	ECJ-2VBIH272K	Digi-Key	PCC272BINR-ND	\$0.02	Manufacturer/Vendor and P/N are flexible.
3	1	SMD	Capacitor : 0.01 uF	0805	C27	Panasonic	ECJ-2VBIH103K	Digi-Key	PCC103BINR-ND	\$0.01	Manufacturer/Vendor and P/N are flexible.
4	6	SMD	Capacitor : 0.022 uF	0805	C31	Panasonic	ECJ-2VBIH223K	Digi-Key	PCC223BGTNR-ND	\$0.01	Manufacturer/Vendor and P/N are flexible.
5	10	SMD	Capacitor : 0.1 uF	0805	C9, C13, C28, C29	Panasonic	ECJ-2VBIH104K	Digi-Key	PCC1840CT-ND	\$0.16	Manufacturer/Vendor and P/N are flexible.
6	1	SMD	Capacitor : 1 uF	0805	C26	Kemet	C0805C105K4RACTU	Digi-Key	389-1284-2-ND	\$0.02	Manufacturer/Vendor and P/N are flexible.
7	4	SMD	Capacitor : 1 uF (Tantalum A)	Tant-A	C17, C18, C19, C20	Kemet	B45196H5105K109	Digi-Key	495-2268-2-ND	\$0.05	Manufacturer/Vendor and P/N are flexible.
8	1	SMD	Capacitor : 10 uF (Tantalum C)	Tant-C	C25	Kemet	T494C106K025AT	Digi-Key	389-3842-1-ND	\$1.43	Manufacturer/Vendor and P/N are flexible.
9	2	SMD	Resistor : 30 ohm	0805	R5, R8	Vishay	CR070305030R0FKEA	Digi-Key	541-3010CT-ND	\$0.09	
10	1	SMD	Resistor : 49.9 ohm	0805	R1	Panasonic	ERJ-6ENF4993V	Digi-Key	F49-90CT-ND	\$0.09	
11	1	SMD	Resistor : 80.6 ohm	0805	R11	Panasonic	ERJ-6ENF8063V	Digi-Key	F80-80CT-ND	\$0.09	
12	1	SMD	Resistor : 100 ohm	0805	R4, R10	Panasonic	ERJ-6ENF1000V	Digi-Key	P1000CT-ND	\$0.09	
13	2	SMD	Resistor : 402 ohm	0805	R2	Panasonic	ERJ-6ENF4020V	Digi-Key	P4020CT-ND	\$0.09	
14	1	SMD	Resistor : 2 kohm	0805	R3, R6, R9	Panasonic	ERJ-6ENF200TV	Digi-Key	P210K0CT-ND	\$0.09	
15	3	SMD	Resistor : 4.99 kohm	0805	R4	Panasonic	ERJ-6ENF499TV	Digi-Key	P499K0CT-ND	\$0.09	
16	2	SMD	Ferrite Bead Core Inductor	SMTF	FB1, FB2	Panasonic	EXC-CLJ532U1	Digi-Key	P9812CT-ND	\$0.61	
17	1	SMD	Inductor : 3.9 nH	0402	L1	Murata Electronics	LOPT15MN3N9B02D	Digi-Key	490-1131-1-ND	\$0.20	
18	1	SMD	Inductor : 10 nH	0805	L2	Panasonic	ELJ-ND10NKF	Digi-Key	PCD1160CT-ND	\$0.35	
19	1	SMD	Inductor : 15 nH	0805	L3	Panasonic	ELJ-ND15NKF	Digi-Key	PCD1162FR-ND	\$0.12	
20	2	SMD	Fixed Attenuators : 2 dB	PAT-X	U8, U15	Mini-Circuits	PAT-2	Mini-Circuits	PAT-2	\$2.95	
21	1	SMD	LED-Blevel : Green	TH	D1	Dialight	592-2222-002F	Allied	Electronics 511-0642	\$3.34	
22	3	SMD	Header 3x2 (1 inch) : 6-pin header	SMD	U1, U4, U22	Molex/Wabcom electronics Corp	15-91-0060	Digi-Key	WMT7457-ND	\$0.77	
23	1	SMD	Lowpass Filter : DC to 120 MHz	YY101	U11	Mini-Circuits	SALF-146	Mini-Circuits	WMT7457-ND	\$6.95	
24	1	SMD	Lowpass Filter : DC to ??? MHz	YY101	U16	Mini-Circuits	???	Mini-Circuits	???	Unknown part #.	
25	3	SMD	2 Way power divider	PL-058	U10, U17, U19	Mini-Circuits	LRPS-2-1J	Mini-Circuits	LRPS-2-1J	\$8.95	
26	1	SMD	4 Way power divider	PL-073	U1	Mini-Circuits	SCP-4-1	Mini-Circuits	SCP-4-1	\$24.95	
27	1	SMD	6 dB directional coupler	PL-094	U13	Mini-Circuits	ADC-6-1R	Mini-Circuits	ADC-6-1R	\$7.95	
28	2	SMD	Macom Amplifier	SMTQ-8	U7, U12	Macom	SMA515 or SM51	Richardson Electronics	MAAM0072SMA51	\$233.00	Long Lead Item.
29	1	SMD	Dual Voltage Regulator : 1.8 V/3.3 V	IMSOP-8	U2	National Semiconductor	LP2986	Digi-Key	LP2986MM-1833CT-ND	\$2.33	
30	1	SMD	Power on Reset	LP3470-Reset	U6	National Semiconductor	LP3470M5-2.631NCPB	Digi-Key	LP3470M5-2.63CT-ND	\$1.55	
31	2	SMD	Dual Band PE Synthesizer	MLP-28	U20, U21	Silicon Laboratories	SL133-D-GM	Digi-Key	395-1113-ND	\$10.89	
32	1	SMD	10 MHz Oscillator	ECS-3951	U5	ECS Inc	ECS-3951M-100-BN-TR	Digi-Key	XC2951FR-ND	\$2.78	
33	1	SMD	CoefRunner II CPLD	GFP10X10-G44X.5N	U3	Xilinx	XC2C64A	Electronics	XC2C64A-7VQ44C	\$2.70	Manufacturer : Johnson/Emerson.
34		SMD	MXC Connectors	MXC	120a, 420b 120c, 120d, 120e, 120f, 120g, 420a,			Digi-Key	Check website		Manufacturer : Johnson/Emerson.
35		SMD	SMA Connectors	SMAL	10MHz			Digi-Key	Check website		Manufacturer : Johnson/Emerson.

Note SMD : Surface Mount Design
 TH : Through Hole
 Common manufacturers for Capacitors, Inductors and Resistors are Panasonic, Murata Electronics, Kemet, AVX Corporation, Rohm and Vishay

Figure C.2. Frequency synthesizer bill of materials

RF Transmitter Input

Line #	Qty	Style	Description	Package	Ref Design	Manufacturer	Manufacturer P/N	Vendor	Vendor P/N	Price/Part	Notes
1	1	SMD	Capacitor : 100 pF	0805	C8	Panasonic	ECJ-2VC1H101J	Digi-Key	PCC101CGTR-ND	\$0.01	Verify part #.
2	2	SMD	Capacitor : 2400 pF	0805	C5, C14	Murata Electronics	GFRM2165C1H242JA01D	Digi-Key	490-1629-1-ND	\$0.19	
3	7		Capacitor : 2700 pF	0805	C2, C4, C7, C11, C13, C18, C22	Panasonic	ECJ-2VC1H272J	Digi-Key	PCC2159CT-ND	\$0.21	
4	10	SMD	Capacitor : 0.1 uF	0805	C1, C3, C6, C9, C10, C12, C16, C17, C19, C21	Panasonic	ECJ-2YB1H104K	Digi-Key	PCC1840CT-ND	\$0.16	
5	2	SMD	Capacitor : 10 uF (Tantalum C)	Tant-C	C15, C20	Kemet	T494G108K025AT	Digi-Key	399-3842-1-ND	\$1.43	Polarity Capacitors.
6	1	SMD	Resistor : 50 ohm (High Quality)	0805	R7	American Technical Ceramics	CT11005T0050JBK	Digi-Key			
7	4	SMD	Resistor : 100 ohm	0805	R2, R3, R4, R6	Rohm	MCR10EZHF1000	Digi-Key	RHM100CG1-ND	\$0.04	
8	1	SMD	Resistor : 1 kohm	0805	R5	Rohm	MCR10EZHF1001	Digi-Key	RHM100KCGT-ND	\$0.04	
9	1	SMD	Resistor : 2 kohm	0805	R1	Panasonic	ERJ-6ENF2001V	Digi-Key	P200KCGT-ND	\$0.09	
10	2	SMD	Ferrite Bead Core inductor	SMFB	FB1, FB2	Panasonic	EXC-CL4532U1	Digi-Key	P9812CT-ND	\$0.61	
11	4	SMD	Inductor	0805	L1, L2, L3, L4	Panasonic	EXC-ML20A390U	Digi-Key	P1019TCT-ND	\$0.26	
12	6	SMD	Fixed Attenuators : 2 dB to 20 dB in steps of 1 dB or 2dB when not available	PAT-X	U2, U3, U6, U13, U14, U16	Mini-Circuits	PAT-x+	Mini-Circuits	PAT-x+	\$2.95	
13	2	SMD	Band control switch	DL805	U4, U9	Mini-Circuits	M3SWA-2-50DR+	Mini-Circuits	M3SWA-2-50DR+	\$4.95	
14	1	SMD	Header 1x2 (1 mm)		JP1	Comm Con Connectors		Digi-Key			Unknown part #. But on digikey it can be searched with following filters. 1mm Center .012 inch Square Pin -Single Row Straight SMD Header - with stacking option
15	2	SMD	Lowpass Filter : DC to 55 MHz	2-pin	U5, U12	Bree Engineering	801783	Engineering	801783	\$318.29	
16	2	SMD	Mixer (450 MHz)	PL-052	U8, U15	Mini-Circuits	ADEX-10L	Mini-Circuits	ADEX-10L	\$2.95	Long Lead Item.
17	1	SMD	Mixer (150 MHz)	102S	U1	Synergy Microwave	SMS206	Microwave	SMS206	\$80.95	
18	1	SMD	Hybrid0	PL-052	U10	Mini-Circuits	ADP-2-10	Mini-Circuits	ADP-2-10	\$12.95	
19	1	SMD	Hybrid90	PL-114	U11	Mini-Circuits	HPQ-05	Mini-Circuits	HPQ-05	\$6.95	
20	1	SMD	Ex-OR Gate	LP-3470	U7	Fairchild Semiconductor	NC7ST86M5X	Mouser Electronics	512-NC7ST86M5X	\$0.14	
21	4	SMD	MCX Connectors	MCX		Johnson Components		Digi-Key			Unknown part #. But can be searched on digikey. 50 ohm, straight, end launch jack receptacle-round contact.
22	3	SMD	SMA Connectors	SMAL		Johnson Components		Digi-Key			

Note SMD : Surface Mount Design
Common manufacturers for Capacitors, Inductors and Resistors are Panasonic, Murata Electronics, Kemet, AVX Corporation, Rohm and Vishay

Figure C.3. Transmitter input board bill of materials

RF Transmitter Output

Line #	Qty	Style	Description	Package	Ref Design	Manufacturer	Manufacturer P/N	Vendor	Vendor P/N	Price/Pack	Notes
1	2	SMD	Capacitor : 100 pF	0805	C11, C32	Panasonic	ECJ-2VC1H101J	Digi-Key	PCC1010GTR-ND	\$0.01	Please verify the part #
2	2	SMD	Capacitor : 2400 pF	0805	C28, C31	Murata Electronics	GRM2165C1H242JA01D	Digi-Key	490-1629-1-ND	\$0.19	
3	9		Capacitor : 2700 pF	0805	C4, C6, C10, C16, C21, C23, C25, C27, C30, C2, C3, C5, C7, C9, C12, C13, C15, C17, C18, C19, C20, C22, C24, C26, C28, C33	Panasonic	ECJ-2VC1H272J	Digi-Key	PCC2159CT-ND	\$0.21	
4	17	SMD	Capacitor : 0.1 uF	0805	C1, C8, C14	Panasonic	ECJ-2YB1H104K	Digi-Key	PCC1840CT-ND	\$0.16	
5	3	SMD	Capacitor : 10 uF (Tantalum C)	Tant-C	C1, C8, C14	Kemet	T494C106K025AT	Digi-Key	399-3842-1-ND	\$1.43	Polarity Capacitors.
6	7	SMD	Resistor : 100 ohm	0805	R2, R3, R4, R6, R8, R10, R99	Rohm	MCR10EZHF1000	Digi-Key	RHM100CCT-ND	\$0.04	
7	2	SMD	Resistor : 1 kohm	0805	R11, 1K Ohm	Rohm	MCR10EZHF1001	Digi-Key	RHM100KCT-ND	\$0.04	
8	2	SMD	Resistor : 2 kohm	0805	R1, R7	Panasonic	ERJ-6ENF2001V	Digi-Key	P2.00KCT-ND	\$0.09	
9	3	SMD	Ferrite Bead Core Inductor	SMFB	FB1, FB2, FB3	Panasonic	EXC-CL4532U1	Digi-Key	P9812CT-ND	\$0.61	
10	4	SMD	Inductor	0805	L1, L2, L3, L4	Panasonic	EXC-ML20A390U	Digi-Key	P10191CT-ND	\$0.26	
11	5	SMD	Fixed Attenuators : 2 dB to 20 dB in steps of 1 dB or 2dB when not available	PAT-X	U4, U5, U8, U11, U12	Mini-Circuits	PAT-X+	Mini-Circuits	PAT-X+	\$2.95	Mainly 2dB.
12	2	SMD	Band control switch	DL805	U6, U13	Mini-Circuits	M3SWA-2-50DR+	Mini-Circuits	M3SWA-2-50DR+	\$4.95	
13	2	SMD	Header 1x2 (1 mm)		JP1, JP2	Comm Con Connectors		Digi-Key			Unknown part #. But on digikey it can be searched with following filters. 1mm Center .012 inch Square Pin - Single Row Straight SMD Header - with stacking option
14	1	SMD	Lorch Bandpass Filter : 150 MHz	2-pin	U3	Lorch Microwave	6BP8-150/40-MP	Lorch	6BP8-150/40-MP	\$378.00	Long Lead Item.
15	1	SMD	Lorch Bandpass Filter : 450 MHz	2-pin	U10	Lorch Microwave	6BP8-450/50-MP	Lorch	6BP8-450/50-MP	\$276.00	Long Lead Item.
16	2	SMD	Ex-OR Gate	LP3470	U1, U14	Fairchild Semiconductor	NC7ST86M5X	Mouser Electronics	512-NC7ST86M5X	\$0.14	
17	3	SMD	Macom Amplifier		U2, U7, U9	Macom	SMA515 or SM51	Richardson Electronics	MAAM00727SMA51	\$233.00	Long Lead Item.
18	2	SMD	MCX Connectors	MCX				Digi-Key			Unknown part #. But can be searched on digikey.
19	3	SMD	SMA Connectors	SMAL		Johnson Components		Digi-Key			50 ohm, straight, end launch jack receptacle-round contact.

Note SMD : Surface Mount Design
Common manufacturers for Capacitors, Inductors and Resistors are Panasonic, Murata Electronics, Kemet, AVX Corporation, Rohm and Vishay

Miscellaneous List

Line #	Qty	Style	Description	Package	Ref Design	Manufacturer	Manufacturer P/N	Vendor	Vendor P/N	Price/Part	Notes
1	1		Receiver Coupler Board		CReSIS	Sierra Protoexpress					Or any other PCB manufacturer
2	1		Receiver MCX Board		CReSIS	Sierra Protoexpress					Or any other PCB manufacturer
3	2		cPCI RF Power Board (Tx and Rx)		CReSIS	Sierra Protoexpress					Or any other PCB manufacturer
4	4		MCX(M)-MCX(M) Cable for Tx of length 7 in (approx)		CReSIS	CReSIS				In-house	
5	2		MCX(M)-MCX(M) Cable for Rx of length 1.5 in (approx)		CReSIS	CReSIS				In-house	
6	20		24 AWG wires for power supply connections and band Control - TX		CReSIS						At least 5 different colors
7	8		24 AWG wires for power supply connections - RX		CReSIS						At least 4 different colors
8	1		Data Cable for Rx		CReSIS						
9	1		Aluminum Chassis with lid for Tx		CReSIS	CReSIS				In-house	
10	1		Aluminum Chassis with lid for Rx		CReSIS	CReSIS				In-house	
11	4		Ears for the Chassis		CReSIS	CReSIS		Digikey			
12	3		Male-Female Headers (8x2) for data transfer - Rx		CReSIS			Digikey			
13	6		Male-Female Headers (8x2) for power supply - Tx/Rx		CReSIS			Digikey			
14	2		Connector which goes to back plane		CReSIS						
15	14		SMA Connectors for Tx		CReSIS			Digikey			
16	8		SMA Connectors for Rx		CReSIS			Digikey			
17	16		Screws for holding the Tx PCBs		CReSIS			Digikey			
18	26		Screws for holding the Rx PCBs		CReSIS			Digikey			
19	30		Screws for holding the Tx chassis lid		CReSIS			Digikey			
20	38		Screws for holding the Rx chassis lid		CReSIS			Digikey			

Appendix D

Publications

- Marathe K., Jara V., Raghunandan S., Akins T., Kanagaratnam P., Gogineni S., Allen C., Braaten D. and Jezek K., 'Airborne Radar Demonstrator for Imaging of Ice-Bed Interface', Graduate Engineering Association Research Poster Competition 2006, University of Kansas, USA.
- Marathe K., Jara V., Raghunandan S., Akins T., Kanagaratnam P., Gogineni S., Allen C., Braaten D. and Jezek K., 'Airborne Radar Demonstrator for Imaging of Ice-Bed Interface', AGU Fall 2006 Meeting, San Francisco, USA.
- Kiran C. Marathe, Victor A. Jara, 'Advanced Remote Sensing Radar System to Study the Role of Polar Ice Sheets in Sea-Level Change', Graduate Engineering Association Research Poster Competition 2007, University of Kansas, USA.
- Fernando Rodriguez-Morales, Prasad Gogineni, Kenneth Jezek, Christopher Allen, Carl Leuschen, Kiran Marathe, Victor Jara-Olivares, Anthony Hoch, Jilu Li and John Ledford, 'Dual-Frequency and Multi-Receiver Radars for Sounding and Imaging Polar Ice Sheets', EUSAR 2008 conference, Friedrichshafen, Germany.
- K. C. Marathe, V. A. Jara, S. Raghunandan, F. Rodriguez-Morales, J. Ledford, S. Gogineni, C. Allen and K. Jezek, 'Dual-Band Airborne Radar for Mapping the

Internal and Basal Layers of Polar Ice Sheets', CSRE workshop 2008, IIT Mumbai, India.

References

- [1] Haskell Indian Nations University, “Sea Level Rise Maps.” CReSIS Internal Communication and Poster Competition, 2006.
- [2] IPCC, Summary for Policymakers (SPM), ed., *Climate Change 2007: The Physical Science Basis: Contribution of Working Group I to the Fourth Assessment Report of the Intergovernmental Panel on Climate Change*, February 2007.
- [3] Sarah Zielinski, “Climate Change Report Adds to Evolving Debate,” *EOS, Transactions, American Geophysical Union*, vol. 88, p. 84, February 2007.
- [4] Marco Tedesco, “A New Record in 2007 for Melting in Greenland,” *EOS, Transactions, American Geophysical Union*, vol. 88, p. 383, September 2007.
- [5] Rob Larter, Karsten Gohl, Claus-Dieter Hillenbrand, Gerhard Kuhn, Tara Deen, Reinhard Dietrich, Graeme Eagles, Joanne Johnson, Roy Livermore, Frank Nitsche, Carol Pudsey, Hans-Werner Schenke, James Smith, Gleb Udintsev and Gabriele Uenzelmann-Neben, “West Antarctic Ice Sheet Change Since the Last Glacial Period,” *EOS, Transactions, American Geophysical Union*, vol. 88, p. 189, April 2007.
- [6] Harold Sobol and Kiyoo Tomiyasu, “Milestones of Microwaves,” *IEEE Transactions on Microwave Theory and Techniques*, vol. 50, p. 594:611, March 2002.
- [7] S. Mozaffar, “Multiband Multistatic Synthetic Aperture Radar for Measuring Ice Sheet Basal Conditions,” Master’s thesis, University of Kansas, 2005.

- [8] A. Lohofener, "Design and Development of a Multi-Channel Radar Depth Sounder," Master's thesis, University of Kansas, 2006.
- [9] Kenneth Jezek, "Glaciers and Ice Sheets Interferometric Radar." A proposal submitted to NASA Science Mission Directorate in response to Instrument Incubator Project, November 2004.
- [10] Sahana Raghunandan, "Design and Analysis of Frequency Synthesizer for MCRDS/IIP," tech. rep., CReSIS, University of Kansas, February 2006.
- [11] John Paden, Shadab Mozaffar, David Dunson, Chris Allen, Sivaprasad Gogineni and Torry Akins, "Multiband Multistatic Synthetic Aperture Radar for Measuring Ice Sheet Basal Conditions," *IEEE Geoscience and Remote Sensing Letters*, vol. 1, pp. :–139, September 2004.
- [12] John D. Paden, Christopher T. Allen, Sivaprasad Gogineni, Kenneth C. Jezek, Dorte Dahl-Jensen and Lars B. Larsen, "Wideband Measurements of Ice Sheet Attenuation and Basal Scattering," *IEEE Geoscience and Remote Sensing Letters*, vol. 2, p. 164:168, April 2005.
- [13] K. Jezek, E. Rodriguez, P. Gogineni, J. Curlander, A. Freeman and X. Wu, "A Design Concept for Spaceborne Imaging of the Base of Terrestrial Ice Sheets and Icy Bodies in the Outer Solar," *Workshop on Radar Investigations of Planetary and Terrestrial Environment*, p. 6043, February 2005.
- [14] George L. Matthaei, Leo Young and E. M. T. Jones, *Microwave Filters, Impedance-Matching Networks, and Coupling Structures*. Artech House Books, 1980.
- [15] Maxim IC, *Equalizing Techniques Flatten DAC Frequency Response*, June 2006. Application Note 3853.
- [16] Sivaprasad Gogineni, "Private Communication," February 2007.

- [17] JFW Industries, Inc, *Specification Sheet for 50S-1532 1P2T Self Terminating Solid State RF Switch*, December 2006. Data Sheet.
- [18] Christopher T. Allen, Manisha Gandhi, Prasad Gogineni and Ken Jezek, "Feasibility study for mapping the polar ice bottom topography using interferometric synthetic-aperture radar techniques," tech. rep., University of Kansas, January 1997.
- [19] Victor Jara-Olivares, "Glaciers and Ice Sheets Mapping Orbiter (GISMO), EECS891 Graduate Problems," tech. rep., University of Kansas, August 2006.
- [20] Victor Jara-Olivares, "Testing Results for Antenna Array," tech. rep., CReSIS, University of Kansas, March 2006.
- [21] Fernando Rodriguez-Morales, Prasad Gogineni, Kenneth Jezek, Christopher Allen, Carl Leuschen, Kiran Marathe, Victor Jara-Olivares, Anthony Hoch, Jilu Li and John Ledford, "Dual-Frequency and Multi-Receiver Radars for Sounding and Imaging Polar Ice Sheets," *EuSAR*, 2008. In press.
- [22] Torry Akins, "Private Communication," September 2005.
- [23] John Ledford, "GISMO Radar Operator Manual 2007, 1.0," tech. rep., CReSIS, University of Kansas, April 2007.
- [24] CReSIS Team, "Glaciers and Ice Sheets Mapping Orbiter Test Plan," tech. rep., CReSIS, University of Kansas, Mar 2007.
- [25] Anthony Hoch, "Private Communication," Jan 2008.
- [26] Agilent Technologies, *Agilent Spectrum Analysis Basics*, August 2006. Application Note 150.
- [27] Kenneth Jezek, "GISMO: Fall Arctic '07 Flight Planning Document," tech. rep., CReSIS, August 2007.

- [28] Ralph Girard, Pok F. Lee and Kenneth James, "The RADARSAT-2&3 topographic mission: an overview," *Geoscience and Remote Sensing Letters, IEEE*, vol. 3, p. 1477:1479, November 2002.
- [29] K. Jezek and X. Wu, "GISMO Data Review: Range Compressed Data," tech. rep., CReSIS, November 2007.
- [30] Victor Jara-Olivares and Fernando Rodriguez-Morales, "Testing Results for Delta-Sigma Power Amps," tech. rep., CReSIS, University of Kansas, February 2007.
- [31] Mini-Circuits, *Most often asked questions on IQ and QPSK Modulators-Demodulators*, September 1999.
- [32] Robert G. Swartz, "Active Mixer ICs Challenge The Passive Status Quo," September 2003. <http://electronicdesign.com/Articles/Index.cfm?AD=1&ArticleID=5691#>.
- [33] Bill Beckwith and Tom Schiltz, "Active Mixers Deliver High IP3," October 2003. <http://www.mwrf.com/Articles/Index.cfm?Ad=1&ArticleID=6646>.
- [34] Analog Devices, *140 MHz to 1000 MHz Quadrature Modulator AD8345*, December 2005. Data Sheet.
- [35] Analog Devices, *Low Cost, High Speed Differential Amplifier AD8132*, November 2006. Data Sheet.
- [36] Skyworks Solutions, Inc, *SKY73010: 300 2500 MHz Direct Quadrature Modulator*, January 2006. Data Sheet.
- [37] Skyworks Solutions, Inc, *AS216-339, AS216-339LF: GaAs SPDT IC 7 W T/R Switch 300 kHz2.5 GHz*, July 2006. Data Sheet.